NIST-GCR-91-595

Theoretical Investigation of Piloted Ignition of Wood

Lin-Shyang Tzeng
Arvind Atreya

Michigan State University
Department of Mechanical Engineering
East Lansing, MI 48824

U.S. DEPARTMENT OF COMMERCE

NATIONAL INSTITUTE OF STANDARDS AND TECHNOLOGY

NIST

NIST-GCR-91-595

Theoretical Investigation of Piloted Ignition of Wood

Lin-Shyang Tzeng
Arvind Atreya

Michigan State University
Department of Mechanical Engineering
East Lansing, MI 48824

Issued August 1991

NIST Grant Number 60NANB8D0861

Sponsored by:
U.S. DEPARTMENT OF COMMERCE
National Institute of Standards and Technology
Building and Fire Research Laboratory
Gaithersburg, MD 20899

U.S. DEPARTMENT OF COMMERCE
Robert A. Mosbacher, Secretary

NATIONAL INSTITUTE OF STANDARDS AND TECHNOLOGY
John W. Lyons, Director

Notice

This report was prepared for the Building and Fire Research Laboratory of the National Institute of Standards and Technology under Grant Number 60NANB8D0861. The statements and conclusions contained in this report are those of the authors and do not necessarily reflect the views of the National Institute of Standards and Technology or the Building and Fire Research Laboratory.

TABLE OF CONTENTS

LIST OF TABLES

LIST OF FIGURES

NOMENCLATURE

A Pre-exponential factor

C_p Specific heat

C_{pa} Specific heat of unpyrolyzed wood

C_{pc} Specific heat of char

d_q Quenching distance

D diffusion coefficient

D Damkohler number, $D = \dfrac{A\rho^2 C_p h^2}{\lambda} e^{-f_o}$

E Activation energy

F Externally applied heat flux

h Boundary layer thickness

$\bar{h}$ Convective heat transfer coefficient

Le Lewis number, $Le = \lambda/\rho C_p D$

m Mass flux, $m = \rho v$

M Nondimensional mass flux, $M = mC_p h/\lambda$

q Heat release

Q Nondimensional heat release, $Q = q/C_p(T_F - T_\infty)$

R Ideal gas constant

R Nondimensional reaction term, $R = DY_o Y_f \exp\left[\dfrac{-\beta(1-\theta)}{1 - \alpha^o(1-\theta)}\right]$

t Time

T Temperature

v Velocity

x Position coordinate

Y Mass fraction

Greek

α° Nondimensional factor, $\alpha^{\circ} = 1 - T_{\infty}/T_F$

β Nondimensional activation energy, $\beta = \beta^{\circ}\alpha^{\circ}$

β° Nondimensional activation energy, $\beta^{\circ} = E/RT_F$

δ Laminar flame thickness, $\delta \sim \lambda/\rho_o v_o C_p$

ϵ Emissivity

θ Nondimensional temperature, $\theta = (T - T_{\infty})/(T_F - T_{\infty})$

λ Thermal conductivity

λ_a Thermal conductivity of unpyrolyzed wood

λ_c Thermal conductivity of char

ν Stoichiometric coefficient

ξ Nondimensional position coordinate, $\xi = x/h$

ρ Density

ρ_{wd} Initial density of wood

ρ_{wf} Final density of wood char

τ Nondimensional time, $\tau = \lambda t/\rho C_p h^2$

ω Reaction rate of fuel(= $A\rho^2 Y_f Y_o EXP[-E/RT]$)

$\omega_T = q\omega$

$\omega_o = \nu\omega$

σ Stephan Boltzamann Constant = $1.356 * 10^{-12}$ $Cal/cm^2 sec^{\circ}K$

Subscripts

F	Flame
f	Fuel
i	Ignition source
o	Oxygen
s	Surface
∞	Ambient
w	Wood

CHAPTER 1

INTRODUCTION

The burning of wood and other cellulosic materials has long been of central importance to fire research because wood is a primary material for building construction. Therefore, a fundamental study to understand the chemical and physical processes that occur during the combustion of cellulosic materials is a significant step toward achieving effective control and prevention of unwanted fires.

Cellulosic materials (such as wood, cotton, paper, etc.), when subjected to heating with sufficient intensity and for a long enough duration, will ignite to yield sustained combustion. Depending upon whether the ignition occurs with or without the aid of an external ignition source, the result is accordingly classified as spontaneous or piloted ignition.

The objective of this thesis is to study the piloted ignition of wood theoretically. Although there are some theoretical models for the auto-ignition of pyrolyzing materials (further discussion in chapter 5), there is no theoretical model for piloted ignition of wood. Piloted ignition, like auto-ignition, includes the solid pyrolysis and gas-phase chemical reactions. However, the mechanisms for piloted ignition are different from those of auto-ignition. Actually, the detailed mechanisms

are still unclear. From the experimental observations of A. Atreya (1983), the important factors for piloted ignition include: (1) pyrolysis of wood, which produces gaseous-fuels (such as CO, CH_4 and higher-molecular-weight hydrocarbons) and inerts (such as CO_2, H_2O). (2) diffusion and mixing of the fuel with the ambient air, which produces a flammable gas in the boundary layer. (3) pre-mixed flame ignition by a pilot ignition source. (4) quenching by the surface and (5) establishment of a sustained diffusion flame after the pre-mixed flames has vanished.

This thesis develops a theoretical model which attempts to explain and to quantify the above experimental observations. The piloted ignition criterion used in the theoretical model is defined as the development of a sustained diffusion flame after the pre-mixed flash. This ignition criterion is in sharp contrast with ignition criteria used previously, such as: minimum char depth, minimum surface temperature and minimum fuel flow rate. It is important to emphasize that the ignition criterion used in this work is not an arbitrary threshold. Instead, it is a natural consequence of the equation solved in this work. This model would be helpful for understanding the important parameters of fire safety (such as increasing activation energy of wood, decreasing pre-exponental factor of wood and decreasing thermal conductivity of wood).

In order to solve the mathematical model which includes both the pre-mixed and diffusion flames, a new numerical scheme has been developed. This method is herein called "a combined analytical and numerical solution method for chemically reacting flow"; the method is

described in detail in Appendix A. Usually, the numerical calculation of a pre-mixed flame requires very small time steps and grid spacing, but diffusion flame calculations can use a much larger time step, since the changes are slower. Consequently, the numerical calculations for the transient period spanning both pre-mixed flame and diffusion flame requires is very difficult, often causing over-flow for the numerical calculation. The combined analytical numerical method is comparatively stable during this transient period.

In chapter two we present a brief literature review for the development of the numerical scheme for pre-mixed flame propagation, quenching, and pyrolysis and ignition of cellulosic solids.

In chapter three a simplified piloted ignition model for the gas phase is developed. Here, irregular grid spacing is used for the numerical calculation. The finite difference expressions are the same as equation 3-100 of Anderson (1984). The computer program has been validated by the numerical calculation of the pre-mixed flame velocity, which is well known for CH_4-air mixtures. Also, the program has been checked by calculating the minimum fuel flow rate for the steady state diffusion flame in two ways, and the diffusion flame location in three ways. In this model, the solid phase is assumed to provide a constant fuel mass flux at a fixed surface temperature. (In the real case, both heat flux and surface temperature vary with time.) Although this model is simplified, it reveals the basic structure of the piloted ignition process, which includes a pre-mixed flame in the earliest stage of piloted ignition; this flame may be quenched if the fuel flow

rate is too low (lower than required to establish a steady-state diffusion flame) or if the ignition source is too close to the surface (which is the quenching of the pre-mixed flame). This model also shows that as the pre-mixed flames vanish a diffusion flame appears. This investigation also confirms that piloted ignition is related to the extinction of a diffusion flame. The simplified model of chapter three has been published in Combustion and Flame [Tzeng et.al. (1990)].

In chapter four the extinction of a steady diffusion flame is investigated both numerically and analytically. The analytical solution uses large activation energy asymptotics (AEA) to solve for the extinction limit of the steady-state diffusion flame.

In chapter 5 a complete simplified piloted ignition model is developed which includes the details of the solid-phase pyrolysis. In this model, the effect of fuel concentration on the ignition delay time, ignition fuel flow rate, and ignition surface temperature is investigated. It is found that the assumption of 25% fuel and 75% inert (by mass) gives the most accurate prediction of ignition time, ignition fuel flow rate and ignition surface temperature. A parameter study is also conducted, which shows that the activation energy of pyrolysis, pre-exponential factor and thermal conductivity of wood are very important factors for the theoretical model. Finally, chapter 6 summarizes the overall conclusions of this thesis and suggests various possible avenues of future research.

CHAPTER 2

LITERATURE REVIEW

As already discussed, the model developed in this thesis must include descriptions of the thermal decomposition of the solid to produce fuel gases, mixing of fuel and air in the boundary layer, pre-mixed flame propagation originating from the ignition source, quenching of this pre-mixed flame by heat losses to the surface, and establishment of a sustained diffusion flame in the boundary layer. To the author's knowledge, there are no piloted ignition models in the literature, Thus, this review basically includes discussions of (1) gas phase chemistry, and (2) solid phase pyrolysis. The piloted ignition model essentially is a combination of the above two phenomena.

2.1 Gas Phase Chemical Reaction

This part includes ignition, propagation, and quenching of a pre-mixed flame. The laminar pre-mixed flame speed and flame structure have been extensively studied in the past. Spalding [1956] first introduced a time-dependent numerical scheme for the solution of the equations for conservation of mass, energy and different chemical species. He assumed arbitrary initial profiles and then solved the equations using a standard finite-difference method. Difficulties

in the numerical procedure arise because the thickness of the pre-mixed flame is very small (about 0.1-0.5 mm, William 1985), thus a grid spacing much smaller than the flame thickness must be employed. Also, the chemical reaction rate in the governing equations is much larger than the diffusion rate, making the profiles very steep and forcing the use of small time steps. Thus, numerical calculations of pre-mixed flame propagation requires both small grid spacing and small time steps.

A numerical study of laminar flame quenching was performed by Aly and Hermance (1981); they found that the quenching Peclet number Pe, increases with decreasing fuel concentration. The theoretical results are in fair agreement with the available experimental data.

Spalding (1953) found that when a combustible mixture is ignited by heating a slab of gas, the amount of energy added to the gas must exceed a minimum value for ignition to occur. Numerical integration for slabs of various thickness, initially raised to the adiabatic flame temperature, shows that ignition does not occur for slabs thinner than the pre-mixed flame thickness. For thicker slabs, however, a propagating laminar flame develops. This observation is important for numerical simulation of a pilot flame or an ignition source.

2.2 Solid Phase Pyrolysis

Combustible solids can generally be categorised as either (1) those which decompose volumetrically, or (2) those which decompose superficially. Wood belongs to the first group, while some polymers (such as PMMA) belong to the second group. In this study, only wood has been considered.

Physically, the properties of wood are highly dependent upon its microscopic structure. Wood consists of cells or fibers, whose diameters vary from 0.02 to 0.5 millimeters. The length of the cell fibers ranges from 0.5 to 1.5 mm. The porosity (ratio of the volume of pores to the volume occupied by the cell walls) of real woods lies somewhere in the range 40-75%. (Kanury 1970).

Chemically, wood is composed of three major constituients: (1) cellulose (50% by weight), (2) hemicellulose (25%) and lignin (25%) (Stamm 1964). Pyrolysis of cellulose occurs in two distinct path ways (Shafizadeh 1981). At low temperatures (200-280°C) dehydration of cellulose produces dehydrocellulose and water. This process is slightly endothermic (except in the presence of oxygen) and leads to the formation of char, water, and volatile gases such as CO_2, CO, and hydrocarbons. The gases evolved in the dehydrocellulose route are primarily noncombustible and the char which remains can oxidize through surface combustion. At higher temperatures (280-340°C) endothermic depolymerization of cellulose leads to the formation of tar-like

products which are highly condensible and constitute the main gaseous fuel to support a gas-phase flame.

Pyrolysis of thick samples of wood involves both the physics of heat and mass transfer and the kinetics of chemical decomposition. Consider a thick slab of wood, initially at room temperature, exposed to a high-intensity thermal radiation source. The temperature of the solid gradually increases with time, the surface temperature being the highest. Before the surface layer decomposes, evaporation of moisture occurs and a moisture evaporation zone begins to travel into the solid. At later times, the pyrolysis zone begins to develop and then to propagate slowly into the interior of the solid, leaving behind a thermally insulating layer of char.

Regarding the mathematical model of pyrolysis, the formation and growth of a char layer which protects the decomposition zone and the virgin material involves many physical and chemical processes, which makes it very difficult to develop a numerical solution that contains all of them. A few mathematical models of wood pyrolysis have been put forward, starting with the work of Bamford et.al.(1946). They treated wood as a solid of constant thermal diffusivity. Kung(1972) assumed the thermal properties of the solid varied continuously from their values for virgin wood to their values for char. Kansa et.al. (1977) included a momentum equation for the motion of gases relative to the solid and obtained good agreement with Lee et.al's (1976) experimental data for low heat fluxes. At high heat fluxes, however, poor atreement was obtained; this was attributed to ignoring the effects of structural

changes (shrinkage and cracking) and to the assumption of a single step-pyrolysis reaction.

An analytical solution for surface temperature was derived by Atreya (1983) using the integral method. The solution shows excellent agreement with the experimental results. Base on this surface temperature, an analytical solution for the pyrolysis mass flux of wood has been derived by Atreya and Wichman (1989). This equation is obtained by assuming constant wood density. Thus, the solution is only valid in the early stages of pyrolysis. In this research, both the analytical (integral) solution and the numerical solution of the simplified wood pyrolysis equations have been used to describe the solid phase.

CHAPTER 3

A ONE-DIMENSIONAL MODEL OF PILOT IGNITION

In this chapter a simplified model of piloted ignition is analyzed. The two-dimensional coupled solid and gas phase problem is simplified by assuming that the mass evolution rate from the combustible solid is a constant , and by employing a plane rather than a point ignition source. With these assumption the model problem requires only a transient one-dimensional analysis of the gas phase. The model equations are solved numerically using the fast scheme discussed in chapter 1 and Appendix A. The pilot flame is modeled as a thin slab of gas that is periodically heated to the adiabatic flame temperature of the stoichiometric mixture. The effects of : (i) the location of the ignition source, (ii) the fuel mass evolution rate from the surface, and (iii) the surface temperature of the solid are investigated. An explanation is produced for the pre-ignition flashes that are observed experimentally. A criterion for positioning of the pilot flame is proposed. The minimum fuel evolution rate, by itself, is found insufficient for predicting the onset of piloted ignition; heat losses to the surface plays an important role. Also, the conditions at extinction of a steady diffusion flame are found to be practically identical to those for piloted ignition.

3.1 Background

The phenomenon of piloted ignition is rather poorly understood. This is evident from the numerous empirical ignition criteria that have been proposed in the literature. Some of these are: critical surface temperature, critical fuel mass flux, critical char depth and critical mean solid temperature. Of these, critical fuel mass flux at ignition appears physically the most reasonable, but critical surface temperature has proved to be the most useful, since it can be easily related to flame spread.

The physical mechanism of piloted ignition is quite complex. The solid must first chemically decompose to inject fuel gases into the surrounding air. This produces a flammable mixture (in the boundary layer), which is ignited by an ignition source. A plausible physical configuration for this process is illustrated in Figure 3-1.In the early stages of solid pyrolysis, the fuel flow rate is very small and the fuel-air mixture in the boundary layer is not combustible. As the fuel evolution rate increasses with time this mixture becomes rich enough to allow a premixed flame to propagate through the boundary layer. This premixed flame consumes nearly all the available fuel and is quenched by heat loss to the surface, unless the fuel evolution rate is large enough to replenish the consumed fuel. Thus, either a flash (a quenched premixed flame) or a sustained diffusion flame (piloted ignition) is observed. Experimental observations of this phenomenon are shown in Figure 3-2. The momentary rise in surface temperature prior to sustained ignition is due the flashes.

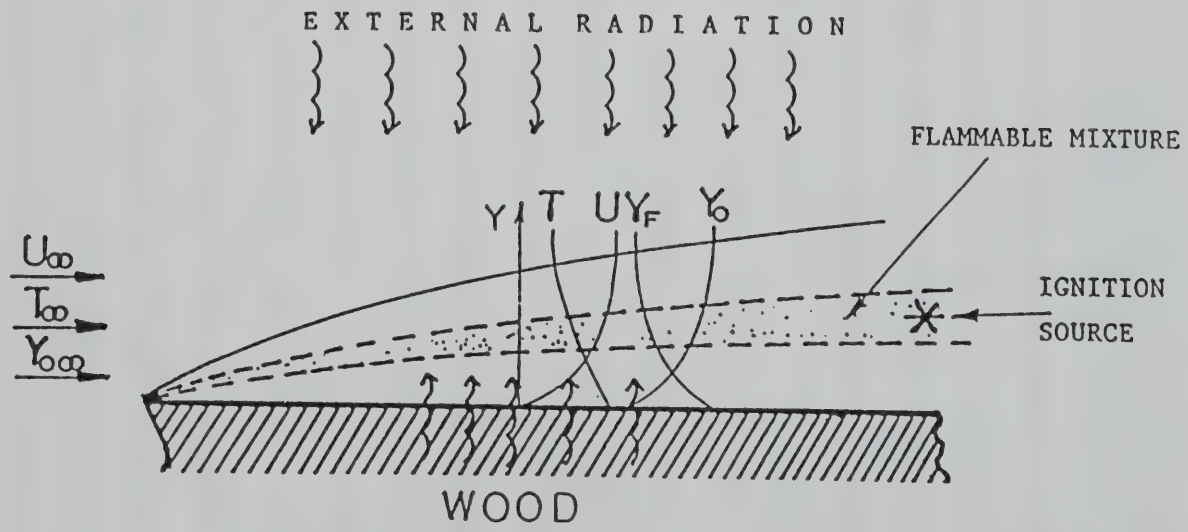

FIGURE 3-1 Piloted ignition of solids -- The physical problem.

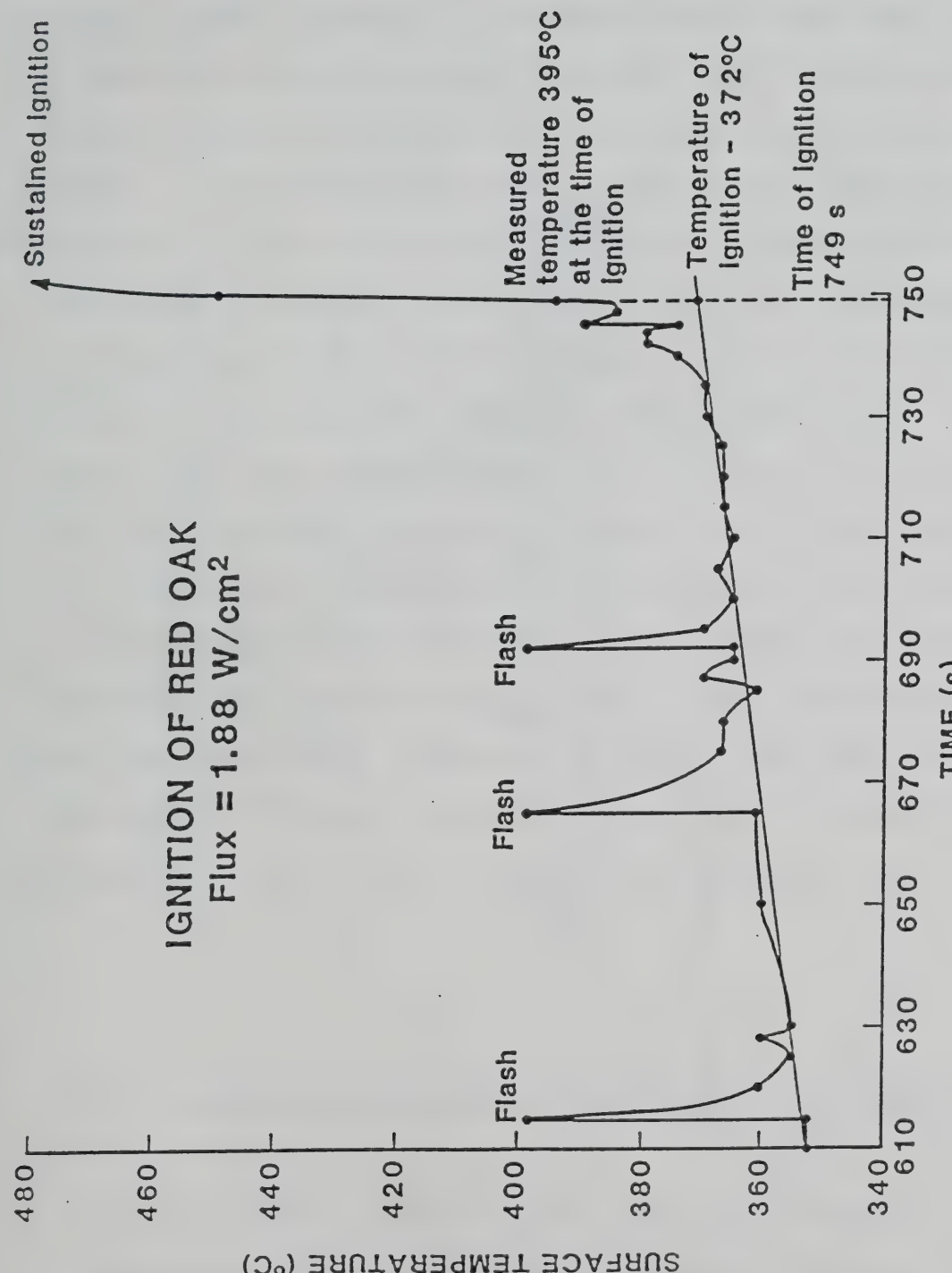

FIGURE 3-2 Surface temperature-time history during piloted ignition of a red oak sample.

From experimental obserations, it is clear that the piloted ignition process involves both premixed and diffusion flames. Also, the true criterion for sustained piloted ignition is determined once the conditions that allow the conversion of a premixed flame to a diffusion flame are known. These conditions include magnitudes of the fuel evolution rate and the surface temperature that determines the heat losses responsible for quenching the premixed flame. Thus, a complete theoretical model of the piloted ignition process must include transient analysis of : (i) thermal decomposition of the solid to produce fuel gases, (ii) mixing of fuel and air in the two-dimensional boundary layer, (iii) premixed flame propagation originating from the ignition source, (iv) quenching of this premixed flame by heat losses to the surface, and (v) establishment of a sustained diffusion flame in the boundary layer. This rather formidable problem is considerably simplified by assuming that the solid-phase thermal response (to the applied heat flux) is a known function of time, and by employing a plane rather than a point ignition source. These assumptions reduce the problem to a transient one-dimensional analysis of the gas-phase phenomena, thus capturing the bare essentials of the piloted ignition process.

3.2 Mathematical Model of One-Dimensional Piloted Ignition

A diagram of the model problem is shown in Figure 3-3. A gas stream containing the fuel is fed uniformly and at a constant rate through a porous plate whose surface temperature is assumed constant.

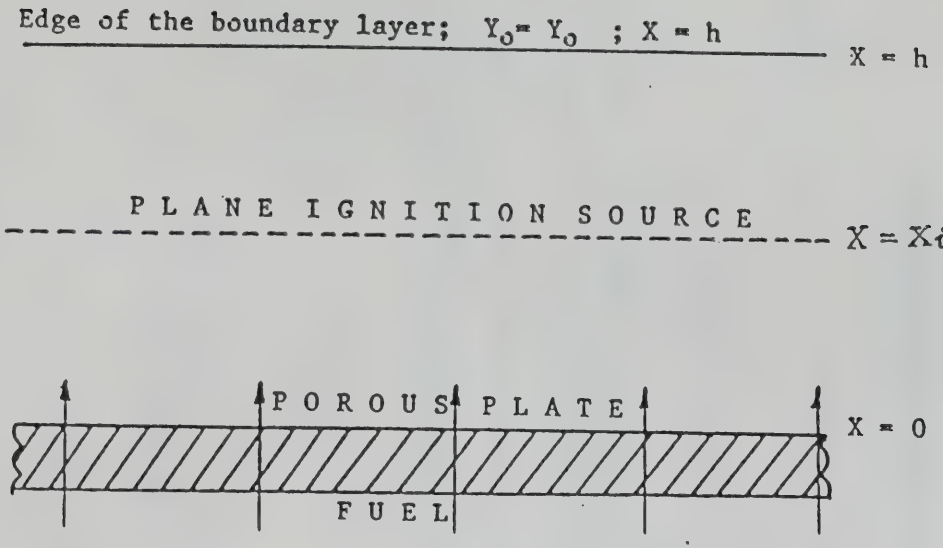

FIGURE 3-3 Piloted ignition of solids -- The model problem.

Conditions at a distance h above the plate are maintained constant by a fast flowing oxidizer stream. A plane ignition source (whose distance from the plate, $0 < x_i < h$, is variable) is placed near the porous plate. This ignition source is periodcally "turned on" to test for piloted ignition. The chemical reaction is assumed to be a simple second-order, one-step irreversible Arrhenius type,

$$\text{Fuel} + \nu\ O_2 \rightarrow \text{Products} + q\ (\text{heat}) \tag{3-1}$$

The governing energy and species equations are:

$$\rho\frac{\partial T}{\partial t} + \rho v\frac{\partial T}{\partial x} = \frac{\partial}{\partial x}\left[\frac{\lambda}{C_p}\frac{\partial T}{\partial x}\right] + q\frac{A}{C_p}\rho^2 Y_f Y_o e^{-E/RT}, \tag{3-2}$$

$$\rho\frac{\partial Y_f}{\partial t} + \rho v\frac{\partial Y_f}{\partial x} = \frac{\partial}{\partial x}\left[\rho D\frac{\partial Y_f}{\partial x}\right] - A\rho^2 Y_f Y_o e^{-E/RT} \tag{3-3}$$

and

$$\rho\frac{\partial Y_o}{\partial t} + \rho v\frac{\partial Y_o}{\partial x} = \frac{\partial}{\partial x}\left[\rho D\frac{\partial Y_o}{\partial x}\right] - \nu A\rho^2 Y_f Y_o e^{-E/RT} \tag{3-4}$$

and the initial and boundary condition are:

at $t = 0$, $0 < x < h$;

$$Y_f = 0,\ Y_o = Y_{o\infty}\ ,\ \text{and}\ T = T_\infty, \tag{3-5}$$

$$\text{at } x = 0,\ t > 0; \qquad \rho D\frac{\partial Y_f}{\partial x} = \rho v(Y_f - Y_{fs}),$$

$$\rho D\frac{\partial y_o}{\partial x} = \rho v Y_o, \tag{3-6}$$

$$T = T_s$$

and at $x = h,\ t>0$;

$$Y_f = 0;\ Y_o = Y_{o\infty};\ T = T_\infty. \tag{3-7}$$

To simplify these equations, ρ is assumed constant, implying that $m = \rho v$ is not a function of x; thus, mass conservation is automatically satisfied. Also, λ, C_p and D are assumed constants.

The above equations are non-dimensionalized as follows:

$$\xi = \frac{x}{h},\ \tau = \frac{\lambda t}{\rho C_p h^2},\ M = \frac{m C_p h}{\lambda}$$

$$\theta = \frac{T - T_\infty}{T_f - T_\infty},\ D = \frac{A \rho^2 C_p h^2}{\lambda} EXP[-\beta^o] \tag{3-8}$$

$$\beta^o = \frac{E}{RT_f},\ Q = \frac{q}{C_p(T_f - T_\infty)},\ \beta = \beta^o\alpha^o$$

$$\alpha^o = 1 - T_\infty/T_f,$$

and with the definitions

$$L\{\bullet\} = \frac{\partial(\bullet)}{\partial\tau} + M\frac{\partial(\bullet)}{\partial\xi} - \frac{\partial^2(\bullet)}{\partial\xi^2},$$

and

$$R = DY_f Y_o EXP\left[\frac{-\beta(1 - \theta)}{1 - \alpha^o(1 - \theta)}\right] ,$$

the governing equations may be rewritten as

$$L\begin{Bmatrix} \theta \\ Y_f \\ Y_o \end{Bmatrix} = \begin{Bmatrix} Q \\ -1 \\ -\nu \end{Bmatrix} R. \qquad (3\text{-}9)$$

The initial and boundary conditions become:

at $\tau = 0$, $0 < \xi < 1$;

$$\theta = 0,\ Y_f = 0,\ Y_o = Y_{o\infty}, \qquad (3\text{-}10)$$

at $\xi = 0$, $\tau > 0$;

$$\left.\begin{aligned} &\theta = \theta_s, \\ &\frac{\partial Y_f}{\partial \xi} = M(Y_f - Y_{fs}) , \\ &\frac{\partial Y_o}{\partial \xi} = MY_o , \end{aligned}\right] \qquad (3\text{-}11)$$

and at $\xi = 1$, $\tau \geq 0$;

$$\theta = 0,\ Y_f = 0,\ Y_o = Y_{o\infty} . \qquad (3\text{-}12)$$

Equations (3-9) along with the initial and boundary conditions are solved numerically by using a finite difference formulation.

3.3 Numerical Solution

A nonuniform grid is used for numerical computations. As shown in Figure 3-4, this grid is closely spaced around the ignition source to

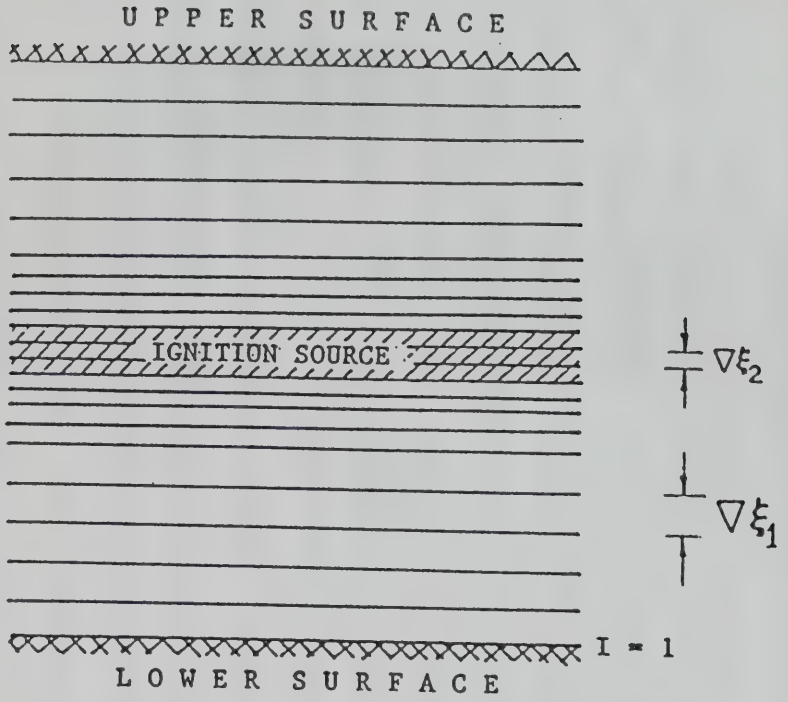

FIGURE 3-4 Computational grid.

ensure satisfactory resolution for the premixed flame propagation stage. An efficient numerical method that splits the solution procedure into a homogeneous reaction (explosion) calculation and a subsequent convective diffusive calculation was developed. This numerical procedure is described in Appendix A.

3.3.1 Premixed Flame Velocity Calculations

First, the premixed flame velocity was calculated in order to: (i) adjust the input parameters, (ii) verify the numerical code, (iii) determine an appropriate grid spacing and time step, and (iv) determine the input energy needed for the ignition source. For these calculations, the fuel is assumed to be methane and essentially the input parameters given by Coffee et.al. (1983) were used. However, the reaction order used in Coffee et.al. (1983) is 3 as opposed to 2 for the present problem. Thus, the pre-exponential factor, A, was slightly modified to obtain the same steady-state premixed flame velocity in a stoichiometric mixture. These input parameters are E = 29.1 Kcal/mole, T_f = 2230 K, T_∞ = 298 K, ν = 4, q = 11355 cal/g fuel, C_p = 0.323 cal/g K, $\lambda = 1.5 \times 10^{-4}$ cal/cm K sec, $\rho = 3.74 \times 10^{-4}$ g/cm^3, $Le = \dfrac{\lambda}{\rho C_p D} = 1$ and $\rho A = 3.56 \times 10^{9}$/sec.

The premixed flame velocity calculations were performed by using the numerical code developed to solve the governing Equations (3-9), with the initial and boundary conditions modified as follows: (i) Initially a stoichiometric mixture of methane and air is assumed to exist above the solid surface and the fuel flow rate from the surface

is set equal to zero (i.e, m = 0). Thus, $Y_f(0,x) = 0.0546$ and $Y_o(0,x) = 0.219$. (ii) The surface temperature is assumed equal to the adiabatic flame temperature, i.e. $\theta = \theta_s = 1$.

Thus, the premixed mixture is ignited at the surface and the flame propagates toward the outer boundary, eventually attaining a steady speed. This steady-state flame velocity is determined by measuring the propagation rate of the temperature profile and by assuming the densities of the burned and the unburned gas mixtures to be identical. A uniform grid was employed for these calculations and the influences of diffenent grid spacings and time steps were investigated. The results of these calculations are summarize in Table 3-1, which shows that the calculated steady-state flame velocity is very close to other calculations, as well as to the experimental result, thus giving credibility the numerical code and the input data.

The grid spacing and the time step for the piloted ignition calculations is determined from Table 3-1, which shows that a grid spacing of $\Delta\xi = 3.7 \times 10^{-3}$ provides sufficient resolution. This corresponds to an actual physical spacing of 0.055 mm, which is smaller than the flame thickness; this value is estimated by using $\delta \simeq \lambda/C_p\rho_o v_o$ Williams (1985), where ρ_o and v_o are the unburned mixture density and velocity respectively, giving a flame thickness of 0.092 mm. A finer grid was not used in order to reduce the CPU time. Since the premixed flame propagation speed is not the desired final result of this piloted ignition study, the largest time step shown in Table 3-1 ($\Delta\tau=2.7\times10^{-5}$) is used to save CPU time. Also, twice this time step ($\Delta\tau = 5.4 \times 10^{-4}$) was used prior to turning on the ignition source.

3.3.2 Numerical Simulation of the Ignition Source

In the numerical code, the ignition source is turned on by simply raising the temperature of a slab of gas to the adiabatic flame temperature. The thickness of this slab is chosen to be three grid spaces, which is approximately twice the premixed flame thickness. Choice of this thickness is based on the observation Williams (1985): "Ignition will occur only if enough energy is added to the gas to heat a slab about as thick as a steadily propagating adiabatic laminar flame to the adiabatic flame temperature." The reason for choosing an ignition source thickness larger than the premixed flame thickness is that the gas mixture is not stoichiometric. Thus, the chosen thickness ensures ignition if the fuel/air mixture in the boundary layer has reached its lean flammability limit.

It is important that the amount of energy added to the system by the ignition source be minimized. Thus, the pilot cannot be left on continuously. This is especially critical because a plane rather than a point ignition source is used to render the model problem one-dimensional. To overcome this difficulty a novel method has been devised. When the ignition source is turned on the data for temperature and species is placed into a temporary file. After calculating for several time steps the occurrence of ignition is determined by observing the development of the temperature and species profiles. If ignition is not observed, then the data from the temporary file is recalled and the calculation is restarted at that point. This procedure eliminates any accumulation of energy from periodic trials prior to the occurrence of piloted ignition.

3.3.3 Steady-State Diffusion Flame Calculations

In the latter stages of piloted ignition, the premixed flame develops into a diffusion flame, which slowly moves toward its steady-state location. The governing equations and the boundary conditions describing this steady diffusion flame are simply the steady-state versions of Equations (3-9), (3-11) and (3-12). Thus, the location of the steady diffusion flame and the corresponding temperature and species concentrations may be found either from the large time solution of the time dependent Equations (3-9), (3-11) and (3-12) (i.e., in the later stages of piloted ignition) or by directly solving the steady-state versions of Equation (3-9),(3-11) and (3-12). It may also be obtained analytically in the thin flame sheet Burke-Schumann limit, which gives Kanury (1975).

$$x_f = 1 - \frac{1}{M} \ln \left\{ 1 + \frac{Y_{o\infty}}{\nu Y_{fs}} \right\} \qquad (3\text{-}13)$$

Table 3-2 shows a comparison of the diffusion flame location calculated by all three methods. The transient piloted ignition calculations were terminated after about 4 seconds (elapsed real time) because changes in the diffusion flame location had become negligibly small. In these calculations the surface temperature of the solid was assumed to be 298 K and the ignition source was located at the minimum distance from the surface. (This minimum distance for the ignition source will be discussed in Sec. 3.4.4)

Numerical solution of the steady-state versions of the Equations (3-9),(3-11) and (3-12) was obtained by iteration. Calculations were

started by guessing the location of the diffusion flame and the corresponding temperature and specied profiles. Using this initial guess, the non-linear reaction rate term (R; See Equation (3-9)) was calculated and then the energy and species equations were solved to obtain a new set of conditions. This iteration was performed until the solution converged to within a prescribed error.

It is evident from Table 3-2 that the results of all three calculations compare quite satisfactorily. These calculations further confirm the validity of the numerical code for the piloted ignition calculations.

3.4 Results and Discussion

After verifying the piloted ignition model for the limiting cases of premixed flame propagation (the early stage) and development of a steady-state diffusion flame (the later stage), several aspects of the piloted ignition process were investigated. In this investigation the fuel concentration in the solid phase was taken as unity (Y_{fs} =1), and unless otherwise specified, the solid surface temperature was T_∞ ($T_s = T_\infty$ = 298 K). Various case studies are summarized below.

3.4.1 Piloted Ignition Phenomena

To investigate the details of the piloted ignition process, the following conditions were assumed: h = 1.5 cm, m = 8.34 x 10^{-5} g/cm^2 sec T_s = 298 K, Y_{fs} = 1, and the ignition source is placed at x_i = 1.186 cm (which corresponds to the theoretically predicted location of the steady diffusion flame). Note that in experiments both surface temperature and fuel mass flux will increase with time as the solid is heated by a contant heat flux. Also, the fuel concentration in the solid is typically less than 100% (i.e., $Y_{fs} < 1$) because of the presence of moisture. Thus, the calculated time for piloted ignition cannot be compared with experimental values. However, the gas-phase ignition process (which is the focus of this study) is not expected to be different. Furthermore, in the numerical model, it is fairly straightforward to assign the experimentally measured values of m, T_s and Y_{fs} once they become available.

Figures 3-5 and 3-6 show the results of piloted ignition calculations. The mixture was ignited at t = 1.089 seconds, as seen by the sharp temperature peak and corresponding dips in the fuel and oxidizer concentrations. The premixed flame then travels quickly into the unburnt mixture in both directions i.e., both toward and away from the porous plate. This can be seen more clearly from the heat flux profiles (which are proportional to the temperature gradient) show in Figure 3-6. At t = 1.102 seconds (i.e. 13 milliseconds later) the premixed flame has consumed nearly all the available oxygen on the fuel side and all the available fuel on the oxidizer side of the ignition

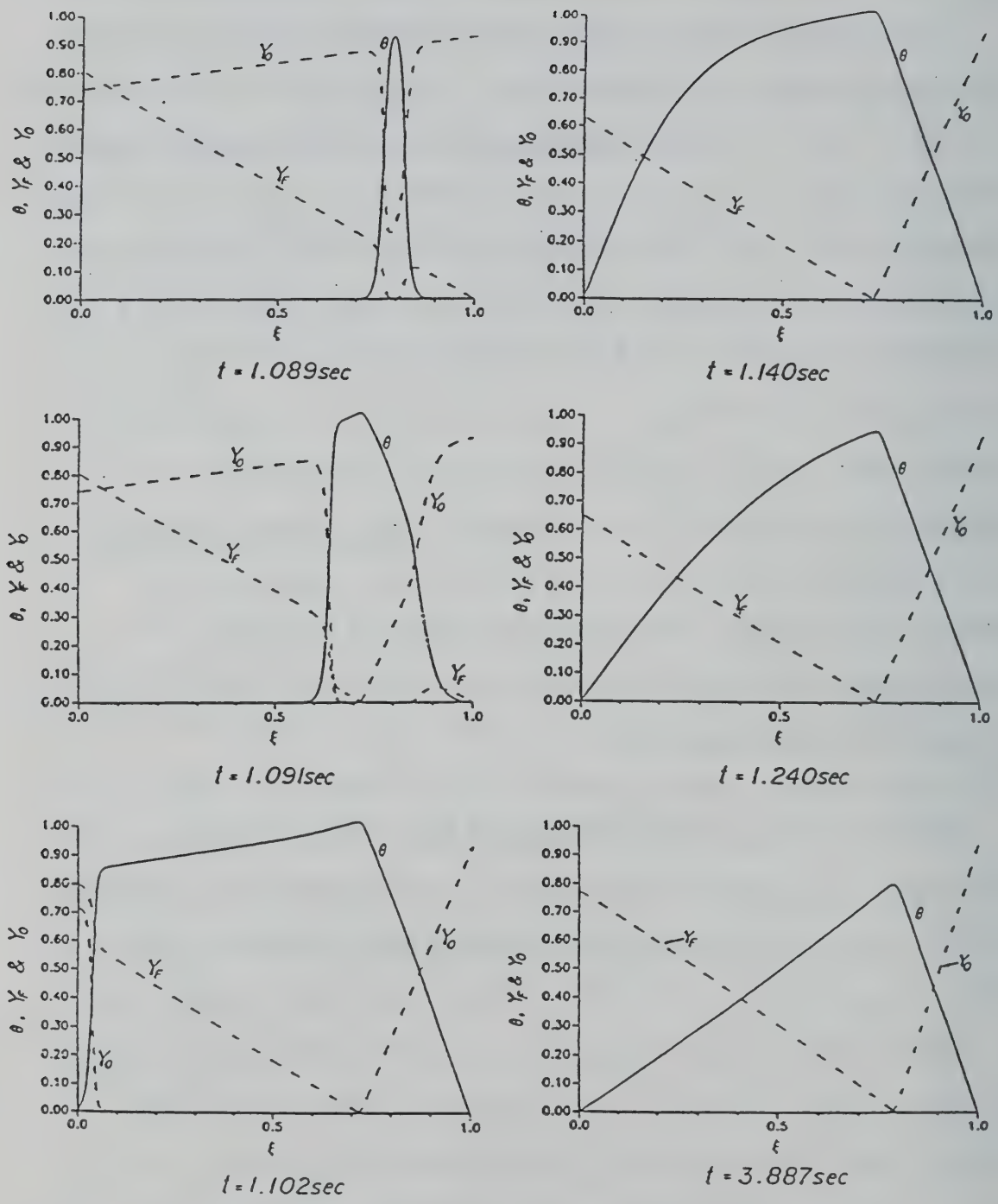

FIGURE 3-5 History of the piloted ignition process from ignition (t = 1.089 s) to development of a steady diffusion flame (t = 3.887 s). Note: the scales for Y_o and Y_F are not shown for clarity. They differ from the scale for θ by a constant factor that is 0.250 for Y_o and 0.167 for Y_F.

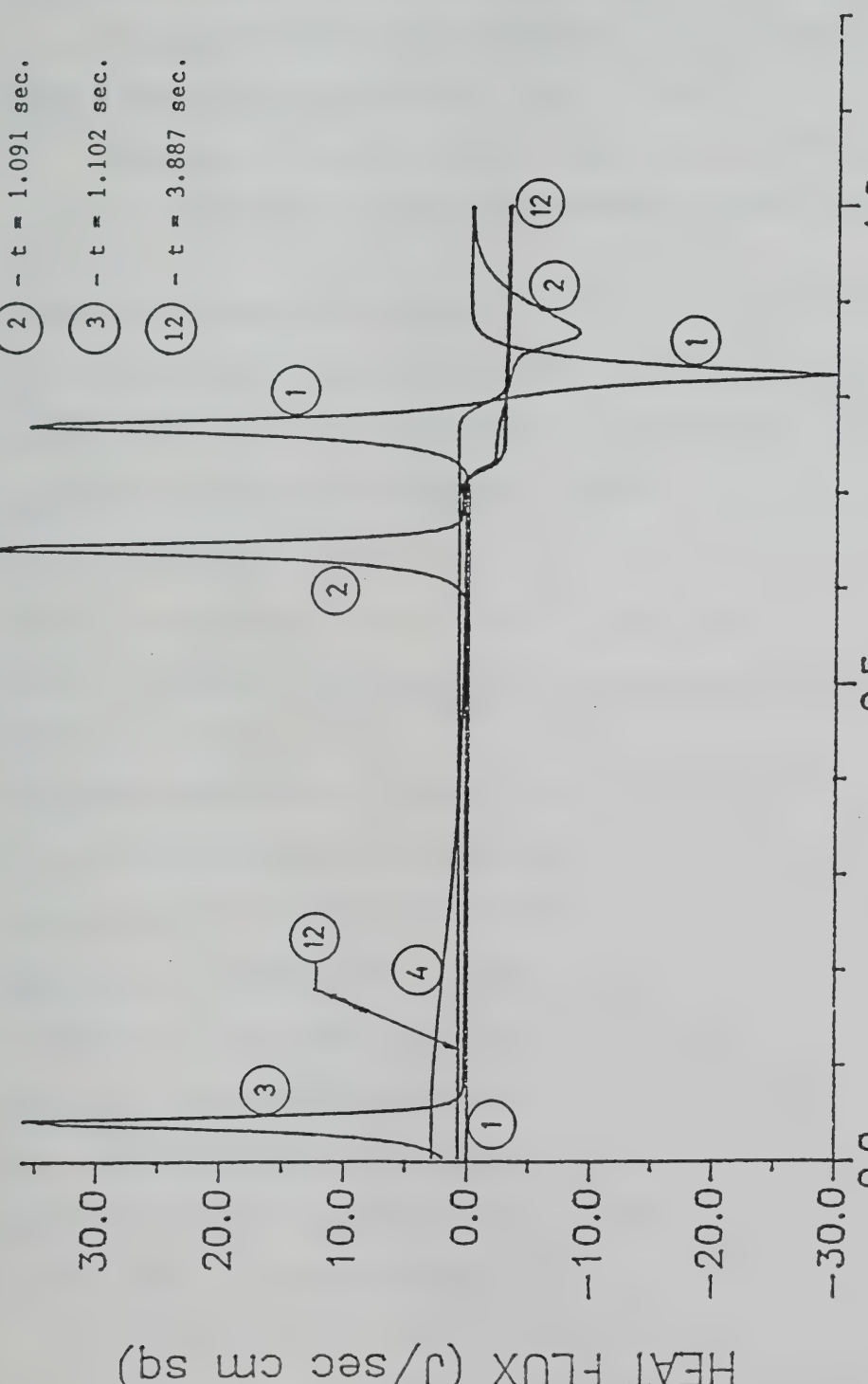

FIGURE 3-6 Heat flux profiles (proportional to temperature gradient) for the propagating pre-mixed flame during piloted ignition.

source, thereby establishing conditions appropriate for the formation of a diffusion flame. At this time the surface experiences a large heat flux (see curve (3) in Figure 3-6), which is probably responsible for the sharp momentary rise in temperature observed during the experiment shown in Figure 3-2. Note that during the premixed flame stage the heat flux is very large. However, once conversion to a diffusion flame begins the magnitude of the heat flux drops sharply.

At times larger than 1.102 seconds, the temperature, fuel and oxygen concentrations slowly adjust to those for a steady state diffusion flame, which is finally established at $t \approx 4$ seconds. Note that its final location is nearly identical to that of the ignition source ($\xi \simeq 0.8$).

3.4.2 Quenching of the Premixed Flame (Flashes)

If the ignition source is too close to the cold porous wall (or the sample surface) then thermal quenching of the premixed flame prevents the development of a diffusion flame and hence the occurrence of piloted ignition, resulting in a flash. Similar behavior is observed if the fuel flow rate is lower than the lean flammability limit. This is discussed in the next section. In the case discussed here, the fuel flow rate is the same as that for the case in Section 4.1, but the ignition source is placed closer to the surface (i.e., at $x_i = 0.193$ cm, as compared with $x_i = 1.186$ cm for the previous case). For this case, gas ignites at 0.1 seconds (much smaller than 1.089 seconds for the previous case) but the ignition is not sustained.

Figure 3-7, 3-8, 3-9 and 3-10 show respectively the temperature, fuel concentration, oxygen concentration and the heat flux profiles during this momentary flaming. It can be seen that nearly all of the oxygen on the fuel side and the fuel on the oxygen side are consumed, but the temperature eventually decays and the fuel and oxygen are subsequently replenished.

It is interesting to note that the fuel concentrations at the location of the ignition source for both this and the previous case are nearly the same ($Y_f = 0.0418$ for the present case and $Y_f = 0.0414$ for the previous case) and yet sustained ignition was not achieved here. Table 3-3 shows the fuel concentration at the location of the ignition source and at the time of piloted ignition for different fuel flow rates and ignition source locations. Note that the value of Y_f is remarkablely constant (average is 0.0445) despite the fact that in many cases the flame was quenched. This value of Y_f is approximately 80% of the stoichiometric mass fraction and is about 1.74 times the stated lean flammability limit for CH_4 [Kanury(1975)]. The reason for the difference between the lean flammability limit and Y_f at ignition is not clear to the authors. It may occur because of the assumption of one-step chemistry or because of the difference between the initial and boundary conditions. Further theoretical and numerical analysis of this phenomenon are obviously necessary. However, regardless of their outcome, it is clear i) that piloted ignition cannot be predicted solely on the basis of the lean flammability limit, and ii) that heat losses to the solid surface play a very important role.

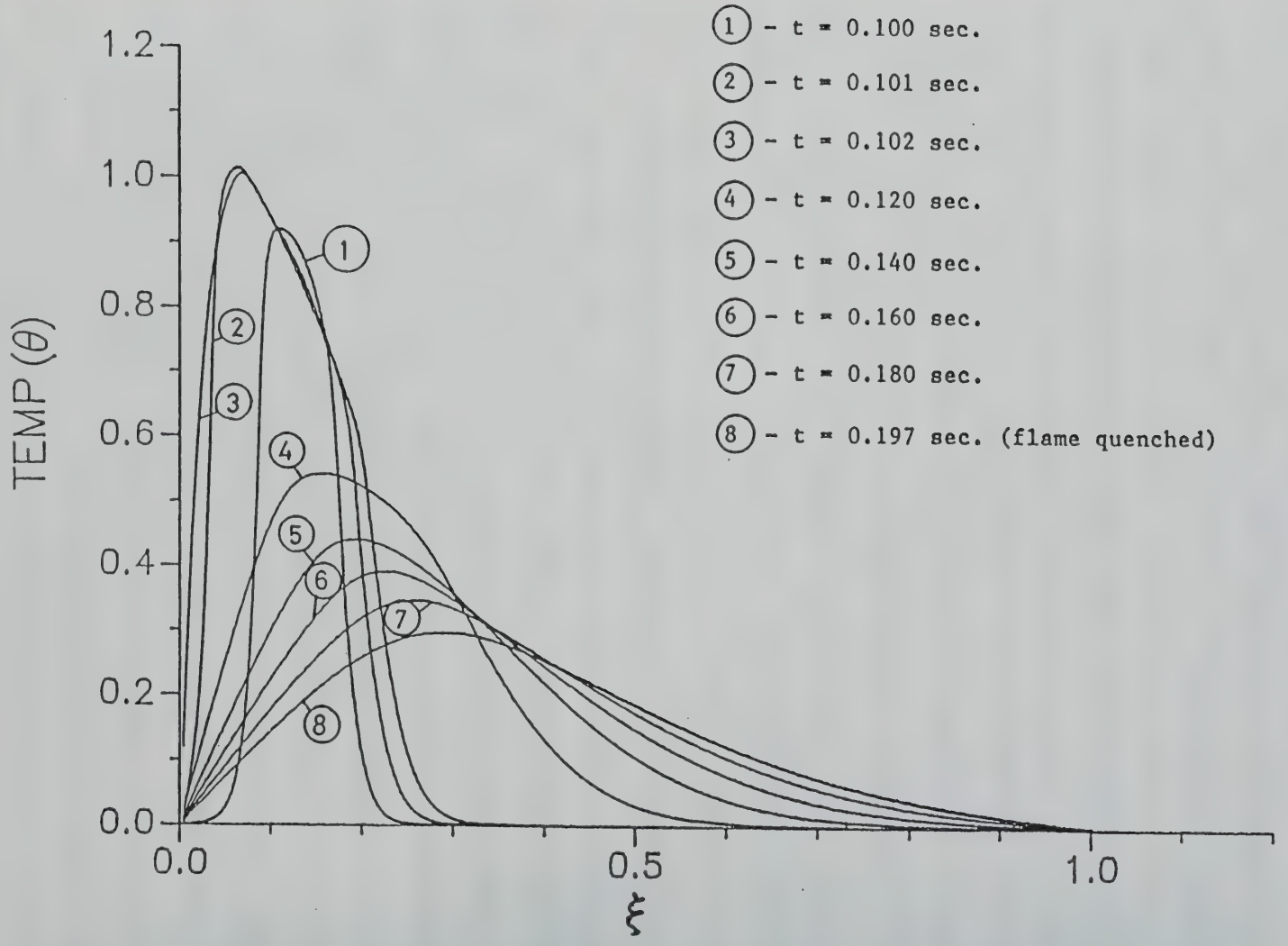

FIGURE 3-7 Temperature profiles for the quenched pre-mixed flame (resulting in a flash).

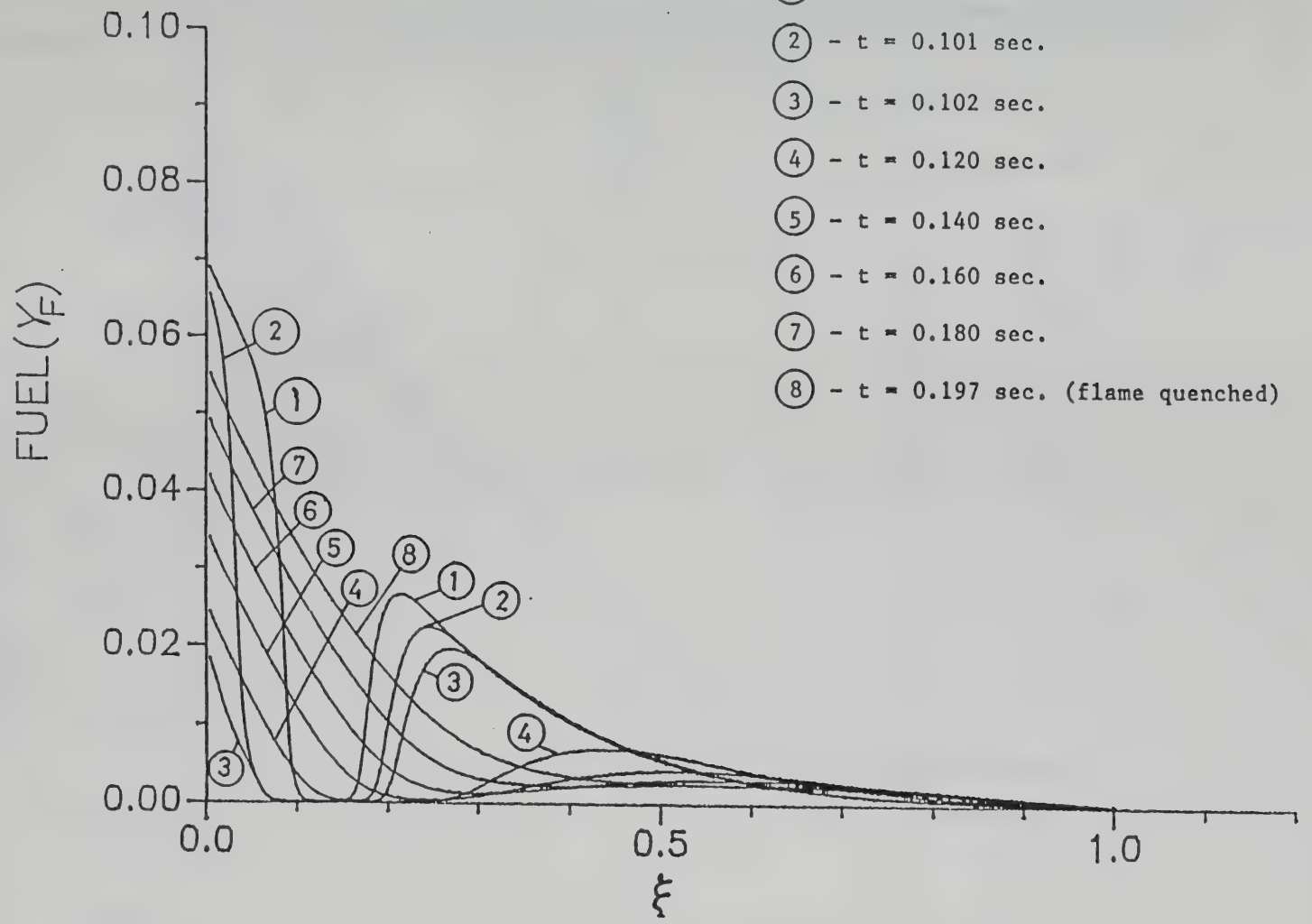

FIGURE 3-8 Fuel concentration profiles for the quenched pre-mixed flame (resulting in a flash)

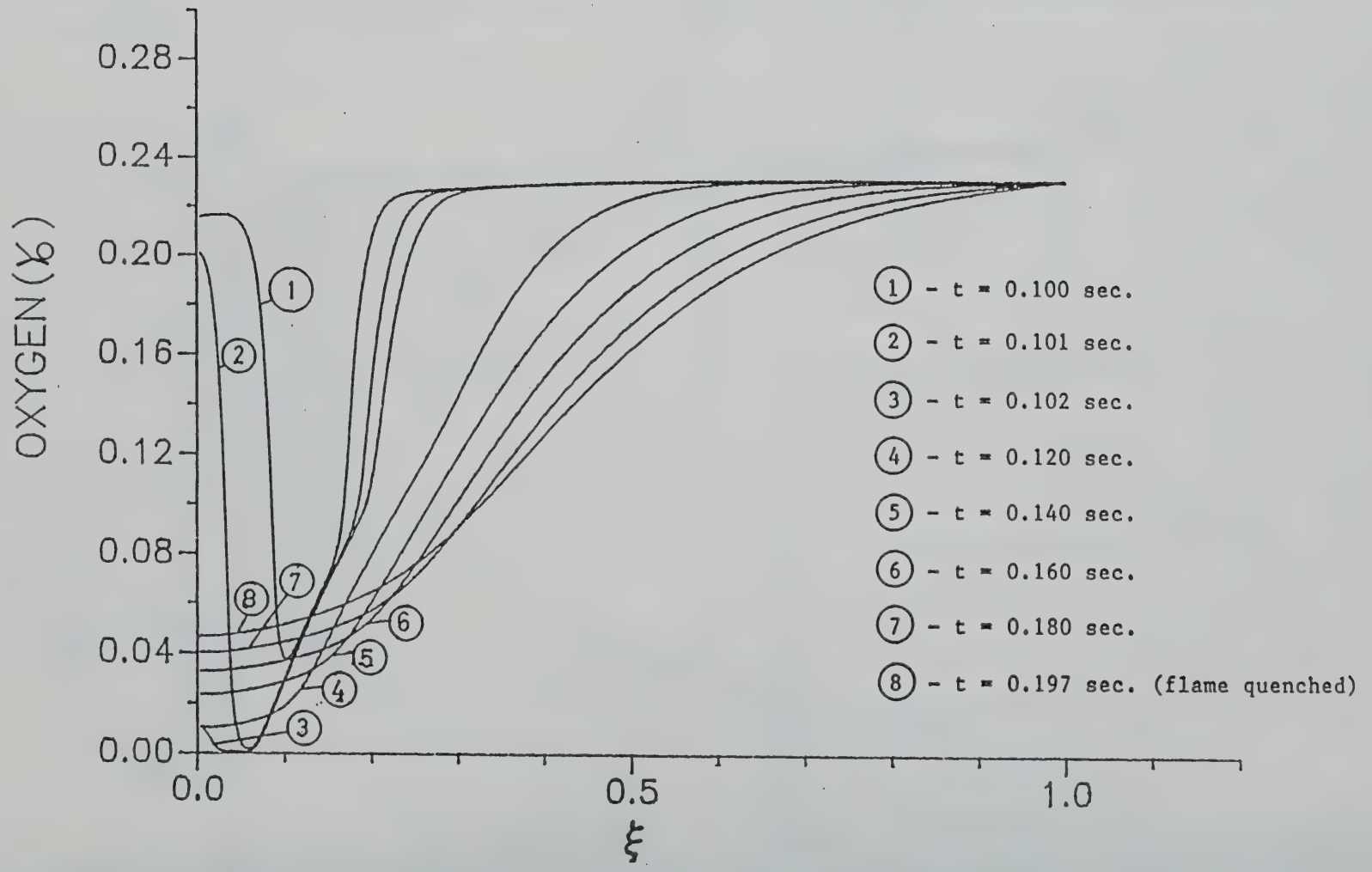

FIGURE 3-9 Oxygen concentration profiles for the quenched pre-mixed flame (resulting in a flash)

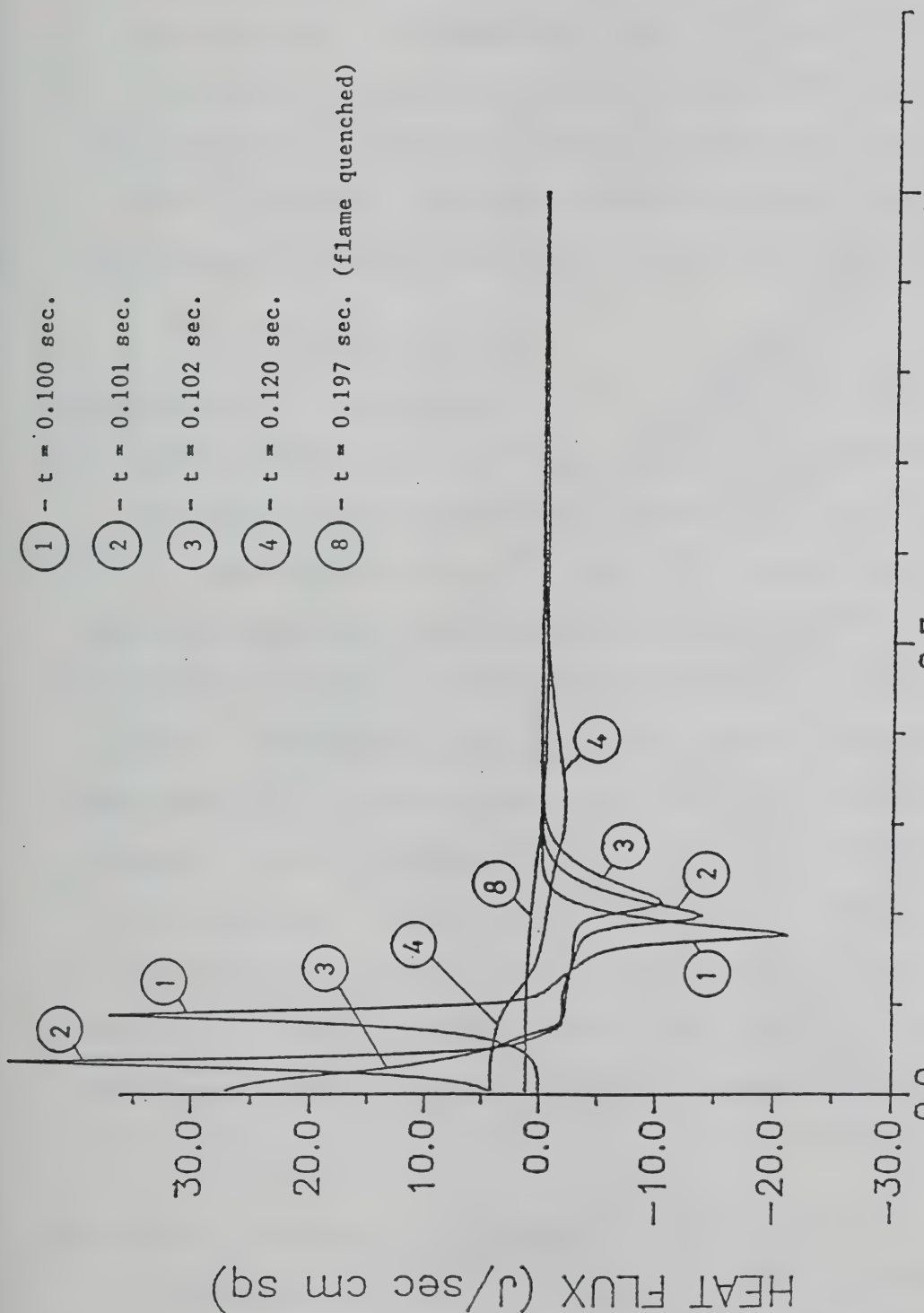

FIGURE 3-10 Heat flux profiles for the quenched pre-mixed flame (resulting in a flash)

3.4.3 Minimum Fuel Rate for Piloted Ignition

In this case the fuel flow rate was reduced to 3.128×10^{-5} g/cm^2 sec, which is slightly less than the minimum fuel flow rate listed in Table 3-3 (3.34×10^{-5} g/cm^2 sec) for which piloted ignition was possible. Note that this fuel flow rate is roughly one-third the fuel flow rate used in the previous two cases. Here, regardless of the location of the ignition source, a sustained diffusion flame was not obtained.

Figure 3-11 through 3-14 show the temperature, fuel concentration, oxygen concentration and heat flux profiles during flashes caused by the low fuel flow rate. For the results presented in these figures, the ignition source was located at 0.67 cm from the surface, which corresponds to the theoretical location of the steady diffusion flame. It can be seen that although most of the oxygen on the fuel side and the fuel on the oxygen side are consumed by the premixed flame, the fuel supply rate is too low to enable the establishment of a diffusion flame. Hence, the temperature quickly falls to its ambient value. A comparison of Figure 3-8 and 3-12 shows how slowly the fuel is replenished. In Figure 3-8, the fuel concentration at the surface recovers to about 75% of its initial value in 0.1 seconds, whereas in Figure 12 the fuel concentration at the surface recovers to only about 50% of its original value in 0.5 seconds.

Since for successful piloted ignition it is necessary to establish a steady diffusion flame, the minimum fuel flow rate at extinction of the steady diffusion flame is expected to be close to that required for piloted ignition. The minimum fuel flow rate at extinction is

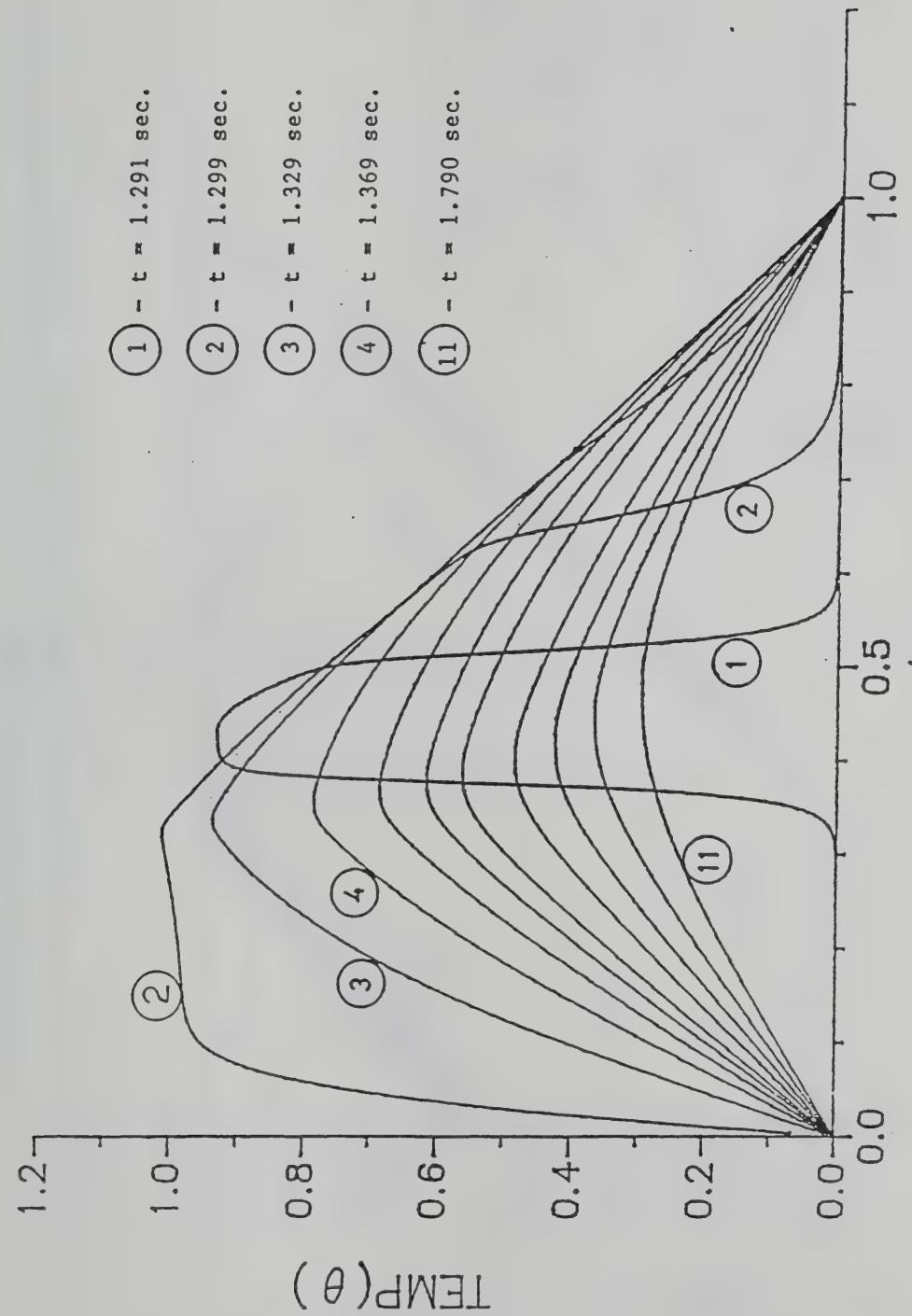

FIGURE 3-11 Temperature profiles during flashes caused by the fuel flow rate being below the lean flammability limit.

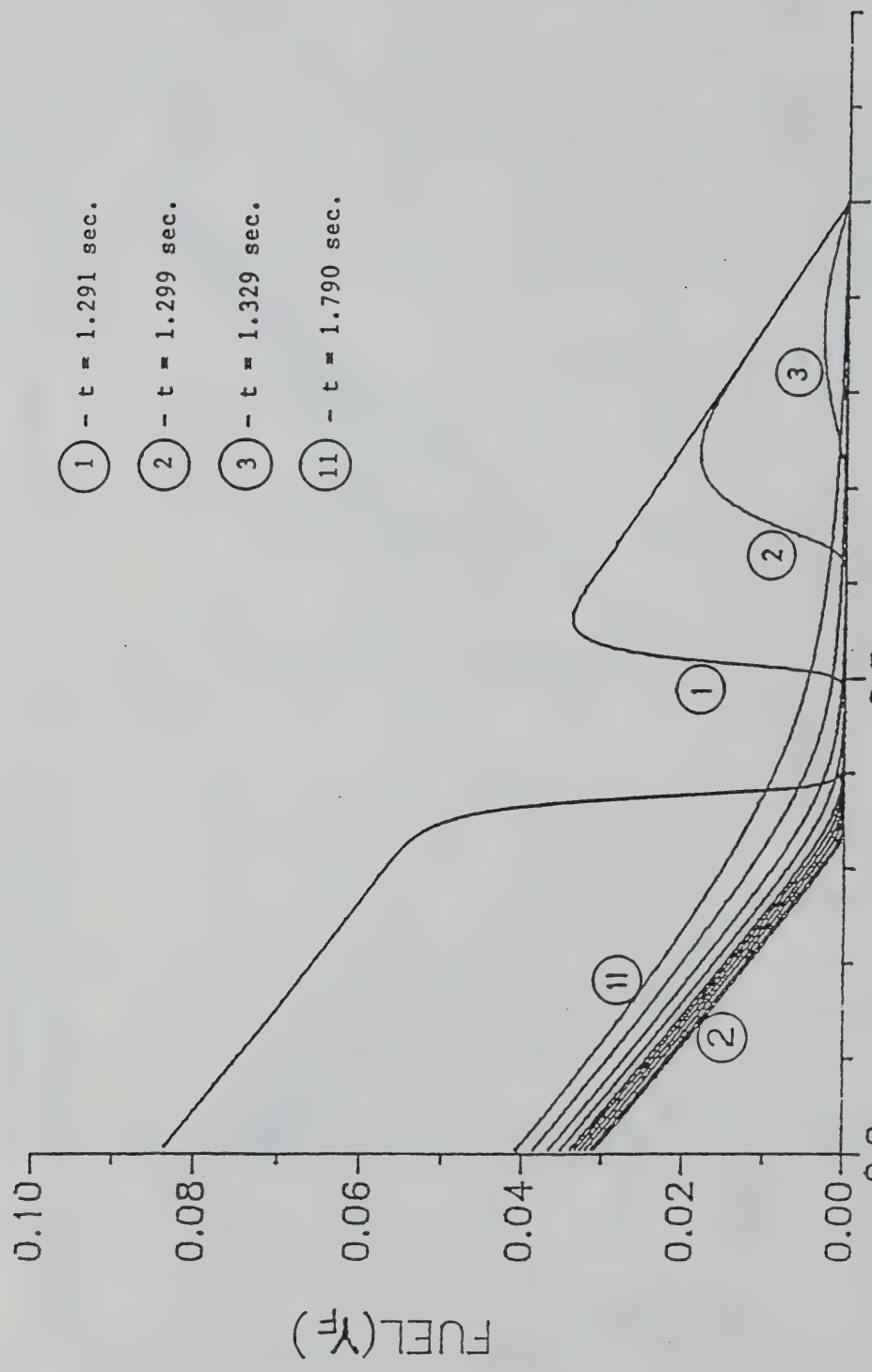

FIGURE 3-12 Fuel concentration profiles during flashes caused by the fuel flow rate being below the lean flammability limit.

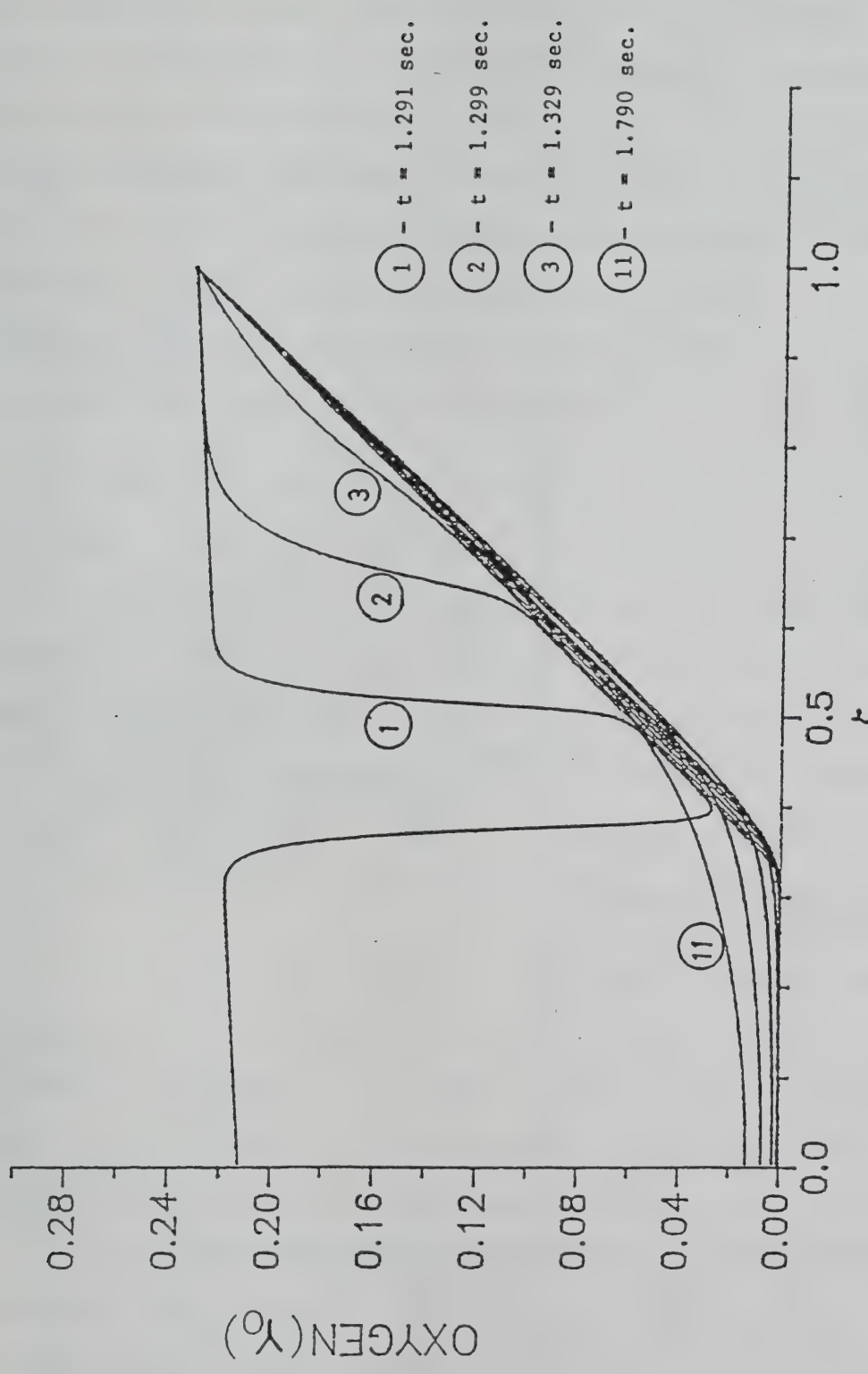

FIGURE 3-13 Oxygen concentration profiles during flashes caused by the fuel flow rate being below the lean flammability limit.

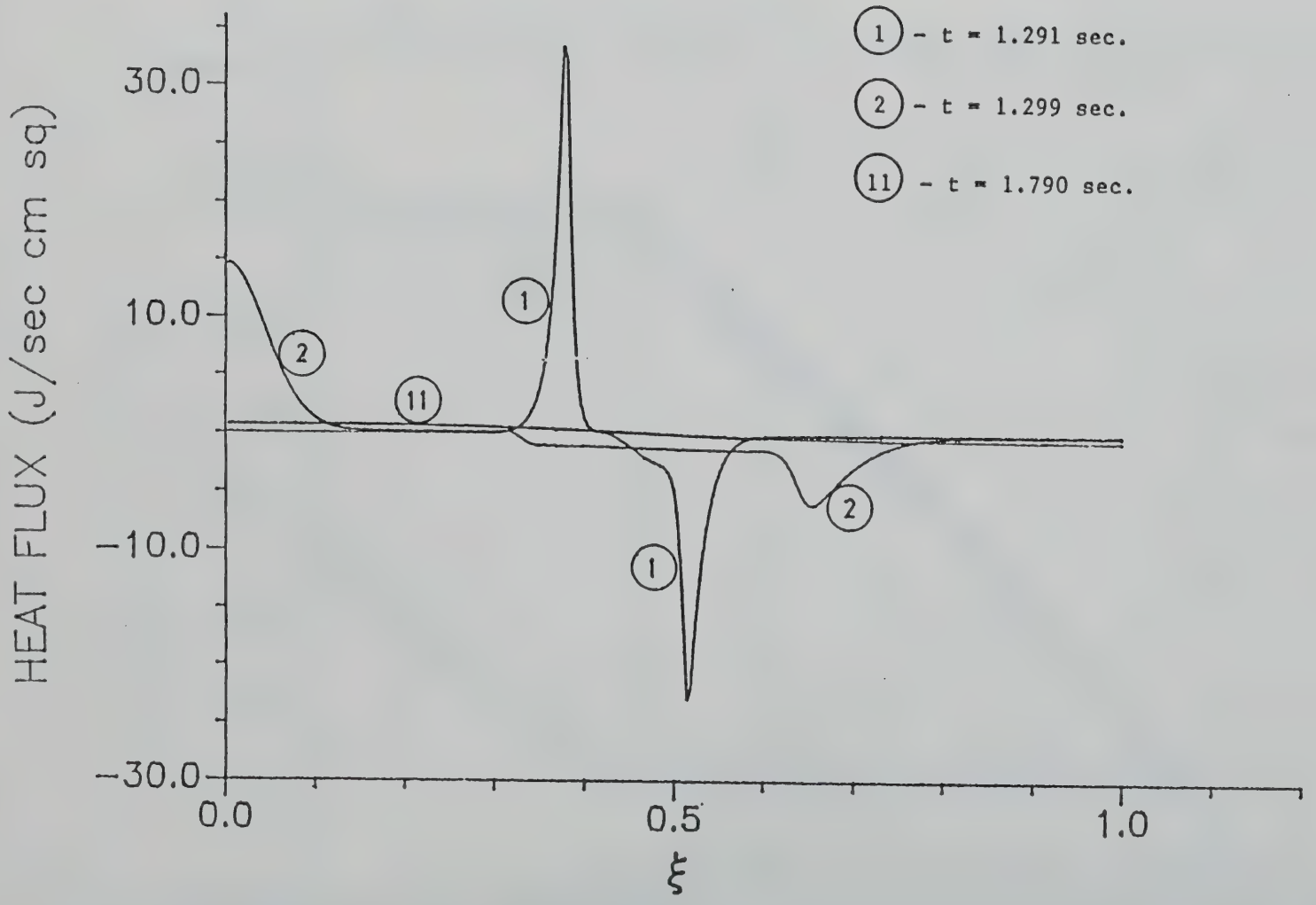

FIGURE 3-14 Heat flux profiles during flashes caused by the fuel flow rate being below the lean flammability limit.

determined by numerically solving the steady-state version of the governing Equations (3-9). For this calculation the temperature and species profiles are first calculated for conditions under which the steady diffusion flame is known to exist. These results are then used as an initial guess for subsequent calculations with slightly lower fuel flow rate. This procedure is continued until the temperature and species profiles are the same as those with no chemical reaction, i.e., no diffusion flame exists. This rather stringent condition for extinction produces a lower bound for the fuel flow rate.

By using the above procedure the minimum fuel flow rate at extinction is found to be 2.88×10^{-5} g/cm^2 sec. This fuel rate is only 8% lower than the minimum fuel flow rate for piloted ignition (3.128×10^{-5} g/cm^2 sec). This result seems to substantiate the hypothesis that conditions at extinction of a steady diffusion flame are similar to those at piloted ignition. This hypothesis was used by Atreya and Wichman (1987) to obtain an approximate analytical solution for the piloted ignition problem (solid-phase solution only).

All results presented thus far assume that the surface temperature of the solid is held constant at T_∞ (i.e., $T_s = T_\infty = 298$ K). As T_s is increased, heat losses to the surface are decreased; this is expected to reduce the minimum fuel flow rate required for the establishment of a steady diffusion flame and for sustained piloted ignition. Calculations with $T_s = 491$ K show that the minimum fuel flow rate at extinction of a diffusion flame reduces to 2.43×10^{-5} g/cm^2 sec and that for sustained piloted ignition reduces to 2.71×10^{-5} g/cm^2 sec. Once again, the fuel flow rate at extinction of a diffusion flame is about 10% lower

than for sustained piloted ignition.

3.4.4 Location of the Ignition Source

As noted in Section 3.4.2 the location of the ignition source is very important in determining whether or not sustained piloted ignition will occur. This fact was experimentally observed by Simms (1963), who states: "The pilot ignition time depends not only upon the intensity of radiation and the density of wood, but also upon the position and possibly upon the size of the pilot flame as well."

Table 3-3 summarizes the calculations for different locations of the ignition source at a given fuel flow rate. It can be seen that there exists a minimum location of the ignition source for sustained piloted ignition regardless of the fuel flow rate. For ignition source distances lower than the minimum location, the flame is quenched (see Section 3.4.2). As the fuel flow rate is decreased, the minimum location approaches the theoretical location of the steady-state diffusion flame. Thus, the optimum location of the pilot is the location of the steady-state diffusion flame, which can be estimated from Equation (3-13). Note that in the experiments, the fuel flow rate and surface temperature slowly increases as the solid is exposed to a given external radiation. Thus, to find the minimum time (or fuel flow rate) at which sustained ignition occurs, the pilot must be located at the eventual position of steady diffusion flame.

As the surface temperature increases both the minimum fuel flow rate for sustained piloted ignition and the minimum distance of the

ignition source decreases. A plot of the minimum distance of the ignition source versus fuel flow rate at surface temperatures of 298 K and 491 K is shown in Figure 3-15. For T_s = 491 K the minimum distance is generally much lower than for T_s = 298 K. However, at the higher fuel flow rates both curves approach the same vertical asymptote, x_i = 0.18cm. It is interesting to compare this value to the theoretically predicted quenching distance for premixed flame propagation. Thus (see Williams (1985). pp. 268-276, and Sec. 3.3.1), $d_q = a\delta = a(\lambda/C_p\rho_o v_o) \approx 40(0.092\ mm) = 0.37cm$, which is twice the value of x_i found here. This is reasonable, because the ignition source is periodically raised to the adiabatic flame temperature while quenching temperatures are usually much lower. In addition, the constant factor a may vary significantly with chioce of parameters (up to 50%,see Williams (1985); also,the derivation for d_q in Williams (1985) assumes a circular tube, not a plane wall. The horizontal asymptote in Figure 3-15 suggests a minimum fuel flow rate, below which ignition of the gas is impossible; this may be interpreted as a blowoff limit due to thermal quenching.

3.5. Significance

The simple one-dimesional numerical model presented here reveals the basic structure of the piloted ignition process. In the early stages of piloted ignition a premixed flame quickly propagates through the unburned mixture, consuming nearly all the fuel on the oxidizer side and all the oxygen on the fuel side, thus establishing conditions that are appropriate for the formation of a diffusion flame. This premixed flame

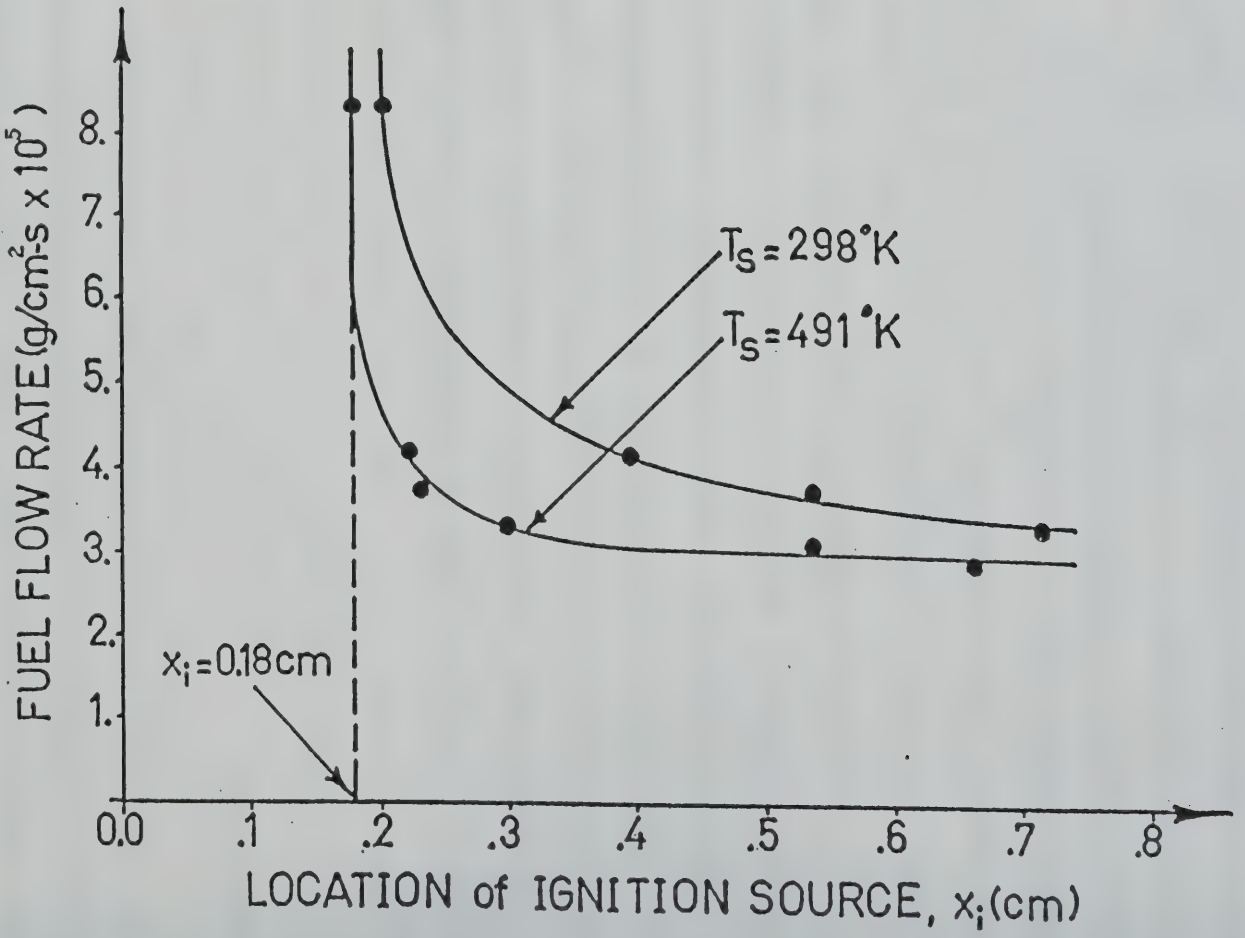

FIGURE 3-15 Minimum distance of the ignition source at surface temperature of 298 and 491 K for various fuel flow rate

may be quenched (resulting in a flash) if the fuel flow rate is too low or if the ignition source is too close to the surface (due to excessive heat losses). The analysis confirms that the sharp rises in surface temperature during experiemnts (flashes in Figure 3-2) occur because of burnout of the accumulated fuel during the premixed flame propagation stage. Note that during this stage the heat flux is an order of magnitude larger than in the steady diffusion flame stage.

Under appropriate conditions a diffusion flame is established, which slowly moves toward the steady-state diffusion flame location. It has been found that the minimum fuel flow rate in itself is not sufficient to predict the onset of sustained piloted ignition (as is often cited in the literature) and that heat losses to the solid surface play an important role. These calculations also confirm the hypothesis that the conditions at extinction of a steady diffusion flame are very nearly identical to those required for piloted ignition.

The optimum location of the pilot flame for actual experiments is found to be the eventual location of the steady diffusion flame. As expected, both the optimum location and the minimum fuel flow rate required for piloted ignition decrease with increase in surface temperature. In experiments where the surface temperature increases with the time of exposure to external radiation, an incorrect placement of the ignition source will eventually result in ignition, but at a higher surface temperature and after a larger ignition delay time. This may partially explain the wide range (300 to 540°C) of measured surface temperatures for piloted ignition of wood.

TABLE 3-1: Flame velocities calculated by using different grid spacing and time steps. (units: cm/sec)

Δr / $\Delta \xi$	2.7×10^{-7}	5.4×10^{-7}	2.7×10^{-6}	5.4×10^{-6}	2.7×10^{-5}
7.4×10^{-4}	38.2	38.3	37.3	36.2	7.4
1.5×10^{-3}	38.2	38.2	37.2	36.1	26.0
3.7×10^{-3}	37.5	37.3	36.5	35.4	25.7

NOTE: Coffee's (1983) calculations--39.8cm/sec.
Estimated from analytical formula of Williams (1985)--39.18 cm/sec.
Experimental measurements from Kanury (1975)--37.3 cm/sec.

TABLE 3-2: Steady state diffusion flame location (x_f)

Fuel flow rate (g/cm^2 sec)	x_f from transient calculations after 4 sec(cm)	x_f from steady-state calculation (cm)	x_f from Equation (3-13) analytical (cm)	Flame temperature	
				Numerical (K)	Analytical (K)
2.5×10^{-4}	1.385	1.384	1.396	2115	2137
8.34×10^{-5}	1.175	1.174	1.186	1840	1868
4.17×10^{-5}	0.866	0.866	0.878	1396	1458
3.75×10^{-5}	0.800	0.800	0.809	1292	1367
3.34×10^{-5}	0.724	0.684	0.723	1109	1253

TABLE 3-3: Location of the ignition source and the fuel concentration at this location. All calculations are for $T_s = T_\infty = 298$ K

Fuel flow rate (g/cm^2 sec)	Location of the ignition source (cm)	Y_f at the ignition source location and at the time of ignition	Time elapaed for piloted ignition (sec)	Observations
8.34×10^{-5}	1.186+	4.14×10^{-2}	1.089	ignition
	0.555	4.57×10^{-2}	0.279	ignition
	0.280*	4.34×10^{-2}	0.141	ignition
	0.204	4.31×10^{-2}	0.106	ignition
	0.170	4.18×10^{-2}	---	flame quenched
4.17×10^{-5}	0.874+	4.48×10^{-2}	1.299	ignition
	0.555*	4.49×10^{-2}	0.609	ignition
	0.397	4.48×10^{-2}	0.457	ignition
	0.390	4.51×10^{-2}	---	flame quenched
	0.280	4.51×10^{-2}	---	flame quenched
3.75×10^{-5}	0.800+	4.49×10^{-2}	1.289	ignition
	0.555*	4.49×10^{-2}	0.709	ignition
	0.540	4.50×10^{-2}	0.691	ignition
	0.445	4.51×10^{-2}	---	flame quenched
	0.280	4.51×10^{-2}	---	flame quenched
3.34×10^{-5}	0.724+	4.48×10^{-2}	1.410	ignition
	0.718+	4.48×10^{-2}	1.358	ignition
	0.710	4.48×10^{-2}	---	flame quenched
	0.555	4.50×10^{-2}	---	flame quenched
	0.280	4.49×10^{-2}	---	flame quenched
3.13×10^{-5}	No sustained diffusion flame regardless of the location of the ignition source.			

+ Location of the steady-state diffusion flame.
* Minimum location of the ignition source for sustained flaming (piloted ignition)

CHAPTER 4

EXTINCTION OF A STEADY STATE DIFFUSION FLAME

In the later stages of piloted ignition, the pre-mixed flames vanish, leaving behind a diffusion flame. This diffusion flame then moves slowly toward its steady-state location. As the flame reaches the steady-state condition, i.e., when all derivatives with respect to time disappear,the governing equations (3-9) become:

Energy:

$$M\frac{d\theta}{d\xi} = \frac{d^2\theta}{d\xi^2} + QR, \qquad (4\text{-}1)$$

Fuel:

$$M\frac{dY_f}{d\xi} = \frac{d^2Y_f}{d\xi^2} - R, \qquad (4\text{-}2)$$

Oxygen:

$$M\frac{dY_o}{d\xi} = \frac{d^2Y_o}{d\xi^2} - \nu R. \qquad (4\text{-}3)$$

In this chapter, the governing equations for the steady-state diffusion

flame have been solved numerically and analytically.

The structure of one-dimensional flames was successfully analyzed by Linan (1974) by using large activation energy asymptotics (AEA) for the model problem of a counterflow diffusion flame. The boundary conditions for the steady state diffusion flame in this thesis are different from Linan's model, whereas the governing equations are very similar.

In section 4-1, the equations are solved by using the finite difference numerical scheme, while in section 4-2, the governing equations are solved using AEA.

4.1 Numerical Solution for the Steady-State Diffusion Flame

The steady-state governing equations of the diffusion flame can be solved numerically. A finite difference method with iteration of the non-linear term was used. The finite difference representations are as follows:

$$d\theta/d\xi=(\theta_{i+1}-\theta_i)/\Delta\xi,$$
$$d^2\theta/d\xi^2=(\theta_{i+1}-2\theta_i+\theta_{i-1})/\Delta\xi^2.$$

Similar definition are applied to the fuel and oxygen concentrations.

The finite difference equations are non-linear and conjugated. An

iteration method has been used to solve these equations. This procedure is described below:

(i) Assume that there exists a diffusion flame, and that the temperature and species profiles are smooth near the reaction zone.

(ii) Use the initial conditions in (i) to calculate the non-linear reaction rate term R, and then solve the temperature equations using the Thomas algorithm.

(iii) Assume that Y_f is the only unknown. Then the equations for the fuel concentrations are linear; again, by using the Thomas algorithm, the equations are easily solved.

(iv) Now assume that Y_o is the only unknown, and solve the oxygen equations.

(v) Compare the solutions to the initial conditions, if the maximum error larger than a prescribed value (say, 10^{-4}), then re-define the new initial conditions as:
(New initial conditions) = 0.7*(old initial condition) + 0.3*(the solutions calculated in steps (ii),(iii) and (iv)).

(vi) Use the new initial conditions to calculate the non-linear term, then solve the temperature equations again and repeat the procedure.

By using this numerical code, the minimum fuel flow rate for diffusion flame is also calculated according to the following algorithm:

(i) First, assume that the fuel flow rate is high, and calculate the temperature and species profiles by using the steady-state numerical code.

(ii) Using the solution in (i) as a new initial condition, then reduce the fuel flow rate slowly, and recalculate the temperature and species profiles.

(iii) Continue step (ii) until there is no steady-state diffusion flame.(ie., the temperature and species profiles are the same as without chemical reaction).

4.2 The Extinction Damkohler Number for Diffusion Flame.

The (AEA) method used here has been successfully applied to other diffusion flame problems as well. C. K. Law (1975) solved the ignition and extinction of droplet burning by following a procedure similar to Linan's (1974). Puri and Seshadri (1986) estimated the activation energy and pre-exponential factor for counterflow diffusion flames by using the extinction Damkohler number of a diffusion flame. The physical configuration for piloted ignition is different from these cases. The objective here is to calculate the minimum fuel flow rate for sustaining the one-dimensional flame sheet by using (AEA) (similar to Linan (1974)).

It is well known that the ignition and extinction Damkohler numbers for a diffusion flame can be described by an S-shaped curve [Williams (1985)]. In such a curve, for Damkohler numbers smaller than

the extinction Damkohler number, having a diffusion flame is impossible (see Figure 4-2). Likewise in the numerical simulation of piloted ignition, when the fuel flow rate is too small, no sustained piloted ignition is possible. Thus, it seems reasonable to assume that sustained piloted ignition can occur only if the Damkohler number for the corresponding boundary layer is at least as large as the extinction Damkohler number, which is determined in the following analysis.

The species and energy equations for the steady state diffusion flame are rewritten as follows:

$$\left(\rho v\frac{d}{dx} - \frac{d}{dx}\begin{bmatrix}\lambda/C_p \\ \rho D \\ \rho D\end{bmatrix}\frac{d}{dx}\right)\begin{bmatrix}T \\ Y_f \\ Y_o\end{bmatrix} = \begin{bmatrix}q/C_p \\ -1 \\ -1/f\end{bmatrix} A\rho^2 Y_f Y_o EXP[-E/RT] \qquad (4\text{-}4)$$

The boundary conditions are:

At x=0:

$$-\rho D\frac{dY_f}{dx} = m(Y_{fs} - Y_f),$$

$$\rho D\frac{dY_o}{dx} = mY_o \quad \text{(for no diffusion flame)},$$

$$Y_o = 0 \quad \text{(for a diffusion flame)},$$

$$T_L = T_L(t),$$

where T_L is the temperature of the lower surface.

At x=h:

$$Y_f = 0,$$

$$Y_o = Y_{o\infty},$$

$$T = T_u = T_\infty.$$

where T_u is the temperature for upper surface.

These governing equations are non-dimensionalized with the following quantities; $L = \frac{\lambda}{mC_p}$ (length), $v = \frac{m}{\rho}$ (velocity), $T_* = \frac{qY_{f,o}}{C_p}$ (temperature), where $Y_{f,o}$ is dependent on the fuel flow rate.

Assuming $\rho v = m =$ constant and $Le = \frac{\lambda}{C_p \rho D} = 1$ $(\frac{\lambda}{C_p} = \rho D)$,

and also defining $y_o = Y_o/\nu Y_{f,o}$, $y_f = Y_f/Y_{f,o}$, $\bar{x} = x/L = x\frac{mC_p}{\lambda}$,

and $a = \frac{\rho\lambda}{C_p m^2}$ (sec), $\bar{D} = \nu\rho A Y_{f,o} a$ = convection time/reaction time,

$\bar{T} = T/T_*$, and $T_a = \frac{E}{RT_*}$ gives

$$\left(\frac{d}{d\bar{x}} - \frac{d^2}{d\bar{x}^2}\right)\begin{bmatrix} \bar{T} \\ y_f \\ y_0 \end{bmatrix} = \begin{bmatrix} 1 \\ -1 \\ -1 \end{bmatrix} \bar{D} y_f y_o \mathrm{EXP}[-T_a/\bar{T}]. \qquad (4\text{-}5)$$

The boundary conditions are:

At $\bar{x} = 0$: $y_o = 0$ (for a diffusion flame),

$y_o = y_{o,o}$ (for no diffusion flame),

$y_f = 1$,

$\bar{T} = \bar{T}_L = \frac{T_L}{T_*}$,

At $\bar{x} = \ell = hmC_p/\lambda$: $y_f = 0$,

$$y_o = \bar{\alpha} = Y_{o\infty}/\nu Y_{f,o},$$

$$\bar{T} = \bar{T}_u = \frac{T_u}{T_*},$$

(where $y_{o,o} = Y_{o,o}/\nu Y_{f,o}$).

Here, $Y_{o,o}$ is dependent on the fuel flow rate with no diffusion flame. To eliminate the convection term (in order to eliminate the convection term, λ must be a constant), define $\zeta = 1 - \frac{e^{\bar{x}}}{e^{\ell}}$. It is obvious that at $\bar{x} = 0$, $\zeta = \zeta_o = 1 - e^{-\ell}$, and at $\bar{x} = \ell$, $\zeta = 0$. Thus, we have

$$\frac{d^2}{dz^2}\begin{bmatrix} \bar{T} \\ y_o \\ y_f \end{bmatrix} = \begin{bmatrix} -1 \\ 1 \\ 1 \end{bmatrix} \frac{\bar{D} y_f y_o \mathrm{EXP}[-T_a/\bar{T}]}{(1/\zeta_o - (1-z))^2}, \qquad (4\text{-}6)$$

where $z = (\zeta_o - \zeta)/\zeta_o$. The boundary conditions are now

At $\bar{x}=0$, $(z=0)$: $y_o=0$ (for a diffusion flame),

$y_o=y_{o,o}$ (for no diffusion flame (dependent on m)),

$y_f=1$, ($Y_{f,o}$ to be determined by m),

$T=T_L$.

Since $\bar{T}_L \geq \bar{T}_u$, let $\bar{\beta} = \bar{T}_L - \bar{T}_u$. Then, using a Schvab-Zeldovich formulation with

$$\left.\begin{aligned} \bar{\beta}_1 &= \bar{T} + y_o, \\ \bar{\beta}_2 &= \bar{T} + y_f, \end{aligned}\right] \qquad (4\text{-}7)$$

gives $d^2\bar{\beta}_i/dz^2 = 0$, $i = 1, 2$. The solutions for $\bar{\beta}_1$ and $\bar{\beta}_2$ are

$$\left.\begin{aligned} \bar{\beta}_1 = \bar{T}+y_o = C_{11}+C_{21}z = \bar{\alpha}z+\bar{T}_f \quad &\text{for a diffusion flame} \\ = \bar{\alpha}z+\bar{T}_f+y_{o,o}(1-z) \quad &\text{for no diffusion flame} \\ \bar{\beta}_2 = \bar{T} + y_f = C_{12} + C_{22}z = \bar{T}_f + 1- z. & \end{aligned}\right\} \quad (4\text{-}8)$$

The frozen flow temperature $\bar{T}_f$ (defined as the temperature when the chemical reaction vanishes) is given by

$$\bar{T}_f = \bar{T}_u + (\bar{T}_L - \bar{T}_u)(1 - z) = \bar{T}_u + \bar{\beta}(1 - z). \quad (4\text{-}9)$$

Therefore,

$$\left.\begin{aligned} y_o = \bar{\alpha}z + \bar{T}_f - \bar{T} \quad &\text{for a diffusion flame} \\ = \bar{\alpha}z + \bar{T}_f - \bar{T} + y_{o,o}(1 - z) \quad &\text{for no diffusion flame} \end{aligned}\right\} \quad (4\text{-}10)$$

and

$$y_f = (1 - z) + \bar{T}_f - \bar{T}. \quad (4\text{-}11)$$

Three local flow regimes exist in the limit $T_a \to \infty$ (infinite activation energy)

(a) Frozen flow:

$$\frac{d^2\bar{T}}{dz^2} = 0 \qquad \text{(no reaction)},$$

(b) Equilibrium flow with $y_o = 0$:

$$\bar{T} = \bar{T}_f + \bar{\alpha}z,$$

(c) Equilibrium flow with $y_f = 0$:

$$\bar{T} = \bar{T}_f + (1 - z).$$

For all regimes

(a) Nearly frozen (Ignition) regime:

Chemical reaction almost equal to zero.

$$\left.\begin{aligned} \bar{T} &= \bar{T}_f = \bar{T}_u + \bar{\beta}(1 - z) \\ y_{of} &= \bar{\alpha}z + y_{o,o}(1 - z) \\ &= (\bar{\alpha} - y_{o,o})z + y_{o,o} \\ y_{ff} &= 1-z \end{aligned}\right\} \quad (4\text{-}12)$$

(b) Partial Burning:

Two frozen flow regimes separated by a thin reaction zone. (see Figure 4-1).

(c) Pre-mixed Flame:

Frozen flow and equilibrium regime separated by the reaction zone.

(d) Diffusion Flame:

Two equilibrium regimes separated by a thin reaction zone. (see Figure 4-2).

4.2.1 Analysis:

Near Equilibrium, Diffusion Flame Regime:

Let z_e be the location of the diffusion flame.

Frozen flow

.....Reaction zone

Frozen flow

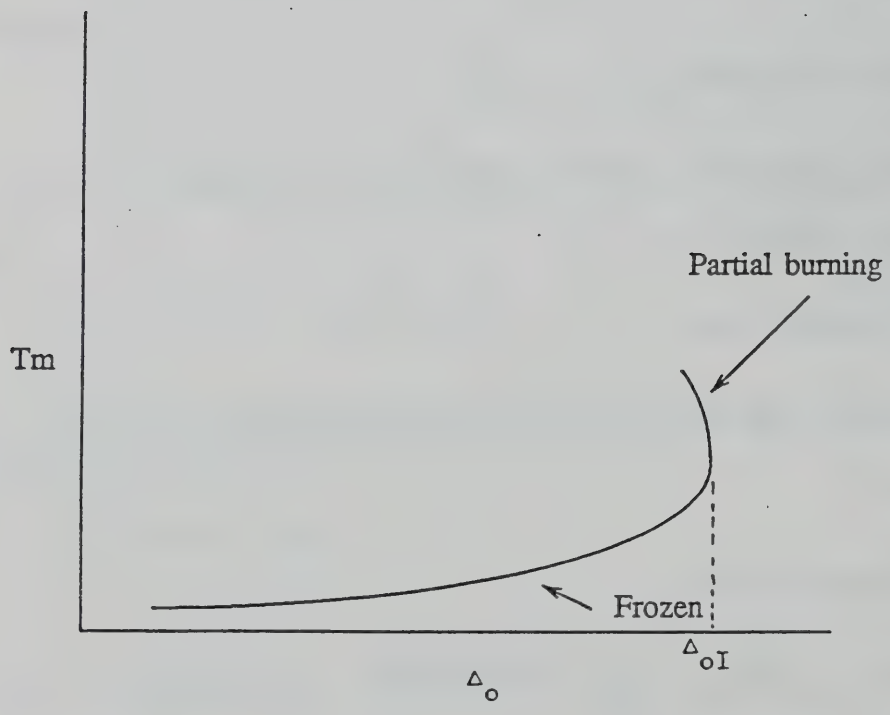

FIGURE 4-1 Partial burning.

Equilibrium

..... Reaction zone

Equilibrium

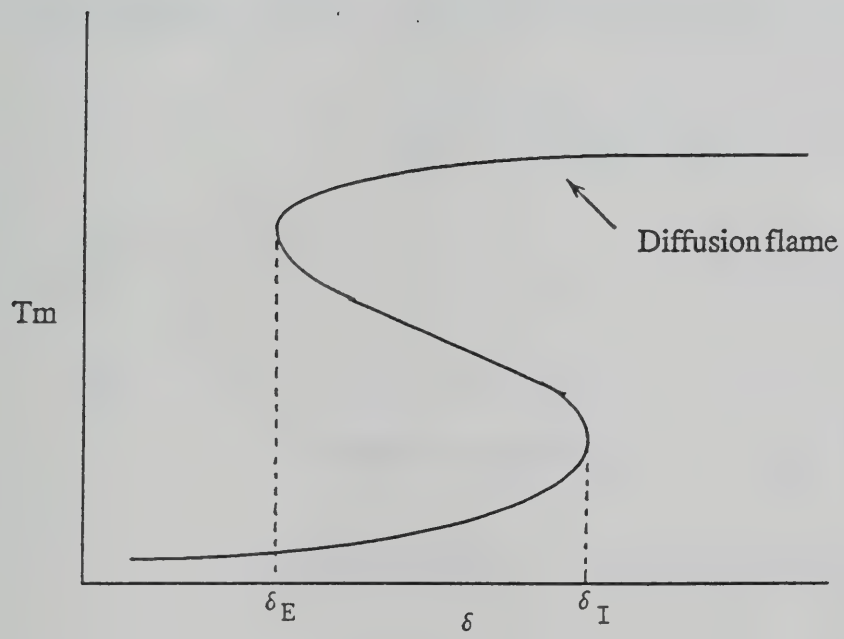

FIGURE 4-2 Diffusion flame.

For $z < z_e$, we have $y_o = 0$, $\bar{T} = \bar{T}_L + (\bar{\alpha} - \bar{\beta})z$, wheras for $z > z_e$, we have

$y_f = 0$, $\bar{T} = \bar{T}_L + 1 - (1 + \bar{\beta})z$. At $z = z_e$, $y_f = y_o = 0$ and

$\bar{T}_L + (\bar{\alpha} - \bar{\beta})z = \bar{T}_L + 1 - (1 + \bar{\beta})z\big|_{z = z_e}$. Therefore,

$z_e = \dfrac{1}{1 + \bar{\alpha}}$, giving $\bar{T}_e = \bar{T}_L + \dfrac{\bar{\alpha} - \bar{\beta}}{1 + \bar{\alpha}}$. For $z - z_e \sim 0(\epsilon)$,

(the reaction zone) we put $\bar{T} = \bar{T}_e - \epsilon k_o \bar{\xi} - \epsilon k_1 \beta_1 - \epsilon^2 k_2 \beta_2 + \ldots$

and $\bar{\xi} = \dfrac{z - z_e}{\epsilon} B$, where $\epsilon = \dfrac{\bar{T}_e^{\,2}}{T_a} \ll 1$, We first match to the

right of z_e, with the same slope for $z > z_e$. Let

$$\frac{1}{k_1}\left[\frac{1 + \bar{\beta}}{B} - k_o\right] = 1;$$

$$\therefore \quad \frac{d\beta_1}{d\bar{\xi}}\bigg|_{\bar{\xi} \to \infty} = 1 \text{ is a boundary condition.}$$

Now matching the slope to the left of z_e, we let

$$\frac{1}{k_1}\left[\frac{\bar{\alpha} - \bar{\beta}}{B} - k_o\right] = 1;$$

$$\therefore \quad \frac{d\beta_1}{d\bar{\xi}}\bigg|_{\bar{\xi} \to -\infty} = -1 \text{ is the other boundary condition.}$$

Again matching the slopes to the right and to the left of z_e, from Equation (4-6) we obtain:

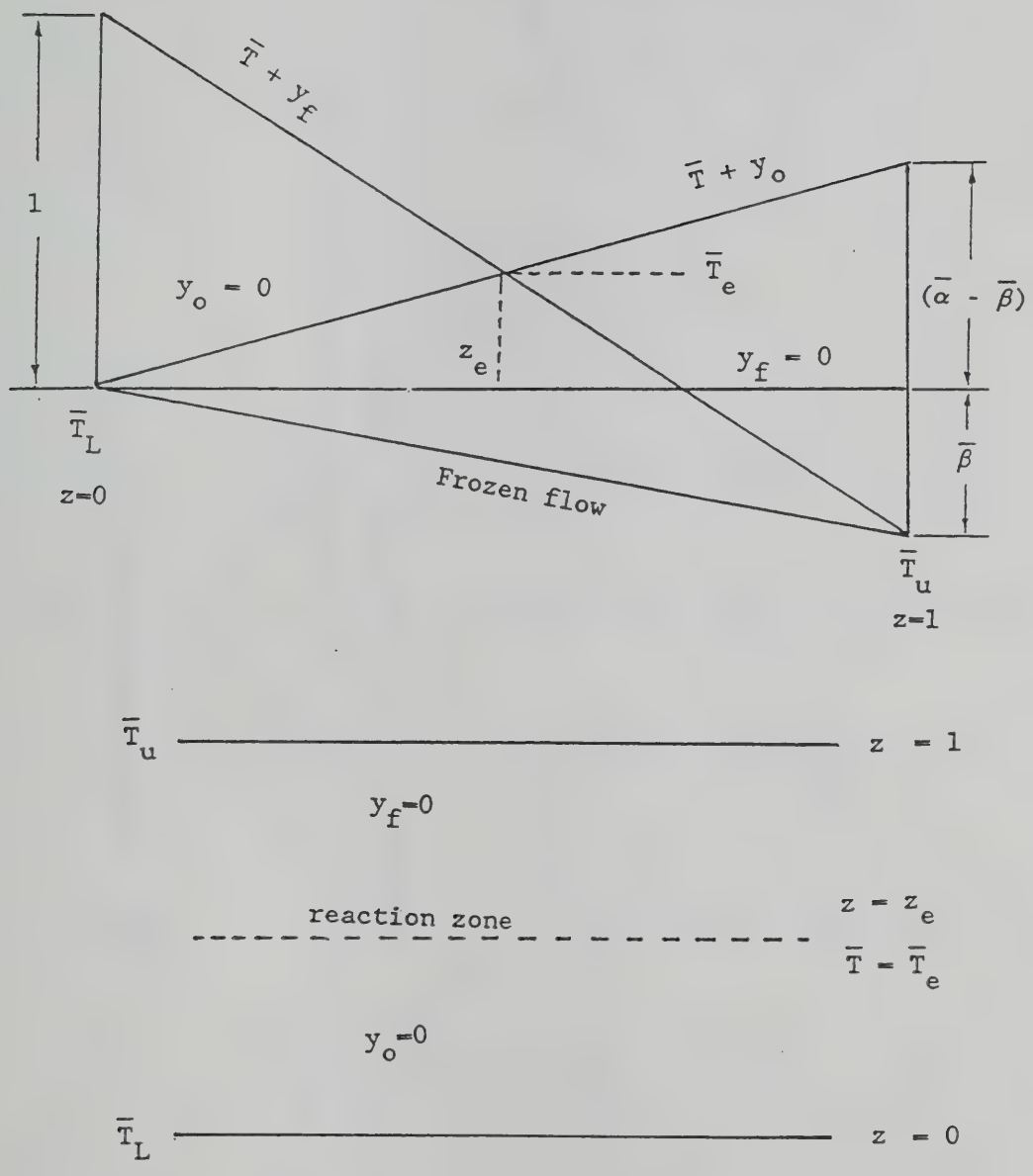

FIGURE 4-3 Near equilibrium, diffusion flame.

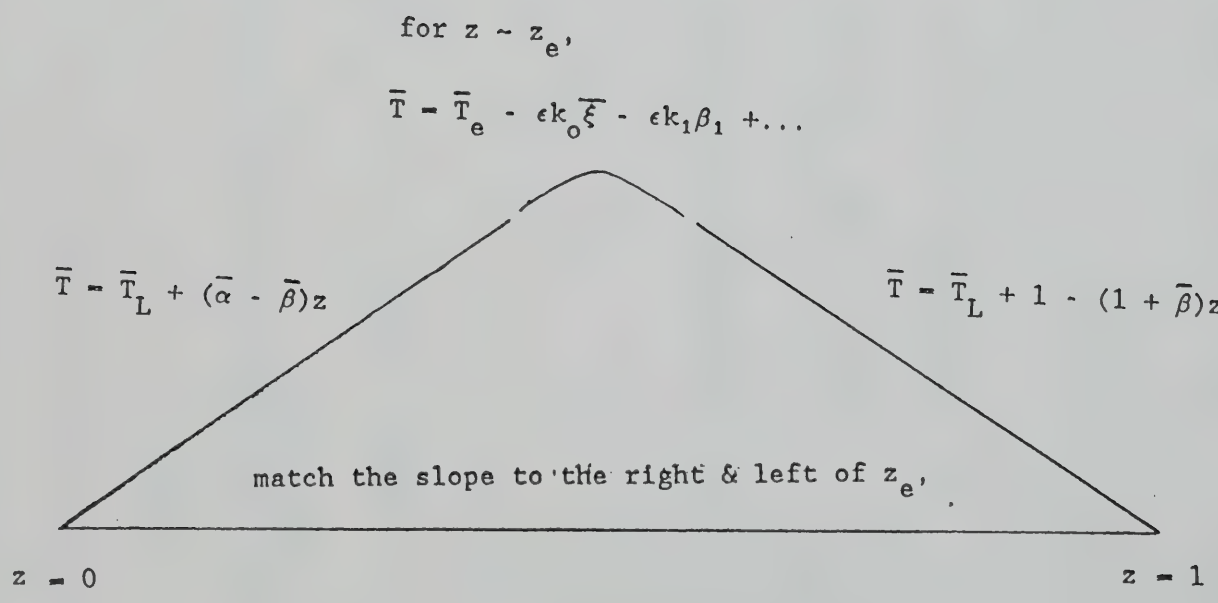

FIGURE 4-4 Match with the same slope.

$$\frac{d^2\beta_1}{d\bar{\xi}^2} = \frac{\bar{D}\zeta_o^{\,2}\epsilon^3 4k_1^{\,3}\exp[-T_a/\bar{T}_e]}{[1-\zeta_o(\bar{\alpha}/(1+\bar{\alpha}))]^2(1+\bar{\alpha})^2}(\beta_1-\bar{\xi})(\beta_1+\bar{\xi})\exp[-(k_o\bar{\xi}+k_1\beta_1)].$$

Defining $k_1^{\,3} = \dfrac{1}{\delta}$ (reduced Damkohler number)

$$\delta = \delta_o + \epsilon\delta_1 + \ldots$$

and

$$\delta_o = \frac{4\bar{D}\zeta_o^{\,2}\epsilon^3 \mathrm{EXP}[-T_a/\bar{T}_e]}{[1-\zeta_o(\bar{\alpha}/(1+\bar{\alpha}))]^2(1+\bar{\alpha})^2} \qquad (4\text{-}13)$$

gives

$$\frac{d^2\beta_1}{d\bar{\xi}^2} = \delta_o\left(\frac{1}{\delta_o+\epsilon\delta_1}\right)(\beta_1-\bar{\xi})(\beta_1+\bar{\xi})\mathrm{EXP}[-(k_o\bar{\xi}+k_1\beta_1)]$$

$$= (\beta_1-\bar{\xi})(\beta_1+\bar{\xi})\mathrm{EXP}[-\delta_o^{\,-1/3}(k_o\delta_o^{\,1/3}\bar{\xi}+\beta_1)].$$

Therefore,

$$\frac{d^2\beta_1}{d\bar{\xi}^2} = (\beta_1-\bar{\xi})(\beta_1+\bar{\xi})\mathrm{EXP}[-\delta_o^{\,1/3}(\beta_1+r\bar{\xi})], \qquad (4\text{-}14)$$

where $r = k_o\delta_o^{\,1/3}$. The boundary conditions are:

$$\frac{d\beta_1}{d\bar{\xi}} = 1 \qquad \text{as } \bar{\xi} \to \infty,$$

$$\frac{d\beta_1}{d\bar{\xi}} = -1 \qquad \text{as } \bar{\xi} \to -\infty.$$

Linan's (1974) analysis shows that when δ_o is too small, there is no solution for the above differential equation; the extinction

Damkohler number δ_{oe} is approximately given as

$$\delta_{oe} = e[(1-r)-(1-r)^2+0.26(1-r)^3+0.055(1-r)^4]. \qquad (4\text{-}15)$$

In other words, when $\delta_o < \delta_{oe}$, there is no diffusion flame (or the flame is extinguished). If the activation energy and the pre-exponential factor are fixed (or a particular fuel is chosen for calculations), the reduced Damkohler number δ_o and the extinction Damkohler number δ_{oe} are then functions of the boundary conditions.

In the one-dimensional piloted ignition model which is of concern here, when the fuel flow rate too small, there is no sustained diffusion flame after the flash. This may occur because the reduced Damkohler number is too small. The calculations of the Damkohler number are presented below.

4.2.2 Calculation of the Extinction Damkohler Number.

The fuel used here is methane and the physical properties are the same as given by Coffee (1983). We put:

$\rho A = 3.56 \times 10^{9}$ (1/sec), $C_p = 0.323$ cal/g K, h = 1.5cm,

$\lambda = 6.2 \times 10^{-5}$ KJ/m K sec (900 K of air), $\rho\lambda = 5.61 \times 10^{-8}$ g cal/cm^4 sec K, $q_f = 11355$ cal/g of fuel, E = 29.1 K cal/mole, R = 0.001983 Kcal/mole K, E/R = 14673 K, and $\nu = 4$. For every M ($M = mC_p h/\lambda$) we have

$$Y_{f,o} = Y_{fs} - \frac{1}{e^M}(Y_{fs} + Y_{o\infty}/\nu), \quad \text{where } Y_{fs} = 1 \text{ for pure fuel, and}$$

$$\bar{\alpha} = \frac{Y_{o\infty}}{\nu Y_{f,o}}, \quad T_* = \frac{q_f Y_{f,o}}{C_p} = 35155\ Y_{f,o}\ \ (K), \quad T_a = \frac{E}{RT_*}, \quad \bar{T}_L = T_L/T_*,$$

$$\bar{T}_u = T_u/T_* \quad (T_u = 298\ K), \quad \bar{\beta} = \bar{T}_L - \bar{T}_u, \quad r = 1 - 2\,\frac{\bar{\alpha} - \bar{\beta}}{1 + \bar{\alpha}},$$

$$\bar{T}_e = \bar{T}_L + \frac{\bar{\alpha} - \bar{\beta}}{1 + \bar{\alpha}}, \quad a = \frac{\rho\lambda}{C_p m^2}, \quad \bar{D} = \nu\rho A Y_{f,o} a, \quad \epsilon = \frac{\bar{T}_e^{\,2}}{T_a}, \quad \ell = hmC_p/\lambda$$

$\zeta_o = 1 - e^{-\ell}$, Also δ_o and δ_{oe} are given by Equations (4-13) and (4-15) and we use $T_L = 298$ K and $Y_{fs} = 1$.

For a given fuel flow rate m, the reduced Damkohler number and the extinction Damkohler are then easily obtained. The extinction Damkohler number is calculated by employing the following procedure.

(i) Assume a higher fuel flow rate,

(ii) Calculate the corresponding values of δ_o and δ_{oe},

(iii) Check if $\delta_o < \delta_{oe}$; if not, reduce the fuel flow rate and repeat step (ii).

This procedure shows that when the fuel flow rate is smaller than 3.127×10^{-5} g/cm^2 sec, δ_o is smaller than δ_{oe}, (δ_o=0.827, δ_{oe}=0.86).

4.3. Comparison of Results

Here the results of minimum fuel flow rate for piloted ignition are compared with the steady state numerical model and the analytical

Damkohler number analysis. The following results are obtained.

1. When the fuel flow rate is smaller than 3.13×10^{-5} g/cm^2 sec, there is no sustained diffusion flame after the flashes. This result is obtained by numerically solving the piloted ignition equation (see chapter 3, see final entry in Table 3-3).
2. When the fuel flow rate smaller than 2.88×10^{-5} g/cm^2 sec, a steady state diffusion flame is not obtained. This calculation was performed for Equation (3-9) without the $\partial/\partial t$ term. The boundary conditions are given by Equations (3-11) and (3-12).
3. Both δ_o and δ_{oe} are functions of the fuel flow rate; for higher fuel flow rates , δ_o is greater than the δ_{oe}. When the fuel flow rate is smaller than 3.127×10^{-4} g/cm^2 sec, the reduced Damkohler number δ_o becomes smaller than the extinction Damkohler δ_{oe}, indicating extinction.

From the above analysis, it seems reasonable to say that for sustained pilot ignition, the Damkohler number for the corresponding boundary condition should be larger than the extinction Damkohler number, which gives a conservative estimate for the minimum fuel flow rate.

Chapter 5

THEORETICAL MODEL FOR PILOTED IGNITION OF WOOD.

5.1 Background

Ignition refers to the appearance of a flame in the volatile gas stream evolved from a solid exposed to external heating (usually radiative). Depending upon whether the ignition occurs with or without the aid of an external ignition source, it is accordingly classified as spontaneous (auto-) or piloted (forced).

Several ignition criteria have been proposed, such as critical surface temperature at ignition [Simms (1963)], critical mass flux [Bamford et.al. (1946)], critical char depth [Sauer (1956)], critical mean solid temperature [Martin(1965)], etc. Of these, critical fuel mass flux at ignition seems to be physically the most correct since it can be related to flammability limits. However, surface temperature has proved to be the most useful ignition criterion since it can be conveniently related to fire spread [Atreya (1983)].

The ignition of cellulosic materials is a complex process involving both the gas and solid phases. When a cellulosic material (such as wood) is exposed to an intense radiant heat flux, the solid

chemically decomposes to inject fuel gases into the surrounding air and produce a flammable mixture which can be ignited by an ignition source. Therefore, this process involves flames of both pre-mixed and diffusion type.

Kashiwagi (1974) suggests a theoretical model for auto-ignition based on the assumption that ignition occurs when the reaction rate in the boundary layer exceeds a value of about 10^{-5} g/cm^3 sec. Gandhi (1986) suggests another model where it is postulated that the auto-ignition point is the gradient reversal in the gas temperature profile at the solid-gas interface. Amos and Fernandez-Pello (1988) suggest a theoretical model for auto-ignition by considering the absorption of radiation by the fuel vapor as a potential source of ignition. Their model also considers the more practical case of the existence of convective flow over the combusting surface. Their analysis of this evolution process provides information about how a diffusion flame is generated from a combustion reaction which has initially premixed character. A similarly detailed analysis of piloted ignition has not appeared in the literature. Recently, Tzeng et.al.(1990) have conducted an investigation of piloted ignition. This predominantly gas-phase investigation did not consider the transient solid-phase decomposition. However, it showed the development of a diffusion flame in an initially premixed gas. This analysis is presented in chapter 3.

The decomposition products of wood are very complex. Schwenker and Beck(1963) have detected 37 volatile compounds, Goos(1952) has identified 213 compounds as products of wood decomposition. The

composition of the pyrolysis products is also a function of the extent of decomposition, the initial density of wood, the temperature at which decomposition occurs, the fraction of char formed, the oxygen concentration in the air, the ambient pressure and the sample moisture content. Abu-Zaid (1988) and Nurbakhsh (1989) investigated the composition of pyrolysis products of wood. They found that the combustible portion is only about 25% (mass fraction) of the total pyrolyzed gas.

5.2 Mathematical Model for Piloted Ignition of Cellulosic Solids

Consider a thick slab of wood placed in an air stream under ambient conditions (as shown in Figure 5-1). The bottom face is considered impervious to both heat and mass transfer and the front face is exposed to a constant radiant heat flux. A part of this incident radiant energy is absorbed at the surface. As the solid surface temperature rises, it radiates a fraction of the energy back to the surroundings. Another fraction is convected to the adjacent air. The rest of the energy is conducted into the solid. Upon further heating, the solid undergoes thermal decomposition. The products of decomposition escape from within the solid through the surface into the gas. These pyrolyzates mix with the heated surrounding air in the boundary layer. Conditions at a distance h above the slab are maintained constant by a flowing oxidizer stream. A plane ignition source is placed near the porous plate. This ignition source is periodically "turned on" to test for piloted ignition. Mathematically

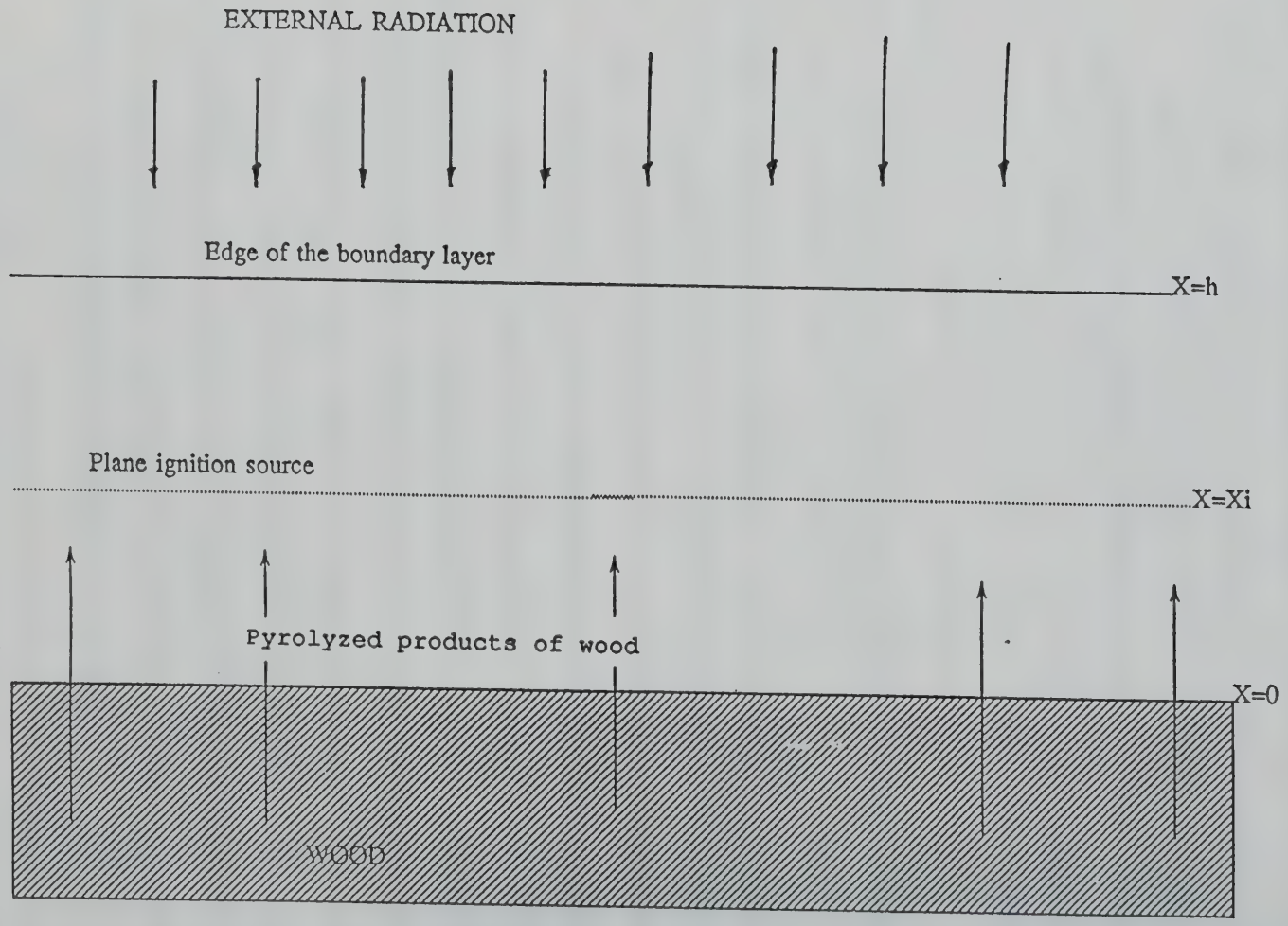

FIGURE 5-1 One-dimensional model of pilot ignition of solids.

this process is described by the following equations.

GOVERNING EQUATIONS:

Gas Phase Equations.

The chemical reaction is assumed to be a simple second-order, one-step irreversible Arrhenius reaction, Fuel + νO_2 → Products + q (heat)

The governing equations are

Energy equation:

$$\rho \frac{\partial T}{\partial t} + \rho v \frac{\partial T}{\partial x} = \frac{\partial}{\partial x} \left(\frac{\lambda}{C_p} \frac{\partial T}{\partial x} \right) + \frac{\omega_T}{C_p}, \qquad (5\text{-}1)$$

Conservation of species

Fuel:

$$\rho \frac{\partial Y_f}{\partial t} + \rho v \frac{\partial Y_f}{\partial x} = \frac{\partial}{\partial x} \left(\rho D_f \frac{\partial Y_f}{\partial x} \right) - \omega, \qquad (5\text{-}2)$$

Oxygen equation:

$$\rho \frac{\partial Y_o}{\partial t} + \rho v \frac{\partial Y_o}{\partial x} = \frac{\partial}{\partial x} \left(\rho D_o \frac{\partial Y_o}{\partial x} \right) - \omega_o, \qquad (5\text{-}3)$$

where:

$$\left.\begin{aligned} \omega &= A \rho^2 Y_f Y_o \, \mathrm{EXP}[-E/RT], \\ \omega_T &= q\, \omega, \\ \omega_o &= \nu \omega. \end{aligned}\right\} \qquad (5\text{-}4)$$

The initial and boundary conditions are:

$$\left.\begin{aligned} &\text{at } t = 0, \quad 0 < x < h: \\ &Y_f = 0, \; Y_o = Y_{o\infty}, \text{ and } T = T_\infty. \end{aligned}\right\} \qquad (5\text{-}5)$$

at t = 0, the radiation source is turned on, resulting in production of the fuel. Thus, the boundary conditions after t = 0 become:

At x = 0;

$$\left.\begin{aligned} \rho D_f \frac{\partial Y_f}{\partial x} &= \rho v (Y_f - Y_{fs}), \\ \rho D \frac{\partial Y_o}{\partial x} &= \rho v Y_o, \\ T &= T_s, \end{aligned}\right\} \quad (5\text{-}6)$$

where ρv, Y_{fs}, and T_s are determined by the heat and mass balance of the solid phase.

$$\left.\begin{aligned} &\text{At } x = h,\ t > 0, \\ &Y_f = 0,\ Y_o = Y_{o\infty},\ T = T_\infty. \end{aligned}\right\} \quad (5\text{-}7)$$

Solid Phase Equations:

Mass balance:

$$\frac{\partial M_w}{\partial x} = \frac{\partial \rho_w}{\partial t} \quad (5\text{-}8)$$

Energy balance:

$$\rho_w C_w \frac{\partial T_w}{\partial t} = \frac{\partial}{\partial x} \left(\lambda_w \frac{\partial T_w}{\partial x} \right) \quad (5\text{-}9)$$

Decomposition kinetics:

$$\frac{\partial \rho_w}{\partial t} = -A_w(\rho_w - \rho_{wf}) \, EXP(-E_w/R\, T_w) \tag{5-10}$$

The boundary conditions and initial conditions are:

$$\left.\begin{aligned} &T_w(x,0) = T_w(\infty,t) = T_\infty \\ &\rho_w(x,0) = \rho_{w\infty},\ M_w(\infty,t) = 0 \end{aligned}\right] \tag{5-11}$$

and the net heat flux into the solid is given by

$$-\lambda_w \frac{\partial T_w(0,t)}{\partial x} = \epsilon\left[F - \frac{\bar{h}}{\epsilon}(T_s - T_\infty) - \sigma(T_s^4 - T_\infty^4)\right] \tag{5-12}$$

The gas phase equations are simplified by introducing the Howarth transformation, $\xi = \frac{1}{\rho_o h_o}\int_0^x \rho \, dx$, $t' = t$. They are nondimensionalized by defining $\tau = \frac{\rho\lambda t}{C_p \rho_o^2 h_o^2}$, $M = \frac{\rho_o^2 v_o C_p h_o}{\rho\lambda}$, $\theta = \frac{T-T_\infty}{T_f - T_\infty}$, where T_f is the adiabatic flame temperature. Also, $\beta^o = E/RT_f$, $\alpha^o = 1-(T_\infty/T_f)$, $\beta = \beta^o * \alpha^o$, $Q = q/C_p(T_f - T_\infty)$, $D = AC_p\rho_o^2 h_o^2 EXP(-\beta^o)/\lambda$, and $R = DY_f Y_o EXP\left[-\frac{\beta(1-\theta)}{1-\alpha_o(1-\theta)}\right]$. Finally, after assuming a Lewis number of unity and $\rho^2 D$ = constant, the energy equation and species conservation become

$$L\begin{bmatrix} \theta \\ Y_f \\ Y_o^f \end{bmatrix} = \begin{bmatrix} \theta \\ -1 \\ -\nu \end{bmatrix} R \tag{5-13}$$

$$\text{where} \quad L(\cdot) = \frac{\partial(\cdot)}{\partial \tau} + \frac{M\partial(\cdot)}{\partial \xi} - \frac{\partial^2(\cdot)}{\partial \xi^2} \tag{5-14}$$

The boundary conditions are:

At $\xi = 0, \tau > 1,$

$$\left.\begin{aligned} &\theta = \theta_s, \\ &\partial Y_f/\partial \xi = M(Y_f - Y_{fs}), \\ &\partial Y_o/\partial \xi = M Y_o, \end{aligned}\right] \tag{5-15}$$

and at $\xi = 1, \tau > 1$

$$\left.\begin{aligned} &\theta = 0, \\ &Y_f = 0, \\ &Y_o = Y_{o\infty}, \end{aligned}\right] \tag{5-16}$$

where M is determined by the mass balance at the solid gas interface. The corresponding non-dimensional solid-phase equations are presented in the next section.

Gas-Phase Parameters for the Model

In Chapter 3, the properties of the gas phase were assumed to be the same as that of a methane-air mixture. The activation energy for the gas phase reaction was assumed to be 29.1 Kcal/mole (as determined by Coffee, 1983). While this activation energy yielded good qualitative results, the results did not compare well quantitatively with the ignition data for wood. Recently, Puri and Seshadri (1986) have studied

the extinction of a methane air diffusion flame. The activation energy calculated from the experimental data is around 45~47 Kcal/mole. Also, Westbrook and Dryer (1981) found that both higher (48 Kcal/mole) and lower values (30 Kcal/mole) of activation energies can predict the premixed flame velocity quite satisfactorily if the pre-exponential factor is adjusted. Now, since the flame velocity in a stoichiometric methane air mixture is 38 cm/sec, the pre-exponential factor is adjusted to $\rho A = 9.068 \times 10^{11}$ (sec^{-1}). The rest of the parameters ($\rho\lambda$, C_p, q, T_f, T_∞) are the same as before (Chapter 3). ($\rho\lambda = 5.61 \times 10^{-8}$ cal g/cm K sec, $C_p = 0.323$cal/gm K, q = 11355 cal/gm fuel, $T_f = 2230$ K, $T_\infty = 298$ K).

The effect of higher and lower activation energies on piloted ignition has been investigated. The result is shown in Table 5-1.

Table 5-1. Effect of the higher (48 Kcal/mole) and lower (30 Kcal/mole) activation energies.
(Assuming the stoichimetric flame velocity is 38 cm/sec)

Activation energy	Min. fuel flow rate for pilot ignition	Flame temperature at min. fuel flow rate
48	4.36×10^{-5}	1401 K
30	3.34×10^{-5}	1284 K

Extensive studies on extinction of opposed-flow diffusion flames by Ishizuka and Tsuji (1981) have shown that near extinction, the limit flame temperature is remarkably constant for most hydrocarbons and is about 1550 K. Thus, it seems that the higher activation energy for methane is closer to the experimental data for diffusion flames. Since piloted ignition essentially represents the minimum requirement for the existence of a diffusion flame, the higher activation energy is used for the rest of this study.

With these parameters, the above partial differential equations and the boundary conditions are solved by a implicit finite-difference method.

5.3 Analytical Solution for Pyrolysis of Wood

An analytical solution of the solid-phase temperature field, heat and mass transfer during piloted ignition of cellulosic solids was derived by Atreya (1983). This solution is used here and is outlined below.

Consider a semi-infinite solid initially at constant ambient temperature (T_∞). At $t > 0$, the solid is exposed to a constant heat flux, F. Surface oxidation and internal heat transfer between the pyrolysis gases and the solid are ignored. The thermal properties are assumed to be temperature-independent and the net heat required to thermally decompose a unit mass of wood is taken to be zero. Since the heat transfer through an inert solid is by conduction only, the energy balance is described by:

$$\rho_w c_w \frac{\partial \theta_w}{\partial t} = \lambda_w \frac{\partial^2 \theta_w}{\partial x^2}, \qquad \text{for } x > 0,\ t > 0,$$

where $\theta_w = T_w - T_\infty$, T_w is the temperature of wood. The solid is assumed to be at the temperature of its surroundings prior to the experiment. Therefore, the initial condition is $\theta = 0$ for $t \leq 0$, $x > 0$. The boundary condition is obtained from the energy balance at the solid surface and is given by

$$-\lambda_w \frac{\partial \theta_w}{\partial x}\bigg|_{x=0} = f_s(\theta_s, T_\infty, t)$$
$$= \epsilon[F - \bar{h}\theta_s - \sigma((\theta_s + T_\infty)^4 - T_\infty^4)],$$

where ϵ = the emissivity (or absorptivity) of the surface and $\bar{h}$ = heat transfer coefficient/ϵ, σ = Stefan - Boltzmann constant, F = the prescribed incident heat flux, $\theta_s = T_s - T_\infty$, where T_s is the surface temperature, f_s = heat flux going into the semi-infinite solid at the surface, and ρ_w, c_w, λ_w are respectively the density, heat capacity and thermal conductivity of the solid. Because of the highly non-linear nature of the problem an exact analytical solution cannot likely be found. An approximate analytical solution for the above problem has been obtained by Atreya (1983) by the use of integral methods. Without entering into the details [see Atreya (1983)], the time as a function of surface temperature is obtained as

$$t = K\left[\frac{\theta_s^2}{2f_s^{*2}} + \frac{r}{\beta^{3/2}}\ln\frac{(2s\theta_s+r-\sqrt{\beta})(r+\sqrt{\beta})}{(2s\theta_s+r+\sqrt{\beta})(r-\sqrt{\beta})} - \frac{\theta_s(r+2s\theta_s)}{\beta f_s^*}\right], \qquad (5\text{-}17)$$

where $K = \frac{2}{3}\frac{\rho_w c_w \lambda_w}{\epsilon^2}$, $r = -(\bar{h} + 4\sigma T_\infty^3)$, $s = -\frac{25}{3}\sigma T_\infty^2$, $\beta = (r^2 - 4Fs)$,

and $f_s^* = \frac{f_s}{\epsilon} = F + r\theta_s + s\theta_s^2$.

In the calculation of the surface temperature, a correction for the energy required to evaporate moisture was made. This quantity was estimated by using the constant weight-loss rate and latent heat of evaporation for water. The result was then substracted from the incident heat flux to obtained the corrected heat flux. This procedure is mathematically correct. The comparison between the experimental surface temperature and the calculated temperature as shown in Figure 5-2, however, is better than expected.

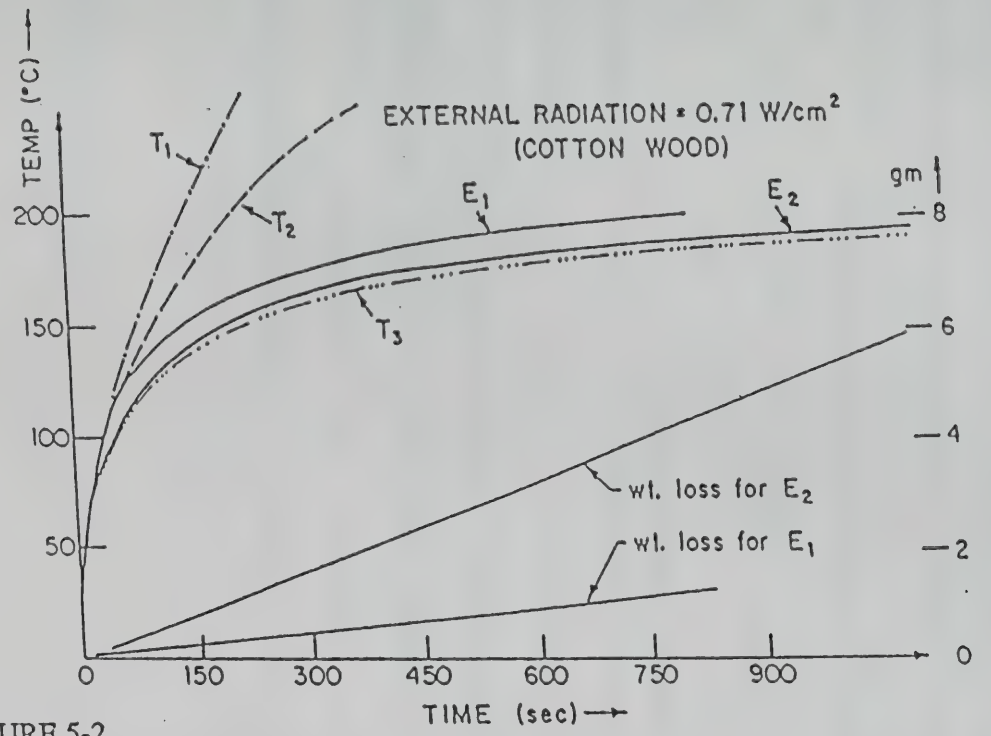

FIGURE 5-2

A comparison of measured and predicted surface temperature showing the effect of radiant emission. Weight loss shown is due to desorption of moisture. E_1: experiments on wood dried at 105°C for 12 hours; E_2: experiments on wood at 70 percent R. H. and 22°C; T_1, T_2 and T_3 are theoretical calculations for a semi-infinite solid based on pure conduction, conduction with convective losses, and conduction with convective and reradiative losses, respectively. Properties used were: $\rho = 470$ kg/m^3, $\epsilon = 0.85$, $c = 1.38$ J/gK, $\lambda = 0.126$ W/mK, and $h = 8.4$ W/m^{2}K. All temperatures shown are above ambient (22°C).

The decomposition of wood is assumed to occur according to a first-order global chemical reaction with a known and fixed char density ρ_f; the mass balance of the one-dimensional decomposition process is given by

$$\frac{\partial M_w}{\partial x} = \frac{\partial \rho_w}{\partial t} .$$

The decomposition kinetics are assumed to be described by

$$\frac{\partial \rho_w}{\partial t} = -A_w(\rho_w - \rho_{wf})EXP(-E_w/RT_w),$$

and the initial and boundary conditions are

$$\rho_w(x,0) = \rho_{w\infty},$$

$$M_w(\infty,t) = 0.$$

To nondimensionalize the equations, a length scale is defined as $L = \lambda_{d\infty}T_\infty/\epsilon F$, which is obtained as the ratio of thermal conductivity and incident heat flux. Also, a diffusion time is defined as $t_d = L^2/(\lambda_{w\infty}/\rho_\infty c)$. The other non-dimensional variables are defined as follows:

$$T^* = T_w/T_\infty,\ \rho^* = \rho_w/\rho_\infty,\ x^* = x_w/L,\ t^* = t/t_d,\ E^* = E_w/RT_\infty,$$

$$A^* = A_w t_d,$$

$$\delta_f^* = \rho_{wf}/\rho_\infty,\quad H^* = \frac{\bar{h}T_\infty}{F},\quad M^* = M_w t_d/\rho_\infty L,\ \Sigma = \sigma T_\infty^4/F,$$

$$\lambda_w^* = \lambda_w/\lambda_{w\infty},\ \theta^* = \theta_w/T_\infty.$$

Hence, the nondimensional mass balance and the decomposition kinetics equations are given by

$$\frac{\partial M^*}{\partial x^*} = \frac{\partial \rho^*}{\partial t^*}$$

and

$$\frac{\partial \rho^*}{\partial t^*} = -A^*(\rho^* - \delta^*)EXP(-E^*/T^*).$$

Upon integration,

$$M_s^* = A^*(1 - \delta^*)\int_0^\infty EXP[-E^*(\theta^* + 1)]dx^*,$$

where M_s^* is the mass flow rate at the solid surface. During the initial decomposition process, the density is almost constant, and ρ^* is nearly unity. Let

$$AA = -(H^* + 4\Sigma),\ BB = -(25/3)\Sigma$$

and $$\Phi_s = 1 + AA\theta_s^* + BB\theta_s^{*2}.$$

For small x^*, $\theta^* \approx \theta_s^* - x^*\Phi_s$; therefore, the upper limit of integration is replaced by $x_{max}^* = \theta_s^*/\Phi_s$. By substituting this into the above equation, integrating, and keeping only the lowest-order terms of the asymptotic expansion for large E^*, one obtains [Atreya and Wichman (1989)],

$$M_s^* = \frac{A^*(1-\delta^*)}{\Phi_s E^*} T_s^{*2} EXP(-E^*/T_s^*)\left[1 - \frac{EXP[-E^*(1-1/T_s^*)]}{T_s^{*2}}\right]. \quad (5\text{-}18)$$

Solid Phase Parameters

The solid phase parameters have been determined by the parameter estimation technique from the experimental data for piloted ignition of Abu-Zaid (1988). The calculations are presented in Appendix D. The physical parameters used for wood are listed below:

$\bar{h}$ (convective heat transfer coefficient) = 2.0 W/m^2K,

A_w (pre-exponential factor for wood) = 6.0×10^7 /sec,

λ_w (thermal conductivity of wood) = 0.167 W/m K ($=\lambda_a$),

ρ_w (density of the wood) = 0.54 g/cm^3 ($=\rho_{wd}$),

E_w (activation energy for wood) = 31 Kcal/mole,

C_w (heat capacity of wood) = 0.33 cal/g K,

δ_f (char yield) = 0.25,

ϵ (surface emissivity) = 0.75,

T_∞ (ambient temperature) = 298 K.

5.4 Numerical Prediction of Piloted Ignition Utilizing Analytical Solid Pyrolysis Solution.

The numerical solution procedure for the gas phase is the same as before (Chapter 3). The surface temperature of the solid wood is calculated by using equation (5-17), and the fuel evolution rate is calculated by using equation (5-18). It is tactitly assumed that the contribution of any gas-phase exothermic reactions to the rise in the solid surface temperature is negligible during piloted ignition.

The uniform grid spacing used in this work is 0.055 mm. A smaller grid spacing was also tested; Figure 5-3 shows the comparison the 0.055 mm grid spacing with the 0.027 mm grid spacing. The heat flux is assumed to be 1.88 W/cm^2 and the fuel is assumed to be 100% methane. Clearly, the temperature fields near the surface for small and regular grid spacings are very similar. The time for start of flashing for the small grid is 64.7 sec, while for the regular grid it is 61.7 sec. The

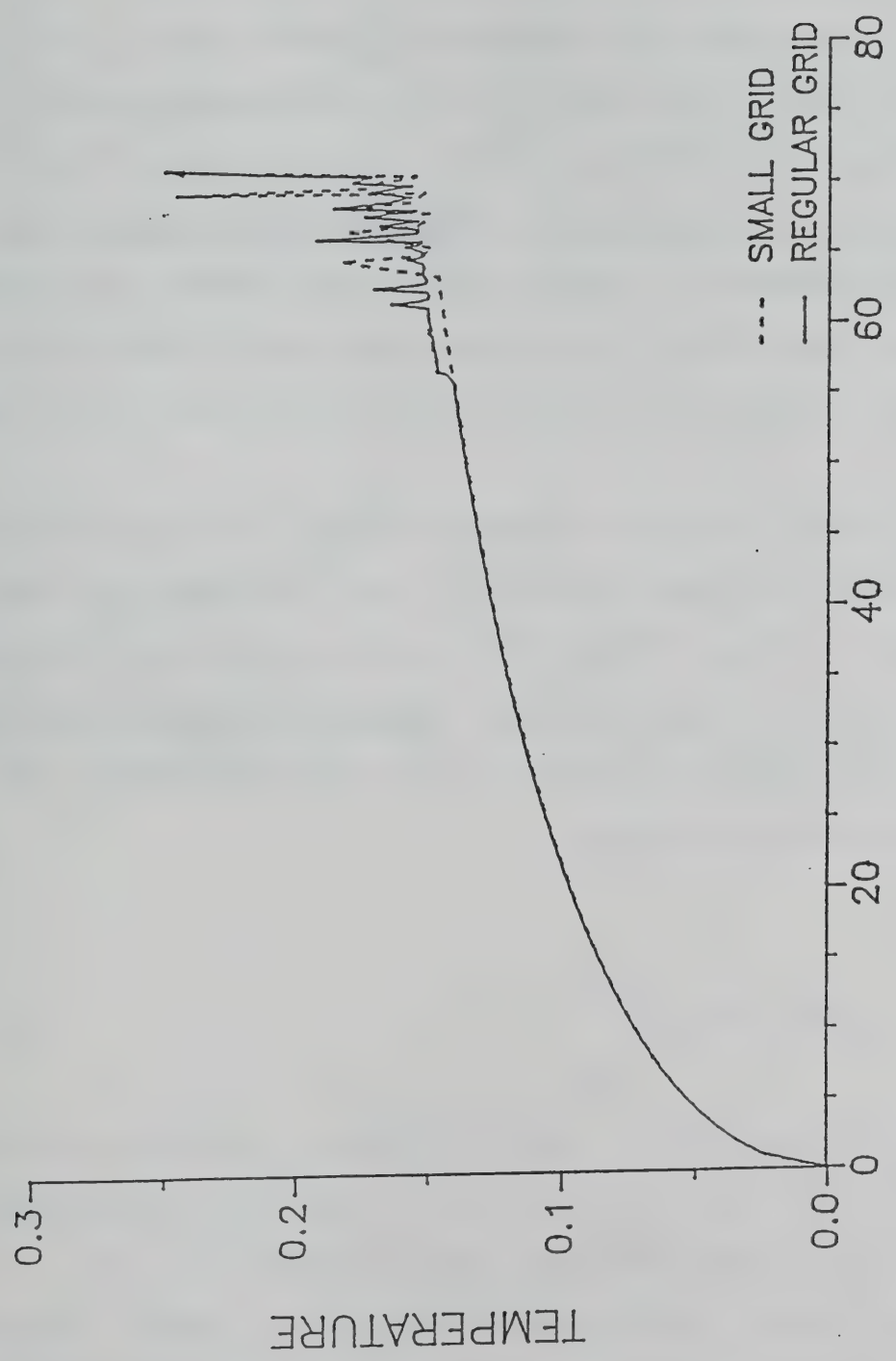

FIGURE 5-3 Comparison of regular grid and small grid.

time for sustained piloted ignition for the small grid is 71.1 sec, while for the regular grid is 70.7 sec. It is noteworthy that the ignition source has been turned on every 0.5 sec; thus the error is within one time period of turning on the ignition source. It is concluded that the grid space used in this study is appropriate for piloted ignition. Furthermore, the most important aspect of piloted ignition is the development of a sustained diffusion flame after the pre-mixed flame. The smaller grid can only predict a more accurate pre-mixed flame velocity. It will not significantly affect the time for sustained piloted ignition but will dramatically increase the CPU time.

Figure 5-4 Shows the temperature history of the gas 0.15mm above the surface. The temperature peaks are due to the flashes and their subsequent quenching. Although it is not immediately obvious from the graphs (due to scaling), it is found that for small heat fluxes, the flashing periods are longer, while for higher heat fluxes, the flashing periods are shorter.

5.4.1 Dilution Study:

As mentioned earlier, numerous products are formed during the decomposition of cellulosic materials. For temperatures between 280 $^{\circ}$C to 500 $^{\circ}$C, the primary pyrolysis products are water, CO_2, CO, hydrogen, methane, ethane, acetic and formic acids, ethanol, aldehydes, ketones, tar and char. Abu-Zaid (1988) have analyzed the time-integrated product mass and composition of pyrolysis products for

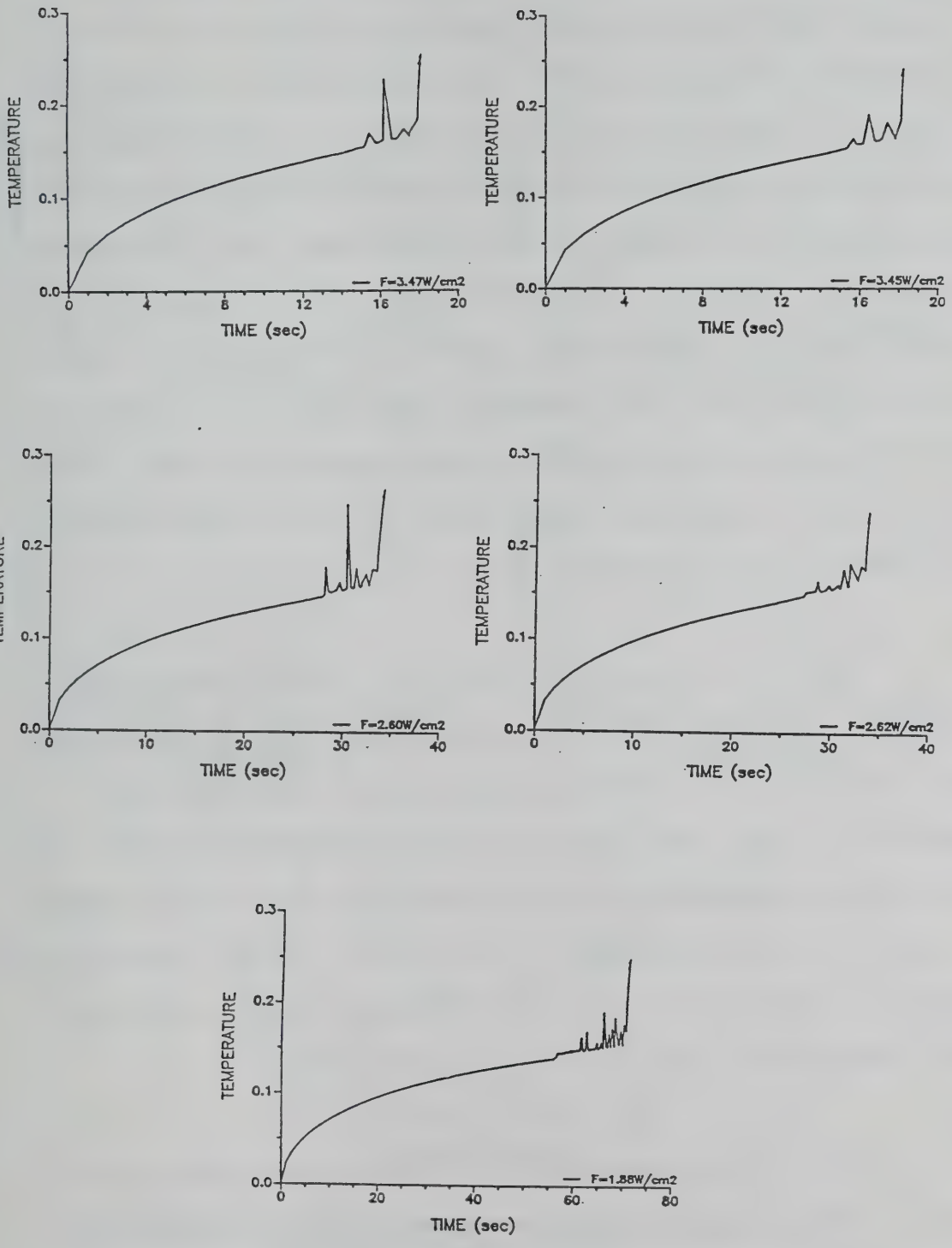

FIGURE 5-4 Temperature history of the gas near the surface.
(Assume fuel is 100% pure)

Douglas fir. He found that the total hydrocarbons and carbon monoxide are only about a quarter of the total gas flux from the solid surface. Thus in this dilution study, the fuel concentration of the pyrolysis products is assume to be equal to 25%. Figure 5-5 is the temperature of the gas near the solid surface for the dilution study. The behavior is basically the same as that for the pure fuel case, only the time for flashes and ignition is a little bit larger. Table 5-2 shows a comparison of the ignition delay times for the experimental, pure fuel assumption and dilute fuel assumption. From Table 5-2, it can be seen that the ignition delay for the pure fuel assumption is about 20~30% lower than the experimental value, while the dilute fuel assumption is very close to the experimental value.

Table 5-3 is a comparison of the fuel evolution rate for the pure fuel assumption and the dilute fuel assumption. The experimental fuel evolution rate is difficult to obtain from the experimental measurment, owing to the weight loss measurement errors. Roughly, the experimental measurment of the fuel evolution rate at piloted ignition is about 0.2 to 0.25 $mg/cm^2 sec$. As can be seen, the fuel evolution rate for pure fuel assumptiom is too low, while the result for the dilute fuel assumption is closer to the experimental data.

Table 5-4 shows the comparison of the surface temperature at ignition for experimental, purefuel assumption, and the dilute fuel assumption. The surface temperature at ignition for pure fuel assumption is lower than the experimental value. Although the surface temperature for the dilute fuel assumption is also slightly lower than the

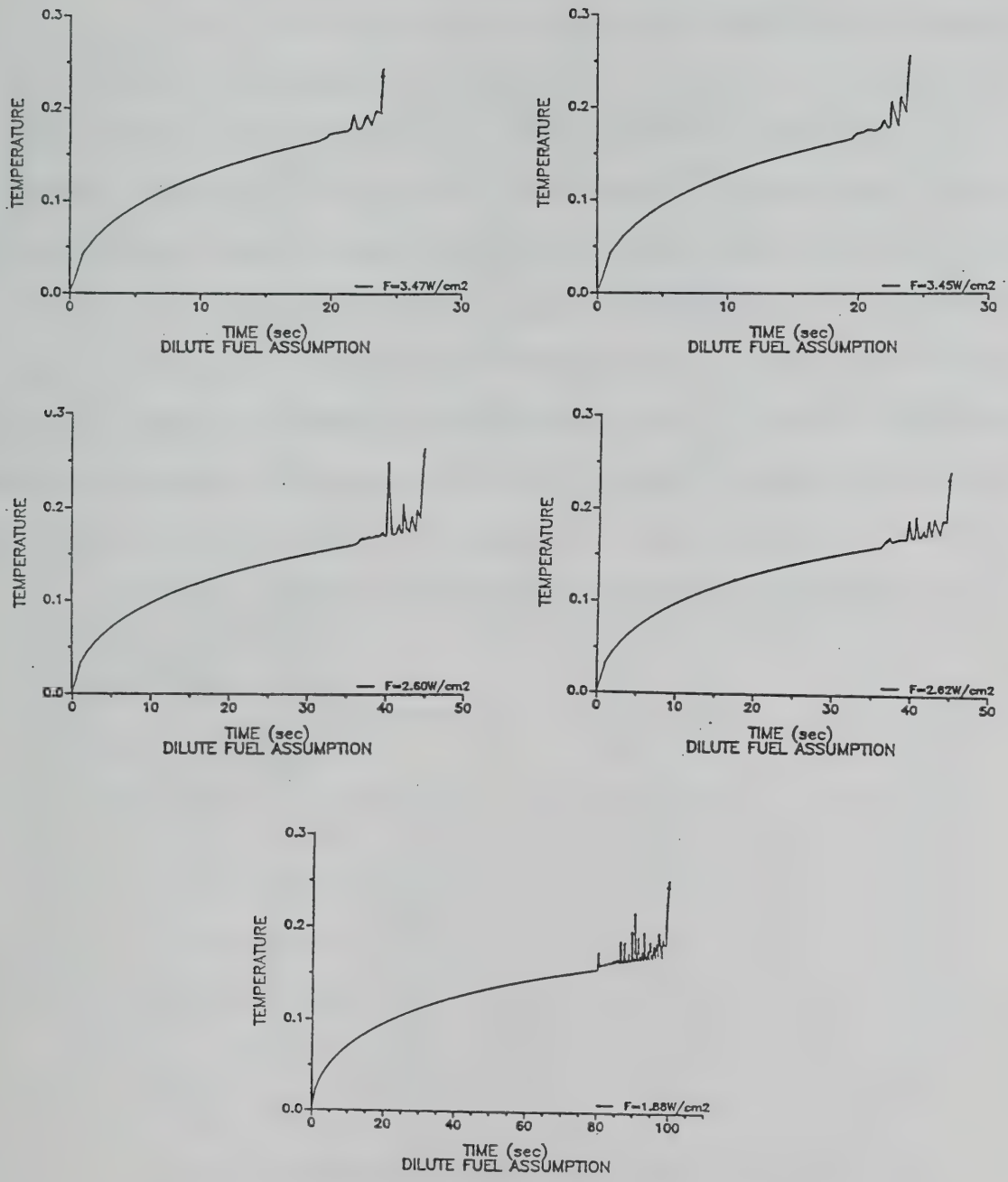

FIGURE 5-5 Temperature history of the gas near the surface.
(Assume fuel mass fraction = 0.25)

experimental value, it is closer to the experimental value. Furthermore, the surface temperature for the dilute fuel assumption is within the range of experimental error.

From Table 5-2 to Table 5-4, it can be seen that the ignition delay time, the ignition fuel evolution rate and the ignition surface temperature for the dilute fuel assumption (25% methane and 75% inert) is close to the experimental data. Although it is within the experimental errors, the experimental results are consistently underestimated. Further dilution (20% methane and 80% inert; results listed in the last column of Tables 5-2 to 5-4), brings the calculations closer to the experimental values. This amount of dilution is within the error of the experimental measurements of Abu-Zaid (1988).

Table 5-2. Comparison of the ignition delay.

External heat flux W/cm^2	Experimental (sec)	Pure fuel assumption (sec)	Dilute fuel assumption (25% CH_4) (sec)	Dilute fuel assumption (20% CH_4) (sec)
1.88	114	70.7	99.0	104.9
2.6	47	33.5	44.5	47.2
2.62	53	33.5	44.3	46.3
3.45	33	18.1	23.6	24.6
3.47	25	18.0	23.8	24.6

Table 5-3. Comparison of the fuel evolution rate at ignition.

External heat flux W/cm^2 $(mg/cm^2 sec)$	Pure fuel assumption $(mg/cm^2 sec)$	Dilute fuel assumption (25% methane) $(mg/cm^2 sec)$	Dilute fuel assumption (20% methane) $(mg/cm^2 sec)$
1.88	0.0364	0.140	0.175
2.6	0.0393	0.144	0.187
2.62	0.0427	0.153	0.186
3.45	0.0418	0.155	0.189
3.47	0.0429	0.170	0.188

(The experimental fuel evolution rate at ignition is about 0.2 to 0.25 mg/cm^2 sec)

Table 5-4. Comparison of the surface temperature at ignition.

External heat flux W/cm^2 ($^{\circ}C$)	Experimental ($^{\circ}C$)	Pure fuel assumption ($^{\circ}C$)	Dilute fuel assumption (25% methane) ($^{\circ}C$)	Dilute fuel assumption (20% methane) ($^{\circ}C$)
1.88	376	318	348	353
2.6	399	330	360	366
2.62	380	332	362	367
3.45	383	340	372	377
3.47	385	341	374	377

5.4.2 Flashes and Quenching

From the experimental observations, there are usually some flashes which are subquently quenched prior to sustained piloted ignition. The sharp rises in surface temperature prior to sustained ignition in Figure 5-6 are due to flashes. These flashes are also observed in the numerical simulation. The sharp rises in temperature (prior to ignition) in Figures 5-4 are also due to flashes.

The time elapsed between flashes and sustained ignition diminishes as the heat flux is increased. Also, the time between flashes and sustained ignition is larger for the dilute fuel than for the pure fuel, i.e., the time interval over which flashes occur is smaller for the pure-fuel case.

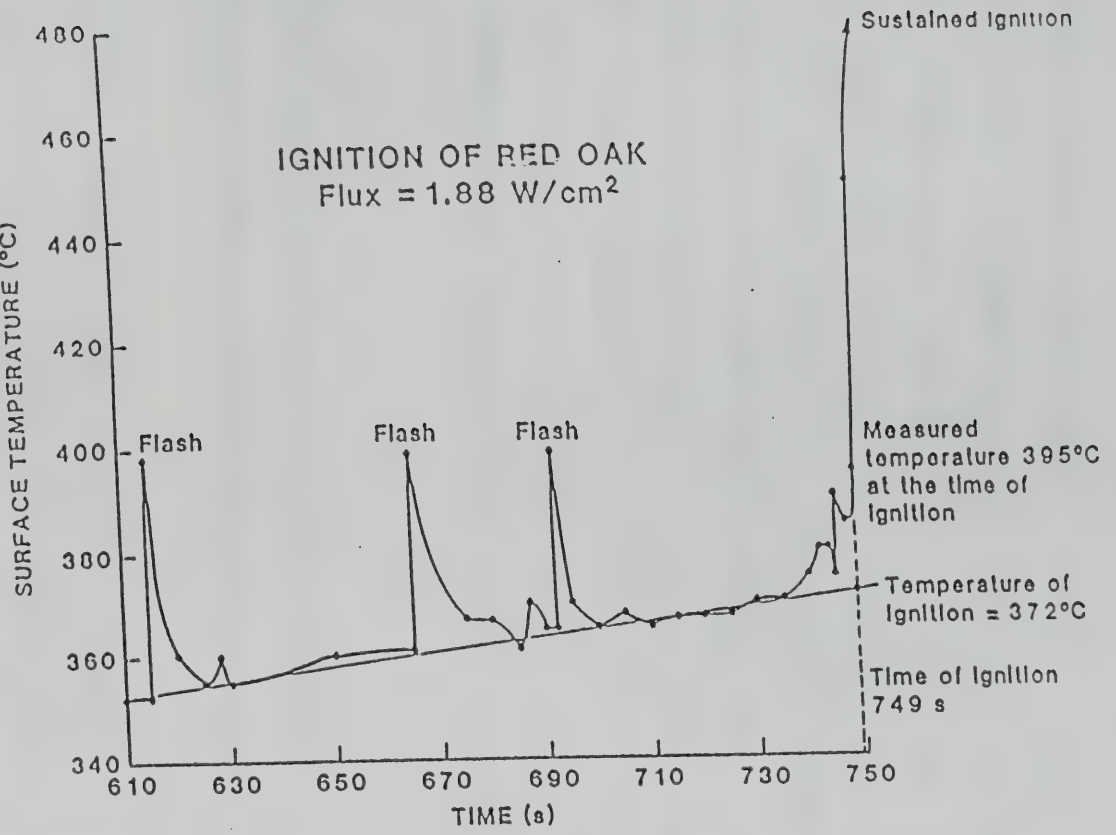

FIGURE 5-6 Surface temperature-time history during piloted ignition of a red oak sample.

5.4.3 Comparison with Experimental Data for Other Woods.

Figure 5-7 shows a comparison of predicted and measured surface temperatures at ignition. The experimental data are obtained from Atreya (1983). The solid line is for the pure fuel assumption, while the dashed lines are for the dilute fuel assumption. From the figure it can be seen that calculations for both of the assumed dilution levels are within the bounds of the experimental measurements. Clearly, the pure fuel assumption under-predicts the ignition temperature. Figure 5-8 shows a comparison of the predicted and experimentally measured ignition delay times. Once again, the pure fuel assumption under-predicts the ignition delay time and the dilute fuel assumption is more accurate.

5.4.4 Comparison of the Minimum Fuel Evolution Rate with the Fuel Evolution Rate at Extinction of a Steady State Diffusion Flame.

The minimum fuel evolution rate of a steady diffusion flame (i.e., near extinction) is calculated with the assumption of constant piloted ignition solid surface temperature. The numerical solution is obtained by solving the steady state version of equations (5-13) through (5-16). The analytical solution is obtained by large activation energy asymptotics (Linan 1974).

Tables 5-5 and 5-6 show the comparison of the fuel evolution rate obtained from numerical simulation of piloted ignition (transient calculation) with the analytical and numerical calculations of the

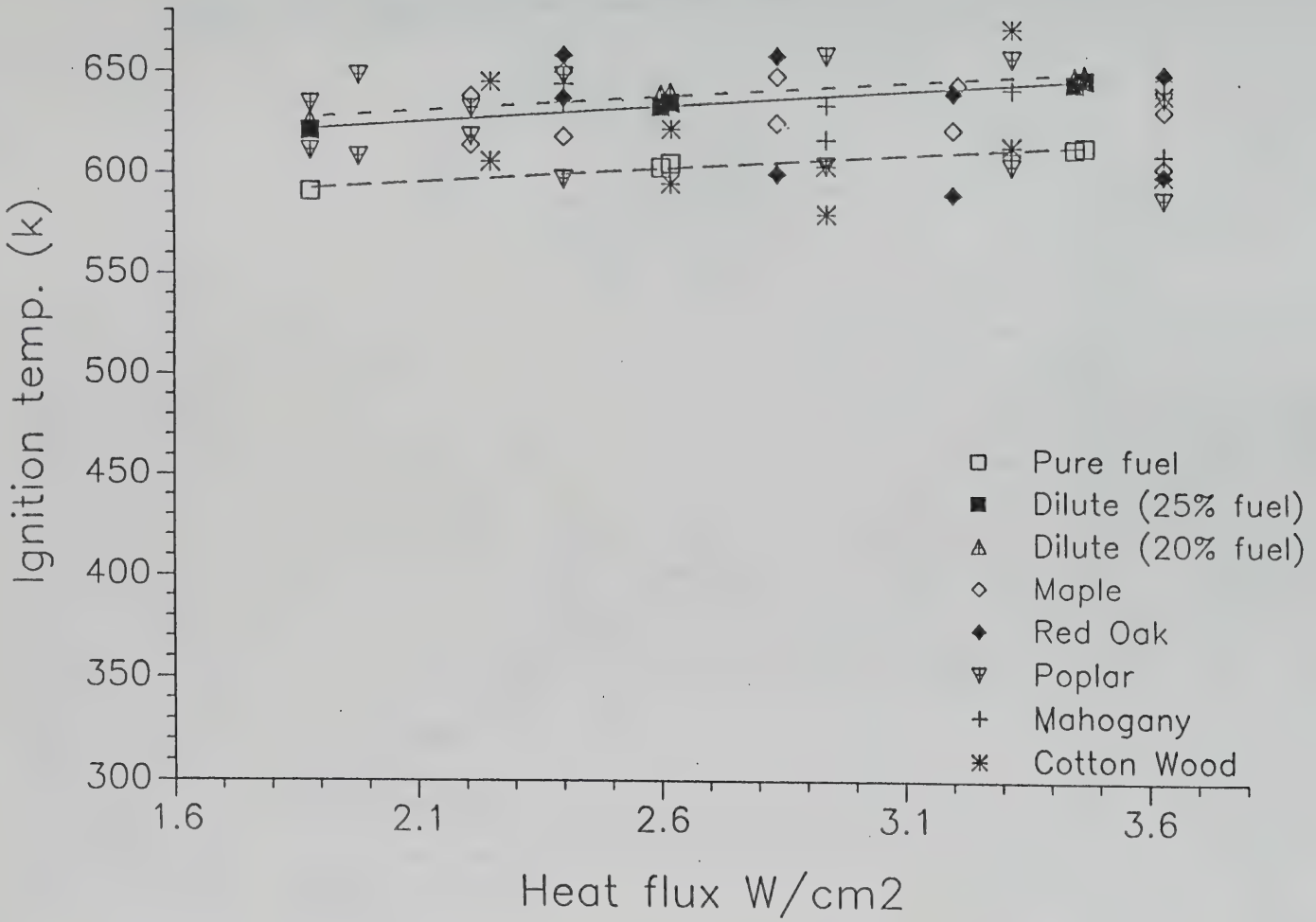

FIGURE 5-7 Comparison of predicted surface temperatures and measured surface temperatures at ignition.

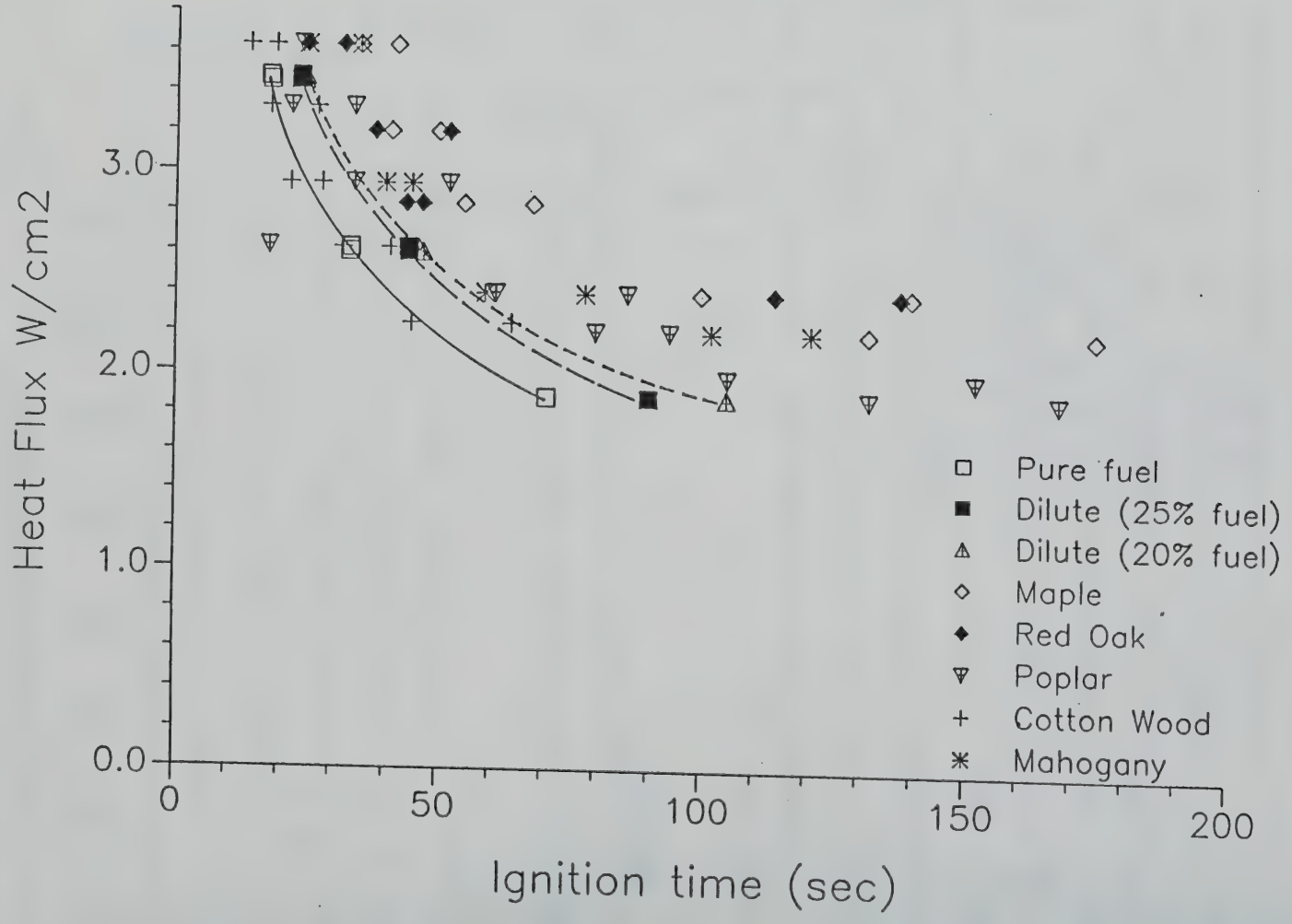

FIGURE 5-8 Comparison of predicted ignition delay time and measured ignition delay time.

minimum fuel evolution rates at extinction of a steady diffusion flame. The diffusion flame is adjacent to a surface whose temperature is the nearly constant surface temperature at piloted ignition for the transient calculation. From these tables, it can be seen that the fuel evolution rate at piloted ignition is quite close to the minimum fuel evolution rate of the steady state diffusion flame (i.e., near extinction). Although the values are slightly larger there is a trend toward increase with increase in heat flux, at least for the values in the first column.

Table 5-5. Comparison of steady state minimum fuel evolution rate with the numerical simulation of the piloted ignition. (pure methane assumption)

External heat flux W/cm^2	Fuel flow rate at piloted ignition, same as in Table 5-3 $mg/cm^2 sec$	Min. fuel flow rate (steady state analytical calculation) $mg/cm^2 sec$	Min. fuel flow rate (steady-state numerical calculation) $mg/cm^2 sec$
1.88	0.0364	0.0328	0.0333
2.6	0.0393	0.0325	0.0330
2.62	0.0427	0.0325	0.0329
3.45	0.0418	0.0323	0.0328
3.47	0.0429	0.0322	0.0328

(The surface temperature for the steady state solution is the same as for piloted ignition)

Table 5-6. Comparison of steady state minimum fuel flow rate with the numerical simulation of the piloted ignition. (25% methane and 75% inert gas)

External heat flux W/cm^2	Fuel flow rate at piloted ignition, same as in Table 5-3 $mg/cm^2 sec$	Min. fuel flow rate (steady state analytical calculation) $mg/cm^2 sec$	Min. fuel flow rate (steady-state numerical calculation) $mg/cm^2 sec$
1.88	0.140	0.128	0.132
2.6	0.144	0.126	0.131
2.62	0.153	0.126	0.131
3.45	0.155	0.125	0.129
3.47	0.170	0.125	0.129

(The surface temperature for the steady state solution is the same as for piloted ignition)

5.4.5 Effect of Air Velocity and Oxygen Concentration

The boundary layer thickness is directly related to the ambient air velocity. Because the theoretical model in this study is one-dimensional, changes in the boundary layer thickness are the only method of simulating the changes due to ambient air velocity. Thus, an air velocity of 0.1 m/sec is assumed to correspond to a boundary layer thickness of 1.5 cm and a convective heat transfer coefficient of 2 W/m^2K. These values correspond to the experimental measurements. An air velocity of 1.0 m/sec will then correspond to a boundary layer thickness of 0.6 cm and a convective heat transfer coefficient of 4 W/m^2K.

Figure 5-9 shows the ignition delay time plotted against incident heat flux for two different air velocities and O_2 concentrations. The ignition delay for 15% O_2 is larger than that for 21% O_2 and the ignition delay time for 1.0 m/sec air velocity is even larger than that for 15% O_2. These results agree with the experimental measurements of Abu-Zaid (1988) qualitatively.

5.4.6 The Effect of Moisture Content

The effect of moisture content manifests itself in changing the physical properties of wood and diluting the products of pyrolysis. Thus,

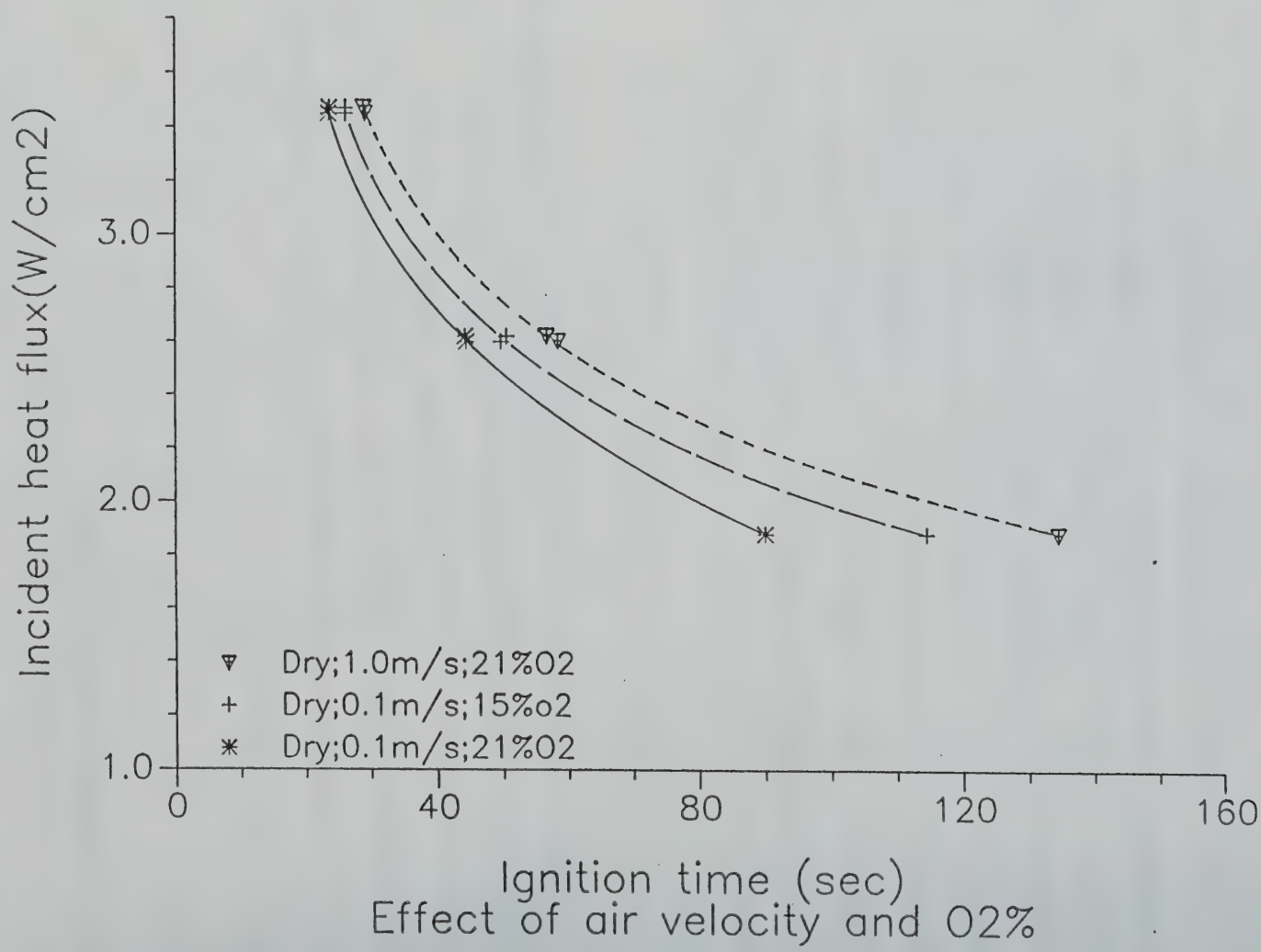

FIGURE 5-9 Ignition delay time for different air velocities and oxygen concentrations.

in this theoretical model, the effect of moisture is studied by changing the thermal conductivity, the heat capacity and the density of wood, The physical properties of wood as a function of moisture content are taken from Parker (1988); these are listed in Table 5-7. The fuel concentration as a function of moisture content is calculated by the following expression:

$$Y_{fs}(M) = Y_{fs}(dry) * \left(\frac{\rho_{dry} - \rho_{char}}{\rho_{M} - \rho_{char}}\right).$$

Here ρ_M is the sample density when moisture is included; hence, $\rho_M \geq \rho_{dry}$. Figure 5-10 is the plot of ignition delay as a function of heat flux for various moisture contents; as expected, the higher the moisture content the larger is the ignition delay.

Table 5-7. Thermal properties of wood as a function of moisture content after Parker (1988).

	ρ (density)	C_p (heat capacity)	λ(thermal conductivity)	fuel concentration
dry	0.54	1.38	0.167	0.25
11% moisture	0.6	1.657	0.197	0.218
17% moisture	0.632	1.786	0.214	0.204
27% moisture	0.686	1.974	0.24	0.184

5.4.7 Correlation of Results

In Equation (5-17), if the surface temperature at ignition, (θ_s), is assumed to be constant, then the following relationship between ignition time and the incident heat flux (F) can be derived,

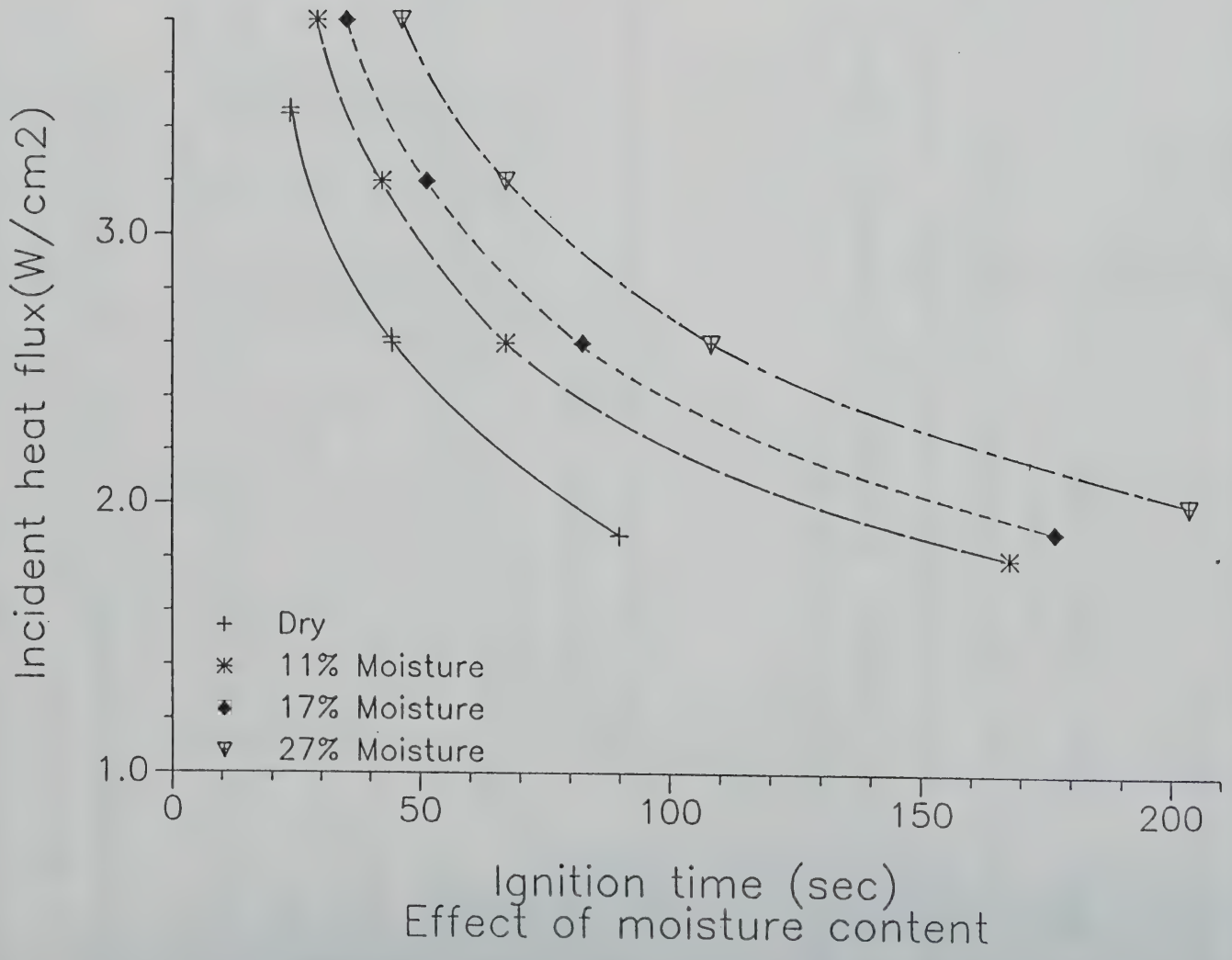

FIGURE 5-10 Ignition delay time for various moisture contents of wood.

$$F = \sqrt{K\theta_s}\, t^{-0.5} + L, \qquad (5\text{-}19)$$

where

$$K = \frac{2}{3}\frac{\rho c \lambda}{\epsilon^2}. \qquad (5\text{-}20)$$

For constant K and L, the relationship between F and $t^{-0.5}$ is linear, $\sqrt{K\theta_s}$ is the slope of the line, and L is the intercept. Here L may be interpreted as the minimum heat flux for ignition, since it is the heat flux required for an infinite ignition delay time. Figures 5-11 and 5-12 show plots of square root of ignition time vs. heat flux. In both Figures 5-11 and 5-12, the intercept is L = 0.4W/cm^2, while the experimental data of Abu-Zaid (1988) show that the intercept is about 1 W/cm^2. The reason for this discrepancy is because the analytical solid pyrolysis solution (Equation 5-18) is obtained by assuming a constant density for wood during pyrolysis. For low heat fluxes, a lot of char is formed prior to piloted ignition, and the density near the surface is considerably lower. This means that the analytical solid phase pyrolysis equation over-predicts the mass flux for low heat fluxes, resulting in a smaller ignition delay time. This motivated us to find a complete numerical solution for wood decomposition.

5.5. Numerical Solution for Decomposition of Wood

The one-dimensional solid-phase mathematical model for the decomposition process studied here is given by equations (5-8) to (5-12). In these equations C_w and λ_w are functions of density. The

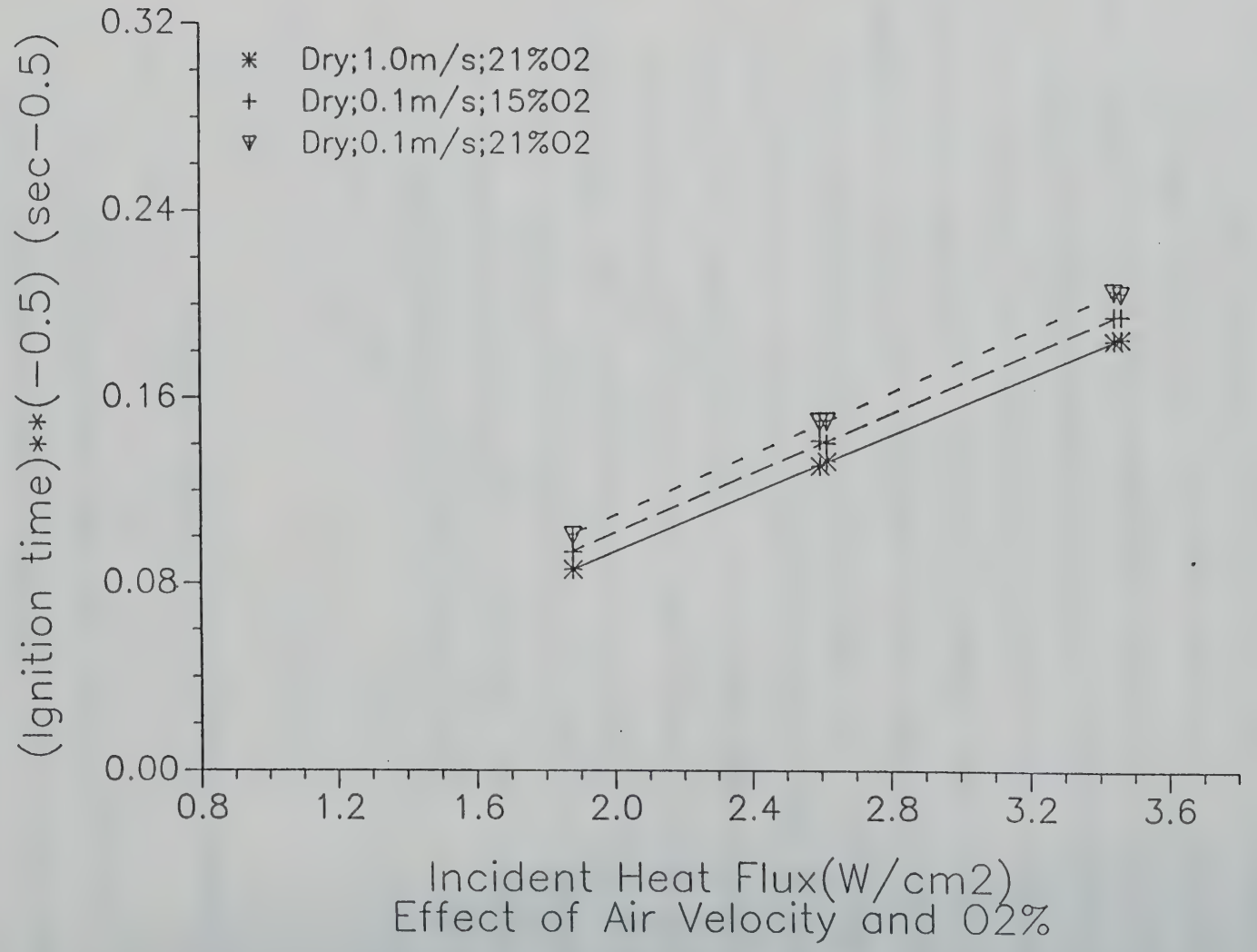

FIGURE 5-11 Plots of square root of ignition time vs heat flux for different air velocities and oxygen concentrations.

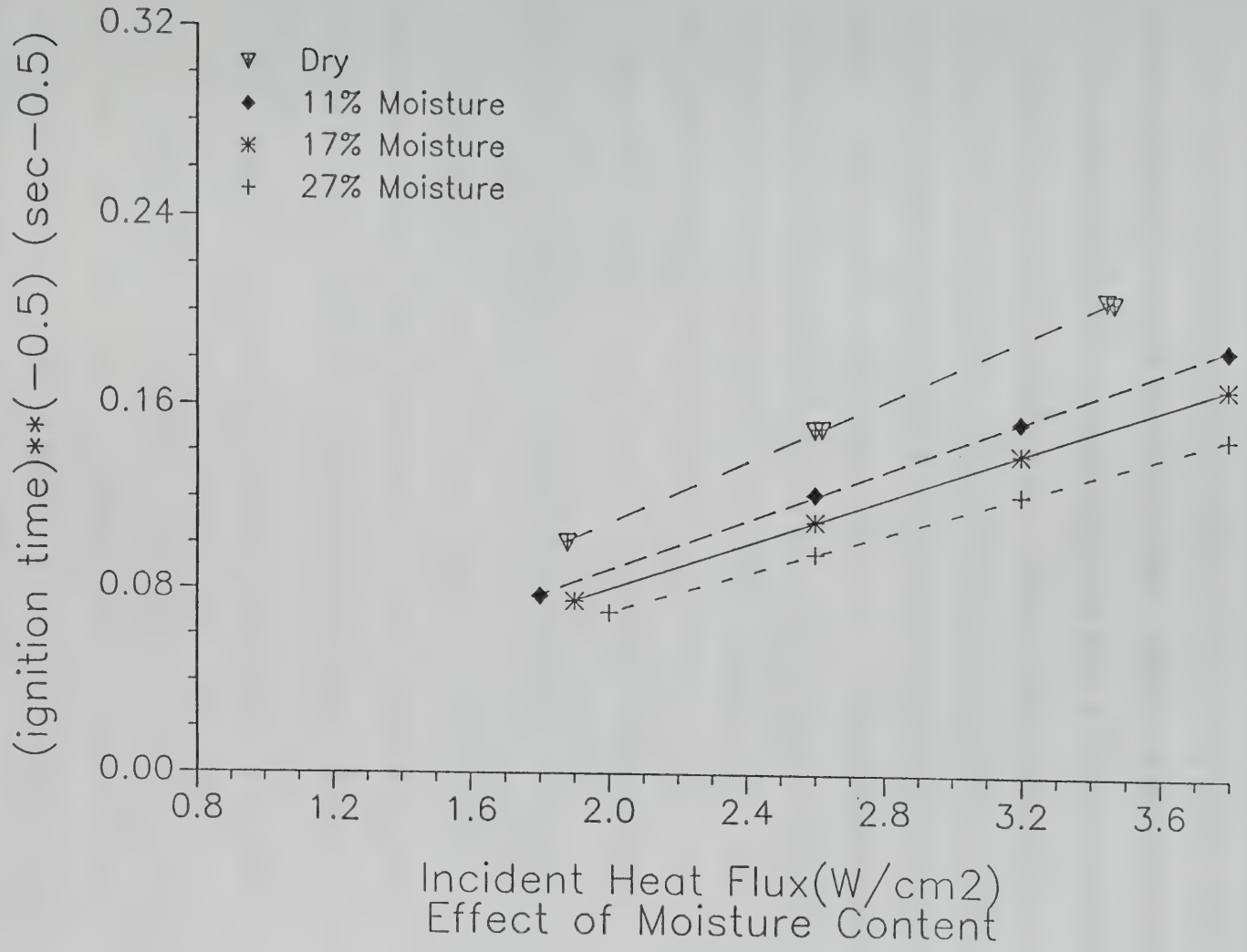

FIGURE 5-12 Plots of square root of ignition time vs heat flux for various moisture contents of wood.

density of the solid in the pyrolyzing zone is assumed to change continuously from the initial density of wood; ρ_{wd}, to the final density of char, ρ_{wf}. At any instant, a partially pyrolyzed element of wood in this zone consists of char distributed throughout the unpyrolyzed active material. Since zero shrinkage is assumed, all densities are based on the original volume of the wood element; thus $\rho_w = \rho_a + \rho_c$, where ρ_a and ρ_c are the densities of the active wood material and char respectively. At $t = 0$, $\rho_w = \rho_{wd}$, and at $t = \infty$, $\rho_w = \rho_{wf}$. The densities ρ_a and ρ_c can be described by the following equations:

$$\rho_a = \rho_{wd} \left(\frac{\rho_w - \rho_{wf}}{\rho_{wd} - \rho_{wf}}\right),$$

$$\rho_c = \rho_{wf} \left(\frac{\rho_{wd} - \rho_w}{\rho_{wd} - \rho_{wf}}\right),$$

while the thermal conductivity of the solid in the pyrolyzing zone is assumed to be given by

$$\lambda_w = \frac{\rho_a}{\rho_{wd}} \lambda_a + \frac{\rho_c}{\rho_{wf}} \lambda_c,$$

where λ_a and λ_c are the thermal conductivities of unpyrolyzed wood and char, respectively. Also, the specific heat of an element in the pyrolysis zone is assumed to be

$$C_{pw} = \frac{\rho_a}{\rho_w} C_{pa} + \frac{\rho_c}{\rho_w} C_{pc} \quad ,$$

where, C_{pa} and C_{pc} are the specific heats of unpyrolyzed wood and char,

respectivity.

The differential equations (5-8) to (5-12) were solved by an implicit numerical scheme, and the numerical code was checked with the numerical program written by Atreya [1983]. The physical properties used for the numerical calculation are $\rho_{wf} = 0.135 g/cm^3$, $\lambda_c = 0.07$ W/m K $C_{pa} = C_w$, $C_{pc} = 0.165$ cal/g K. The remainder of the parameters are the same as before. Figure 5-13 shows the ignition delay time calculations using the numerical code for the pyrolysis of wood. A comparison with Figure 5-10 shows that for higher heat fluxes, the ignition delay time is not much different than the previous result (in which an analytical solution for the wood pyrolysis was used). However, at low heat fluxes, the ignition delay time for the numerical wood pyrolysis calculations is almost four times larger than the analytical wood pyrolysis calculations. This is because a substantial amount of char is formed over an extended exposure at low heat fluxes prior to ignition, as already discussed. Figure 5-14 is the plot of wood density at the time of piloted ignition. From the figure, it can be seen that the density near the surface for the low heat flux is much lower than for the the higher heat flux.

Figure 5-15 is the plot of $(\text{ ignition time})^{-0.5}$ vs incident heat flux. The slope of the line is different for different moisture contents, and the intercept is about 0.9 W/cm^2. This agrees with the experimental results of Abu-Zaid (1988).

In summary, the one-dimensional piloted ignition model presented

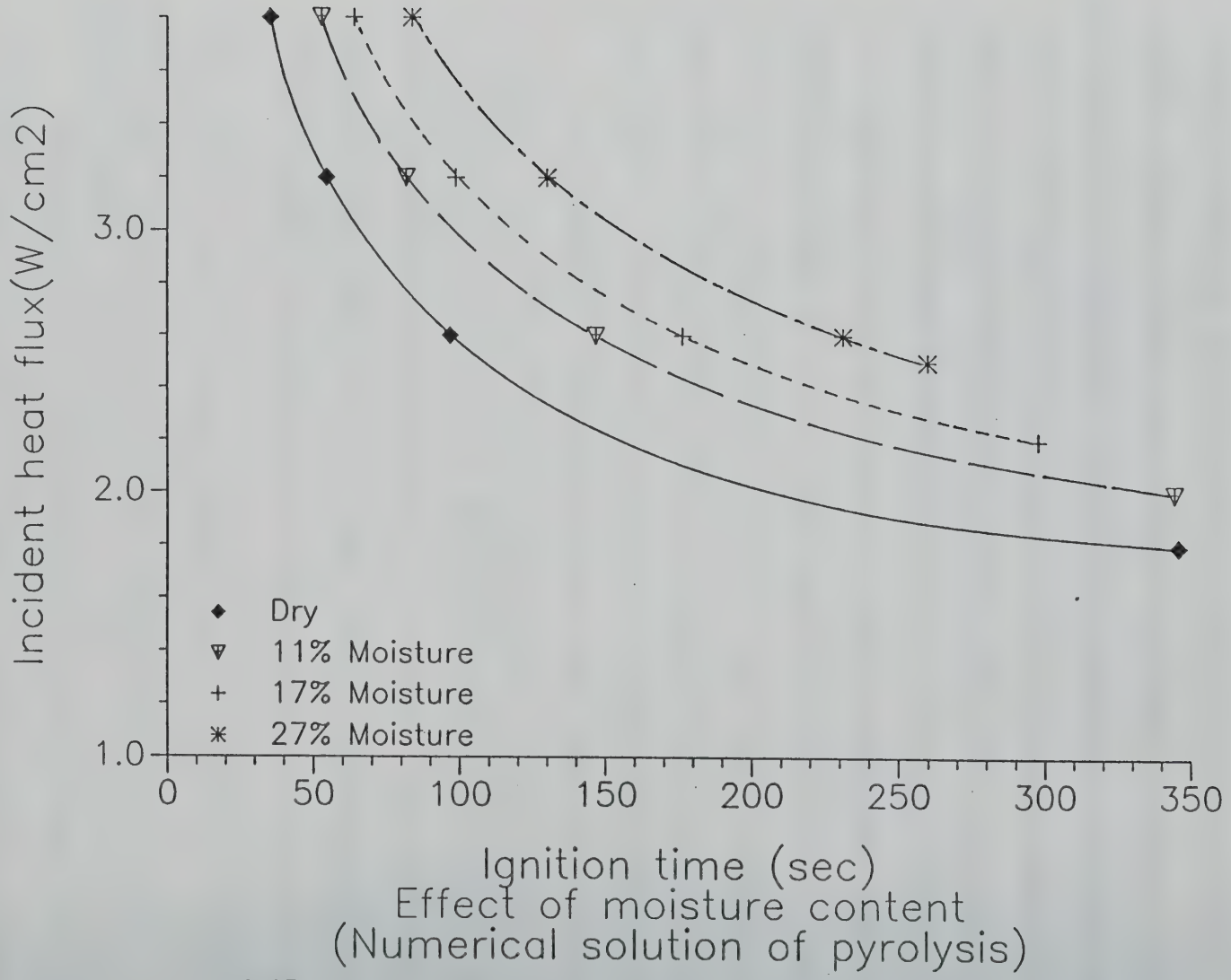

FIGURE 5-13 Ignition delay time for various moisture contents of wood (solid pyrolysis equations have been solved numerically).

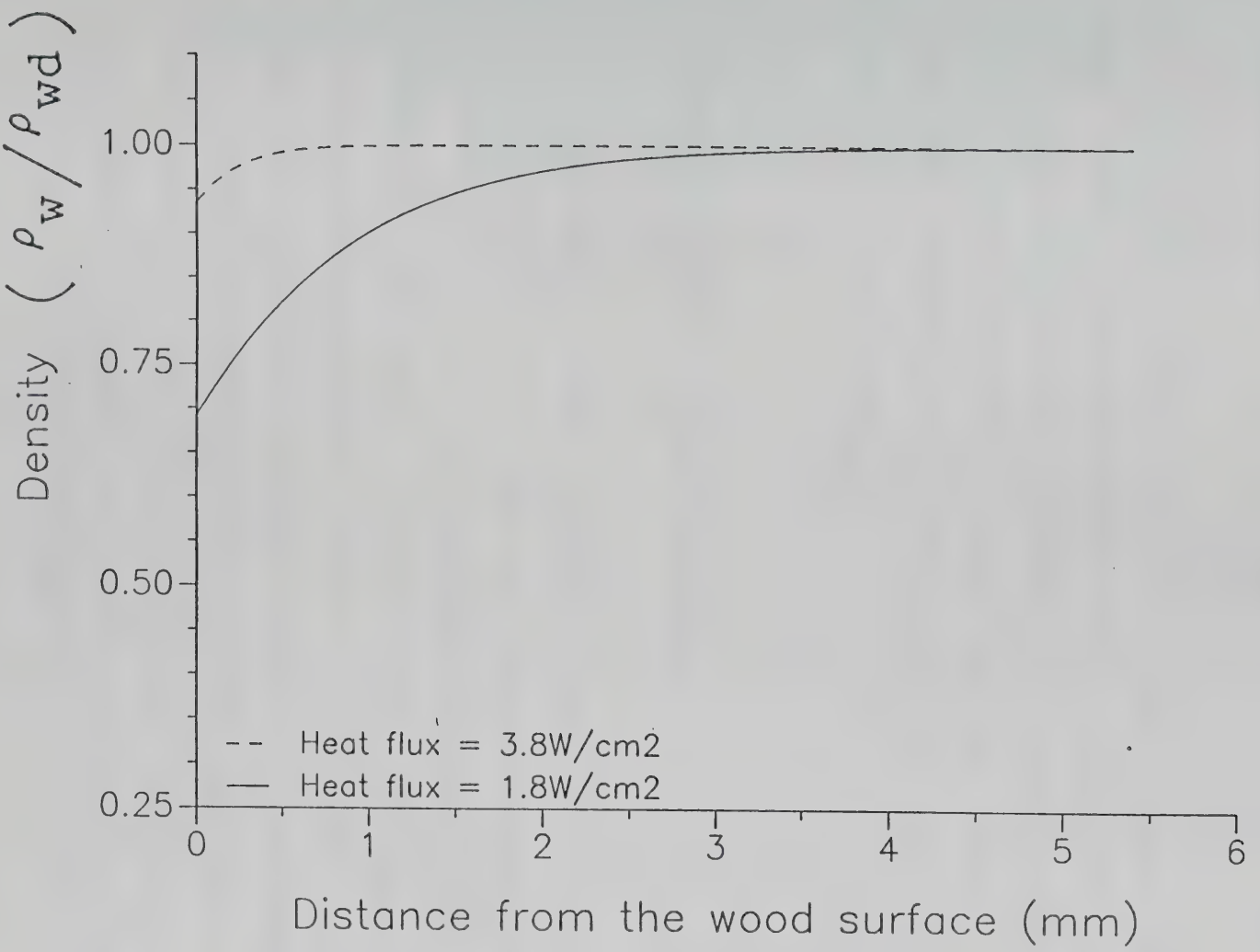

FIGURE 5-14 Density of wood at piloted ignition.
(Assume wood sample is dry).

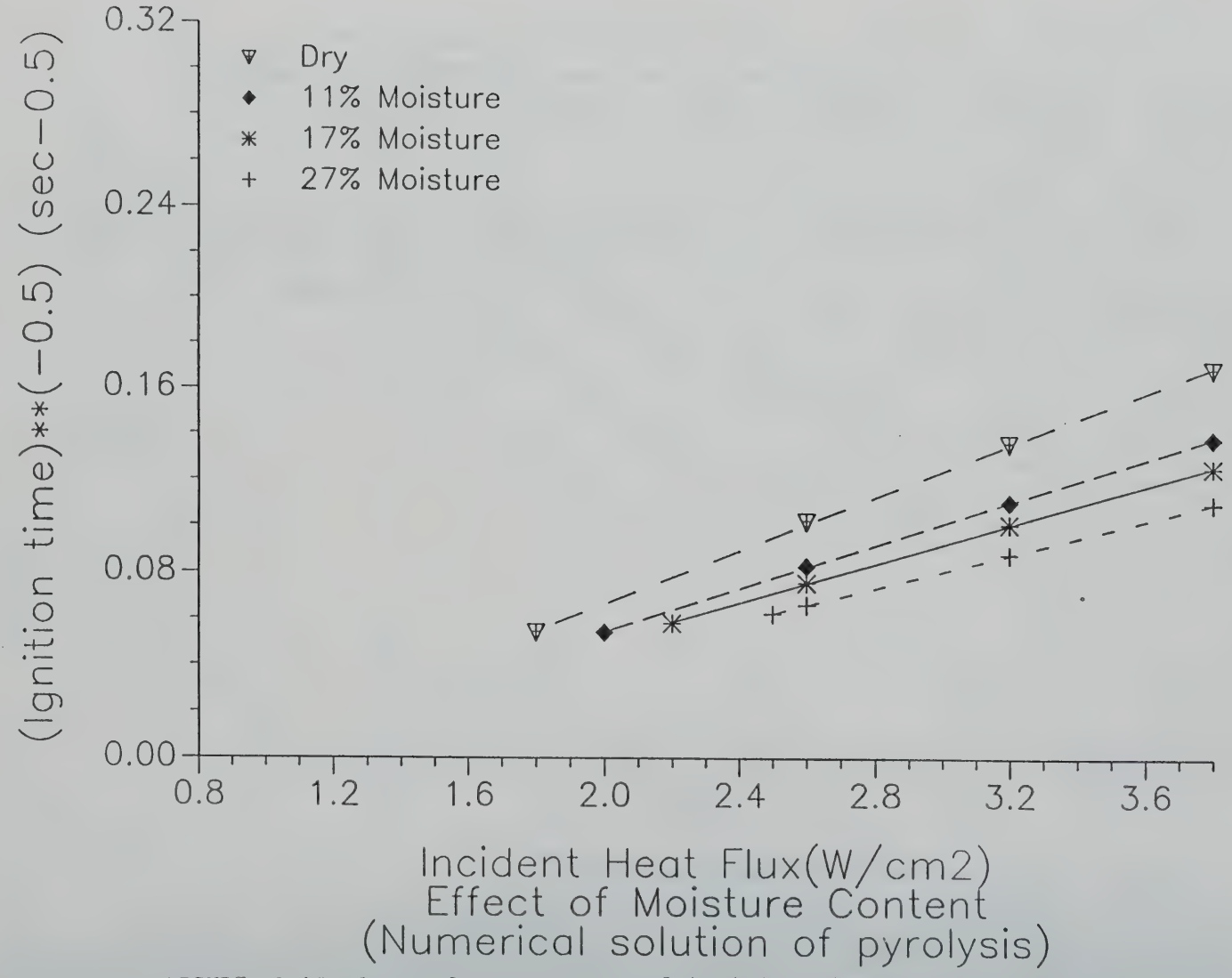

FIGURE 5-15 Plots of square root of ignition time vs heat flux for various moisture contents of wood (solid pyrolysis equations have been solved numerically).

here captures all the essential features of piloted ignition of wood.

5.6 Sensitivity Study

In the above theoretical study of wood ignition, some of the physical properties were difficult to estimate accurately. Thus, the pertinent question is: how will the errors in the various parameters affect the ignition calculations. In what follows, the influence of solid-phase activation energy, frequency factor and thermal conductivity were investigated.

5.6.1 Effect of Solid-Phase Activation Energy

To understand the effect of activation energy on piloted ignition, three different values were used in the calculations. Figure 5-16 shows the ignition delay time calculations for E_w=28 Kcal/gmole, 31 Kcal/gmole and 34 Kcal/gmole. It can be seen that a 10% change in the activation energy significantly changes the ignition delay time. For higher activation energy, the ignition delay time is much longer than that for the lower activation energy. This high sensitivity to activation energy also suggests that piloted ignition measurements may be a very accurate way of determining an overall activation energy for the one-step solid phase decomposition model.

Figure 5-17 is a plot of $(\text{ignition time})^{-0.5}$ vs heat flux. It

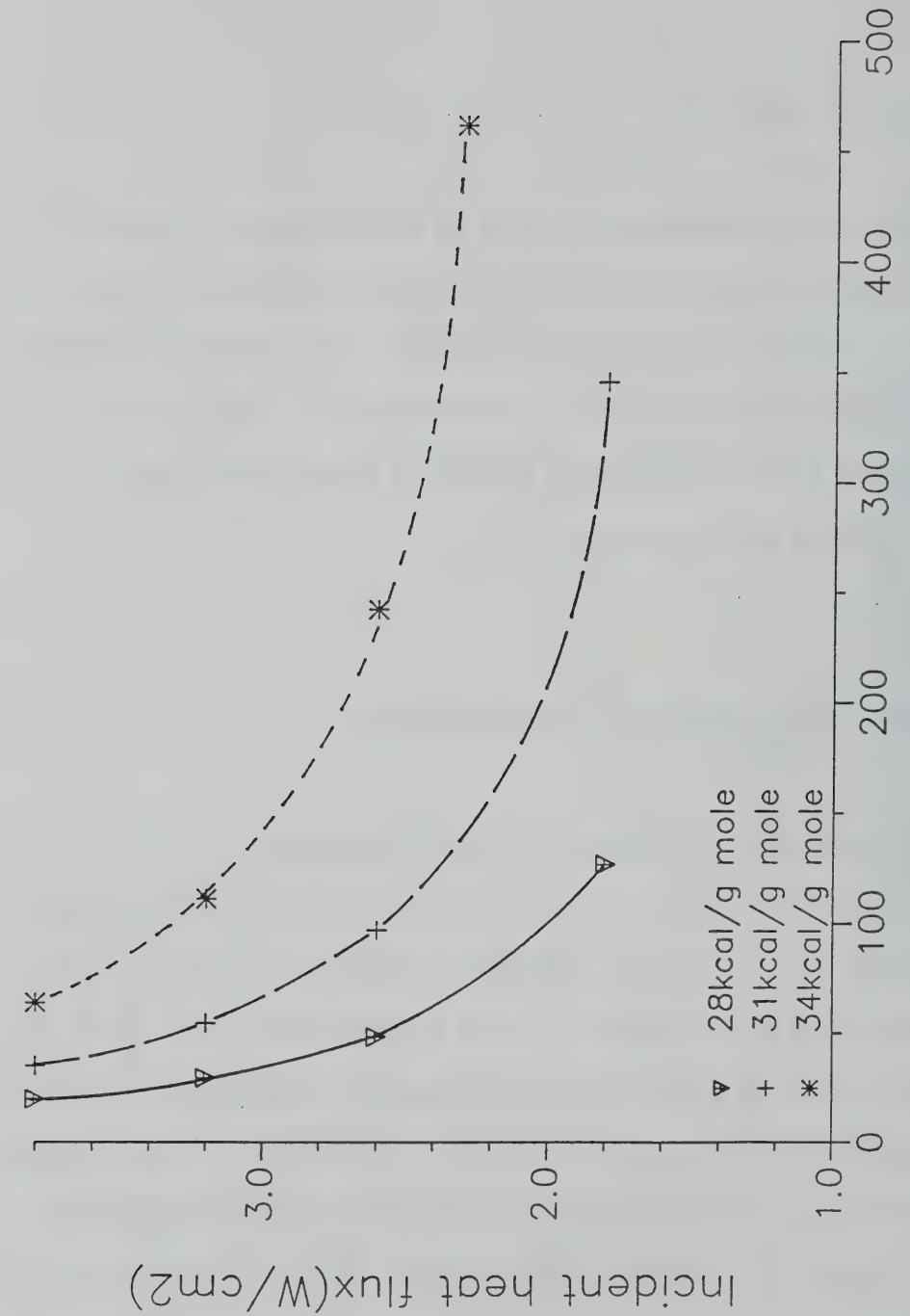

FIGURE 5-16 Effect of activation energy on the ignition delay.

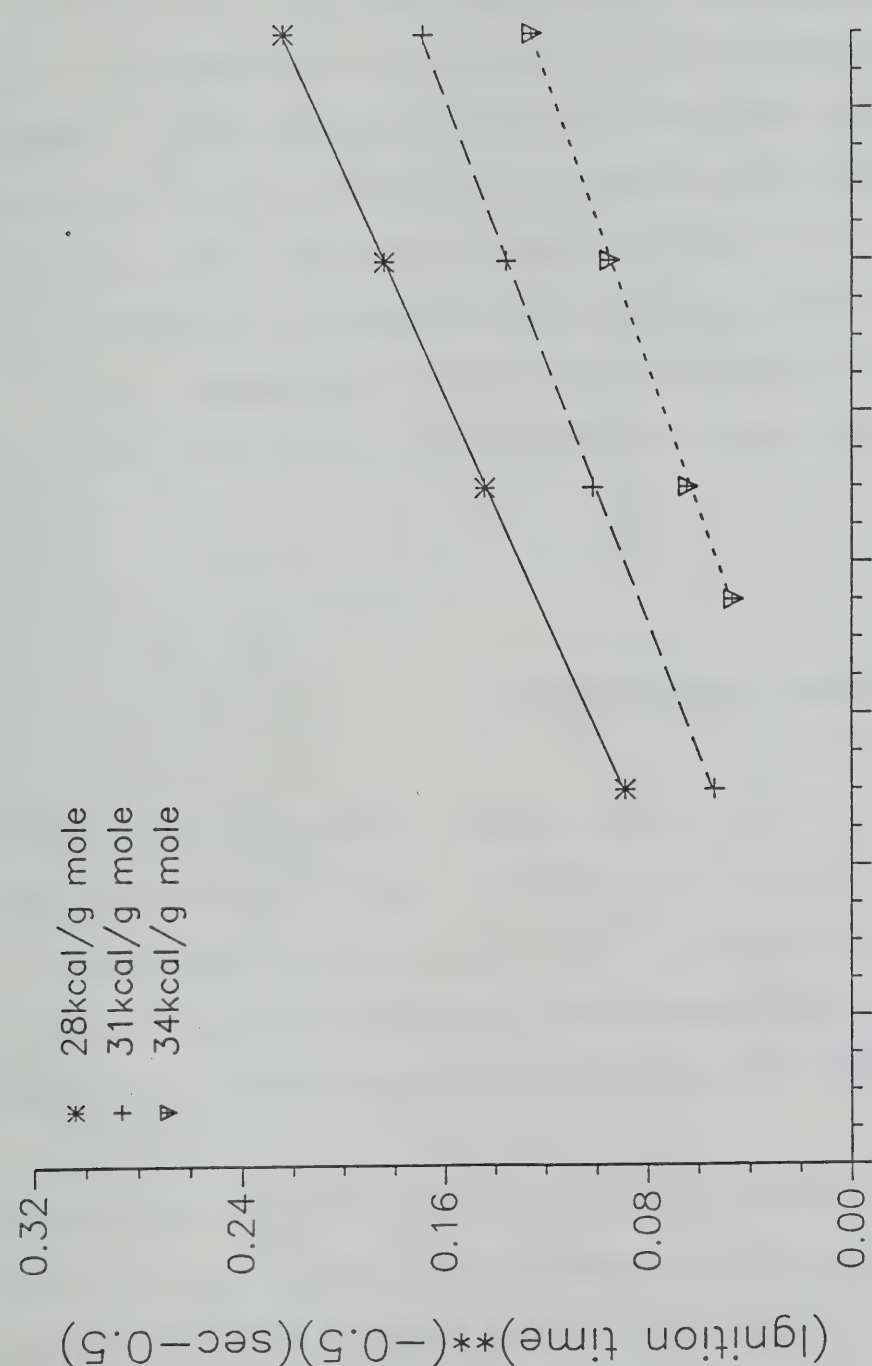

FIGURE 5-17 Plots of square root of ignition time vs heat flux for various activation energy.

can be seen that the intercept is 0.6 W/cm^2 for E_w = 28Kcal/gmole; For E_w = 31 Kcal/gmole the intercept is 0.9 W/cm^2, and for E_w= 34 Kcal/g mole, the intercept is 1.4 W/cm^2. The slope of the three lines is therefore also changed. This is because the surface temperature at ignition (which affects both the heat loss and the slope) is changed with change in activation energy. The surface temperature for the three cases was 350, 410, and 470°C. Since the intercept of the line is interpreted as the minimum heat flux for ignition, the higher activation energy yields a higher minimum heat flux; a 10% increase in the activation energy results in a 50% increase in the minimum ignition heat flux.

5.6.2 The Effect of Frequency Factor

In the literature [Atreya (1983)], the frequency factor for the pyrolysis of wood ranges from 6.0×10^7 to 7.5×10^8. In this study, three frequency factors A_w=6.0×10^7, 0.6×10^7 and 60×10^7 were investigated. Figure 5-18 shows the ignition delay for various frequency factors. As expected, higher frequency factors yield lower ignition delay times.

Figure 5-19 is the plot of (ignition time)$^{-0.5}$ vs heat flux. The trend and the slope of the separate lines is similar to the activation energy case. The intercept for different frequency factors is different. For A_w = 0.6×10^7/sec, the minimum heat flux for ignition is about 1.4 W/cm^2, for A_w = 6.0×10^7/sec the minimum heat flux is 0.9 W/cm^2, while the minimum heat flux for A_w = 60×10^7/sec is 0.6 W/cm^2. In

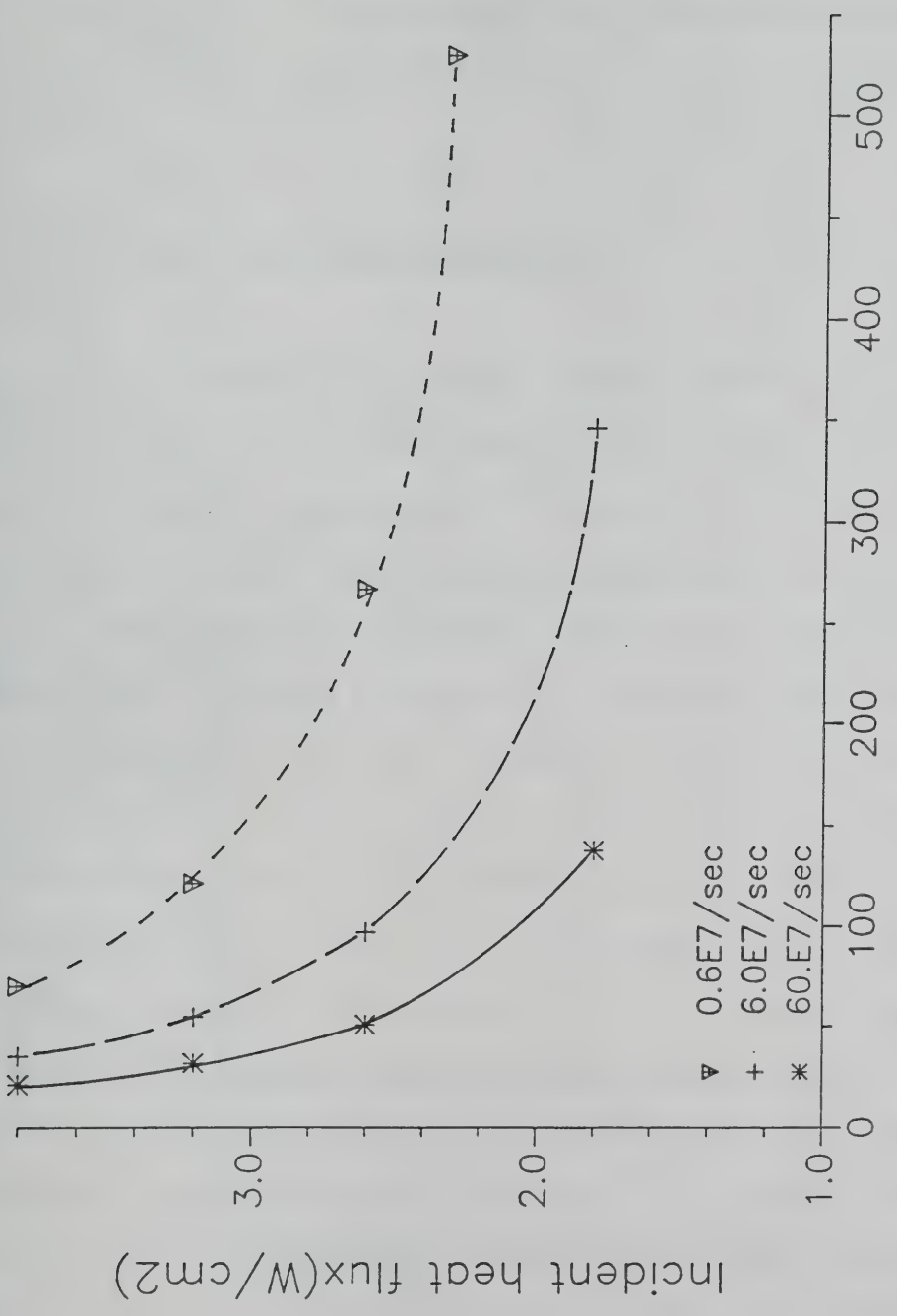

FIGURE 5-18 Effect of frequency factor on the ignition delay.

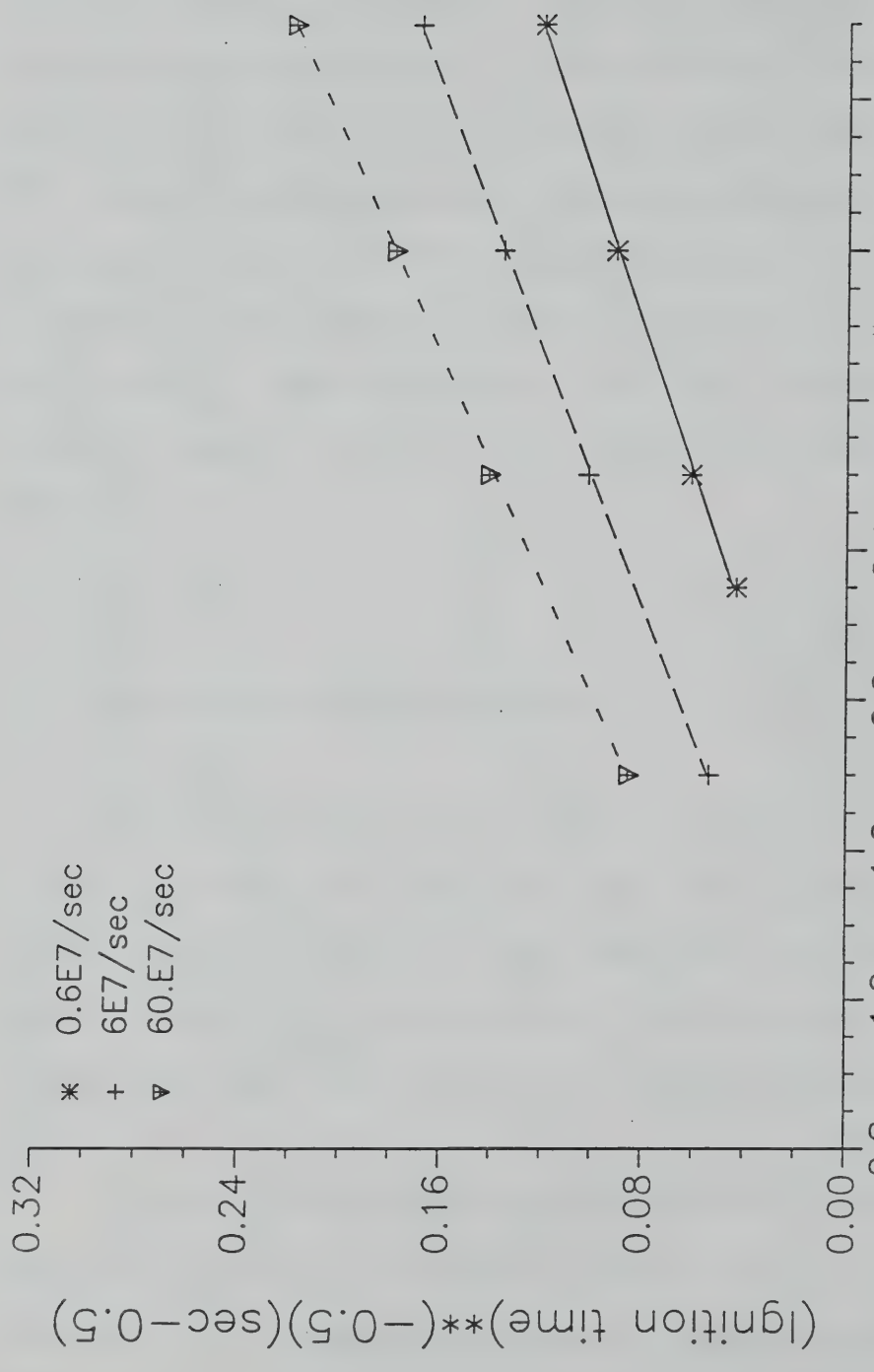

FIGURE 5-19 Plots of square root of ignition time vs heat flux for various frequency factors.

other words, a factor of ten reduction in the frequency factor increases the minimum heat flux at ignition by 50%, whereas a 10% increase in the activation energy has a similar effect. This is caused by the linear dependence of the the reaction rate on A_w, and the exponential dependence of the reaction rate on E_w.

5.6.3 The Effect of Thermal Conductivity

The literature values for the thermal conductivity of wood range from 0.134 W/mK to 0.263 W/mK [Atreya (1983)]. In this study, the thermal conductivity was assigned the values λ_a = 0.25 W/mK, 0.167 W/mK and 0.111 W/mK. Figure 5-20 shows the ignition delay time for these various cases. Although the ignition delay time for lower heat fluxes is very large, the three curves tends to practically the same asymptotic value. Figure 5-21 is the plot of (ignition time)$^{-0.5}$ vs heat flux. For λ_a=0.25 W/mK, the intercept is about 0.8 W/cm^2, for λ_a=0.167 W/mK, the intercept is about 0.9 W/cm^2 and for λ_a = 0.111 W/mK, the intercept is about 1.0 W/cm^2. The thermal conductivity is related to the slope of the line. From equation (5-19), for higher thermal conductivity the slope is smaller and the intercept [or L in equation (5-19)] will be lower. This is confirmed by Figure 5-21. Clearly, the higher the thermal conductivity, the larger is the ignition delay time and the smaller is the minimum heat flux for ignition. Physically, this means that as the thermal conductivity increases, more heat have been conducted into the deeper area, the surface temperature and the pyrolysis product decreases.

From Figures 5-17 and 5-21, it can be seen that for higher activation energy the ignition delay is longer, and the intercept of the line is also larger, whereas, for higher thermal conductivity, the ignition delay is larger but the intercept of the line is lower. This is because the ignition temperature for higher thermal conductivity is lower (for λ_a=0.25 W/mK, T ignition is about 400°C, for λ_a=0.167 W/mK, T ignition is about 410°C, and for λ_a=0.111 W/mK, T ignition is about 420°C). However, the ignition temperature for higher activation energy is larger. (for E_w=34 Kcal/gmole T ignition is about 470°C, for E_w=31 Kcal/gmole T ignition is about 410°C, for E_w=28 Kcal/gmole, T ignition is about 350°C). These changes in the ignition temperature in conjunction with Equation 5-19 explain the observed trends of ignition delay for different activation energies and different thermal conductivities.

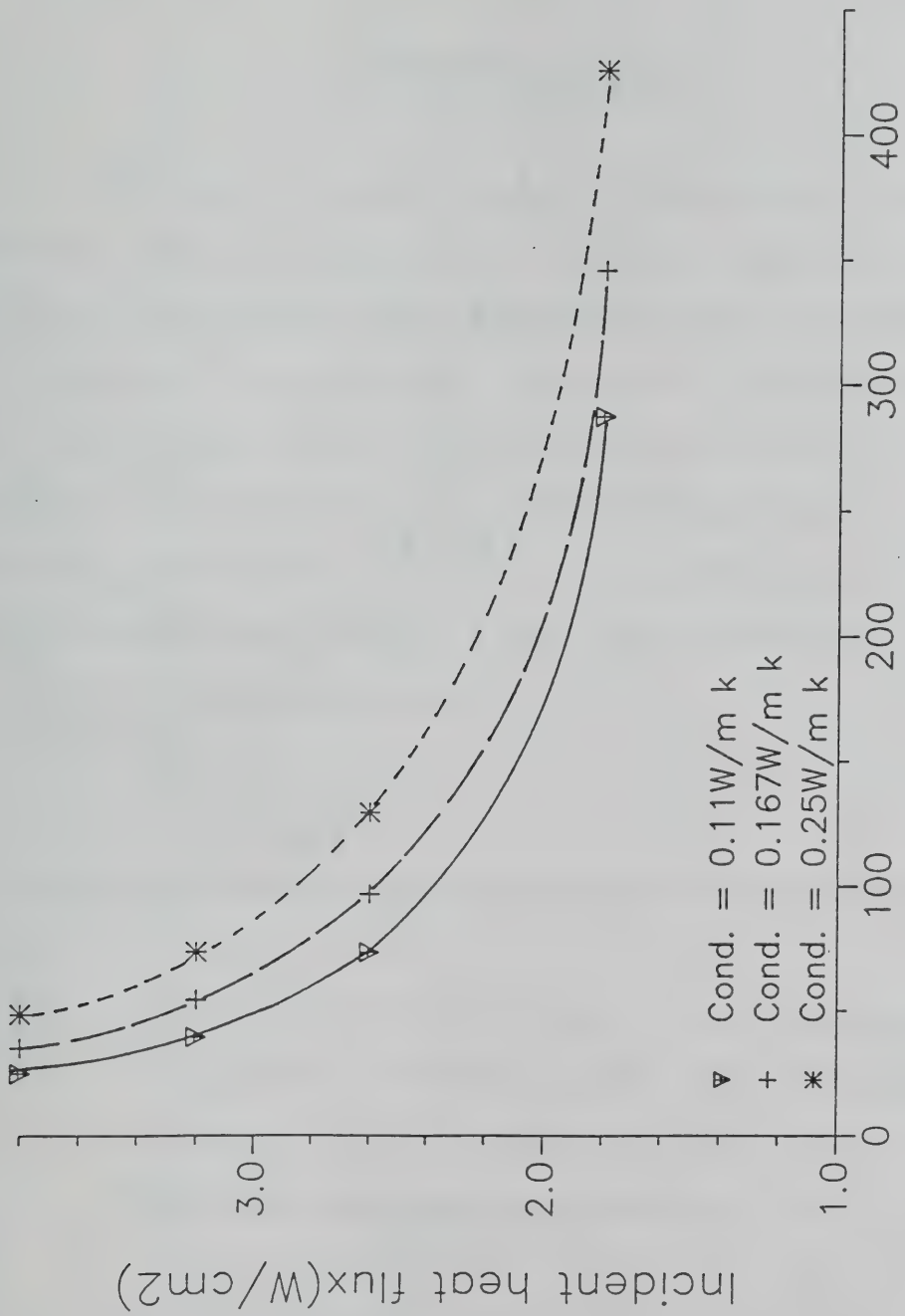

FIGURE 5-20 Effect of thermal conductivity on the ignition delay.

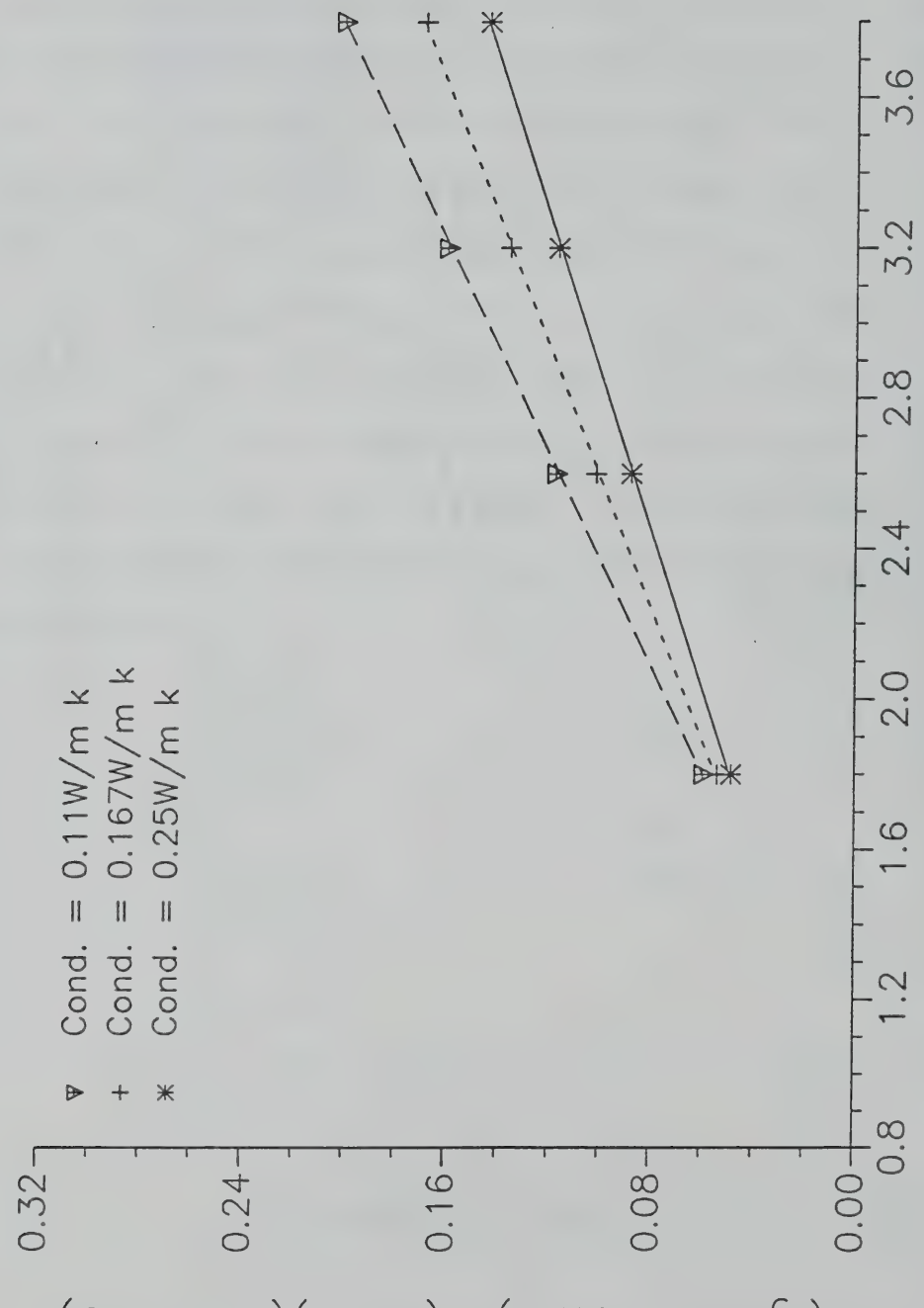

FIGURE 5-21 Plots of square root of ignition time vs heat flux for various thermal conductivity.

Chapter 6

Conclusions

This chapter presents a summary of the important results for different components of this thesis. Section 6.1 summarizes the conclusions of the analytical-numerical method for the chemical reacting flow, section 6.2 summarizes the conclusions of the analytical solution for the extinction of the steady-state diffusion flame, section 6.3 summarizes the conclusions of the one-dimentional model of piloted ignition, and section 6.4 summarizes the conclusions of the numerical simulation of piloted ignition of wood. Some recommedations for future work are presented in section 6.5.

6.1. Analytical-Numerical Method for the Chemically Reacting Flow

6.1.1. The required CPU time for the analytical-numerical method is less than for the implicit scheme. The explicit scheme for the chemical reaction scheme is fastest, but it is less stable when larger time steps are used.

6.1.2. The analytical-numerical scheme is very efficient for the piloted ignition problem. Piloted ignition involves both pre-mixed and diffusion flames. The pre-mixed flame requires very small time steps, while the time step for

diffusion flame can be O(100) times larger than for the pre-mixed flame. The implicit and explicit methods overflow very easily during the transition from pre-mixed flame to the diffusion flame, while the analytical-numerical method does not overflow.

6.2 Analytical Solution for the Extinction of the Steady-State Diffusion Flame.

The extinction limit for a steady diffusion flame can be derived by large activation energy asymptotics (AEA), which provides expressions for the ignition and extinction Damkoher number. By using a higher mass flux, the flame temperature and the flame Damkohler number are obtained; then by reducing the fuel mass evolution rate, the Damkohler number is again calculated. If the Damkolher number is smaller than the extinction Damkolher number, no solution for the diffusion flame exists, and the flame will be extinguished. The minimum fuel evolution rate for piloted ignition is very close to the analytical solution for the steady diffusion flame extinction limit (±10%).

6.3. One-dimensional Model of Pilot Ignition.

6.3.1 The simple one-dimensional numerical model of piloted ignition describes the basic strunture of the piloted ignition process, which includes a pre-mixed flame, the quenching of a flash,

and the development of a diffusion flame after the flash.

6.3.2 The minimum fuel evolution rate in itself is not sufficient to predict the onset of sustained piloted ignition, and the heat losses to the solid surface play an important role.

6.3.3 The optimum location of the ignition source is found to be the eventual location of the steady diffusion flame.

6.4 Theoretical Model of Pilot Ignition of Wood.

6.4.1. Although the thermal conductivity of wood is a function of the exposed heat flux, temperature, moisture content and density, the overall thermal conductivity can be determined by the least square fitting of the experimental surface temperature. The curve fitting uses the analytical solution for the surface temperature of wood derived by Atreya (1983); the calculated thermal conductivity of dry Douglas fir is within the range of values listed in the literature.

6.4.2. The integral analytical solution for the fuel mass production rate in the initial stages of decomposition can be used to determine the pre-exponential factor of the pyrolysis of wood by using the least square fitting of experimental measured mass flux around piloted ignition. The predicted pre-exponential factor for dry Douglas fir is within the

range of values listed in the literature. Since the analytical solution is only valid for the initial stage of decomposition, this model cannot be used for lower heat flux where ignition delay is very large and a lot of char has been formed before piloted ignition.

6.4.3. By using the thermal conductivity obtained by the least square fitting, the analytical solution can predict the experimental surface temperature of wood very accurately.

6.4.4. This numerical model for the piloted ignition of wood can predict the flashes, the quenching and sustained piloted ignition. For lower heat flux, the period of flashes and quenching is longer, while for higher heat fluxes, the flashes and the quenching are not so obvious.

6.4.5. During the flash-quenching period, the fuel evolution rate is much lower than the minimum fuel evolution rate of the steady state diffusion flame, whereas at sustained piloted ignition the fuel evolution rate is very close to the minimum fuel evolution rate. This leads us to believe that conditions for piloted ignition for wood are quite similar to those for extinction of a diffusion flame.

6.4.6. The assumption that the fuel evolute from the solid wood is the same as pure methane underestimates the ignition delay, the ignition surface temperature, and the ignition

mass evolution rate. The predicted ignition delay is about 30% lower than the experimental value, the predicted ignition surface temperature is about 15% lower than the experimental ignition surface temperature, while the predicted mass evolution rate only about 1/5 to 1/7 of the experimentally observed value.

6.4.7 The assumption that the fuel evoluted from the solid wood is 25% methane and 75% inert gas (by mass) enables the experimental ignition delay, the ignition surface temperature and the ignition mass evolution rate to be accurately predicted. From the experimental observations, the gas flow out of the solid in the early stages of pyrolysis is primarily water vapor, CO_2 CO, CH_4, and higher hydrocarbons; it is evident that the concentration of total hydrocarbons and CO is very low at piloted ignition. Both the surface temperature and fuel evolution rate are very important for the piloted ignition, but the dilusion of the fuel is also a very important factor.

6.4.8 The study of the effect of O_2 concentration and ambient air velocity shows that higher air velocities and lower O_2 concentrations increases the ignition delay and increase the minimum heat flux for piloted ignition. This result is agreement with the experimental observation of Abu-zaid (1988).

6.4.9 The study of the effect of moisture content shows that a higher moisture content increases the ignition delay without altering the minimum heat flux for ignition.

6.4.10 The model which use the analytical solution for the wood pyrolysis equations [derived by Atreya and Wichman (1989)] predicts an ignition delay at high heat flux (greater than 2.6 W/cm^2) very close to that calculated from a model which solves the pyrolysis equations numerically. At lower heat fluxes (less than 2.0 W/cm^2), the ignition delay predicted by the analytical solid solution model is only 1/3 of the value predicted by the numerical solid-phase model. The plot of $(t\ ignition)^{-0.5}$ vs heat flux shows that the numerical solid phase model obtains closer value of minimum heat flux for piloted ignition to the experimental observation of Abu-zaid (1988). The analytical solid phase model underestimates the minimum heat flux for piloted ignition.

6.4.11 A sensitivity analysis shows that:

A. The activition energy for thermal decompostition of wood is very important for the prediction of piloted ignition. An O(10%) change in the activation energy makes an O(100%) change in the ignition delay. The plot of $(t\ ignition)^{-0.5}$ vs heat flux shows that the curves for different activation energies have similar slopes, but that the minimum heat fluxes for piloted ignition are different. An O(10%)

increase in the activation energy makes an O(50%) increase in the minimum heat flux.

B. The frequency factor is very important for the prediction of piloted ignition, but is less sensitive than the activation energy. An increase in the frequency factor reduces the ignition delay. The plot of $(t_{ignition})^{-0.5}$ vs heat flux shows that the curves for different frequency factors have the same slope, but the minimum heat flux for pilot ignition is different. (This trend is similar to the effect of activation energy). The effect of a factor of 10 increase in the frequency factor is similar to reducing the activation energy by 10%.

C. The thermal conductivity is very important for the prediction of piloted ignition; the higher thermal conductivity, the larger the ignition delay. The effect of thermal conductivity on the ignition delay is different from the activation energy. The plot of $(t_{ignition})^{-0.5}$ vs heat flux shows that the lines with higher thermal conductivity have a lower slope, and that a higher thermal conductivity produces lower minimum heat fluxes for piloted ignition.

6.4.12 A new definition of piloted ignition is proposed in this work. It is found that the development of a sustained diffusion flame after the pre-mixed flash successfully predicts the experimentally measured ignition delay, ignition surface temperature, ignition mass flux and minimum fuel flow

rate for piloted ignition. This model is helpful in clearifying important parameters for piloted ignition that are not easy observed from the experimental data. (such as quenching effect, location of ignition source, thermal conductivity of wood and activation energy of wood).

6.5. Recommandation for the Future Work

In the present model of piloted ignition, the chemical reaction in the gas phase is assumed to be a one-step irreversible chemical reaction. In some pratical experimental observations, the one-step chemical reaction is too simple and multistep chemical reactions may produce more accurate results. Besides, the composition pyrolysis products are very complex, a great deal of CO and water vapor are contained in the pyrolyzate; thus, a multistep chemical scheme would give a better representation for the effect of water vapor and CO during piloted ignition.

For the time being, the piloted ignition model in the gas phase is one-dimensional. The actural gas phase in the boundary layer is two dimensional. Since piloted ignition involves pre-mixed flames, and since the pre-mixed flame thickness is very small (only about 0.1mm), the grid spacing should be smaller than the flame thickness. A two-dimensional model for the gas phase would be more practical, but such a model might require a more powerful tool, such as a super computer.

Appendix A

A COMBINED ANALYTICAL-NUMERICAL SOLUTION PROCEDURE FOR CHEMICALLY-REACTING FLOWS

A.1. INTRODUCTION

The possibility of exploiting the often vastly different time scales for chemical reaction [$O(10^{-3}$ sec)] and for the subsequent convection and diffusion of this chemical release into the flow field [O(1 sec)] appears to have been first discussed physically by Baum and Corley(1981). (A more detailed history of the "operator-splitting" method is given in the recent study of Wichman (1990)). In their short work Baum and Corley (1981) analyzed the laminar mixing of fuel and oxidizer streams in a plane channel flow for arbitrary Lewis numbers, and for <u>two</u> reaction models; (1) delta-function heat release, and (2) one-step Arrhenius kinetics. For (2), the solution is obtained by dividing each streamwise marching step into two parts. In the first part, a locally homogeneous rate chemistry problem is solved by quadratures (for (1) the analytical solution of this part is trivial). This solution is then applied as a (local) initial condition for the second part, in which this heat release is transported by convection and diffusion to the neighboring fluid elements. Thus, the solution is

obtained by an "operator-splitting" procedure.

The purpose of the present study is to develop a rational motivation for the use of the operator-splitting procedure in combustion theory by analyzing a simple model problem in some detail. A numerical scheme that is consistent with this model is then applied to a simple premixed laminar flame model that has been previously employed as a test for various numerical integration schemes [Peters (1982)], such as the method of lines, adaptive grids explicit and implicit schemes.

A.2. The Model Problem

Consider a purely thermal model, for which the gas-phase energy balance is represented by transient, diffusion and heat-release terms. When properly nondimensionalized, the coefficients of the transient and diffusive terms are unity, while the heat-release term contains the factor $D = \Delta t_d/(\Delta t_c)$, called the Damkohler number. Here Δt_d is the characteristic diffusion (or convection) time, while Δt_c is the characteristic reaction time. Thus, we consider the following initial boundary-value problem,

$$\left.\begin{aligned} &\frac{\partial T}{\partial t} = \frac{\partial^2 T}{\partial x^2} + DQ(x,t), \qquad -\infty < x < \infty,\ t > 0 \\ &T(-\infty,t) = T(\infty,t) = 0, \\ &T(x,t_o) = T_o(x). \end{aligned}\right\} \qquad \text{(A-1)}$$

Note that the heat-release term (analogous to the chemical reaction term

in the combustion equations) is written as a simple function of x and t. The solution for $T(x,\Delta t)$ can therefore be obtained from the solution at the previous time step t_o from the equation (we put $t_o = 0$ with no loss of generality)

$$T(x,\Delta t) = -\int_0^{\Delta t}\int_{-\infty}^{\infty} G(x,\Delta t|\xi,\tau)[DQ(\xi,\tau)]d\xi d\tau - \int_{-\infty}^{\infty} T_o(\xi)\, G(x,\Delta,t|\xi,0)d\xi, \quad \text{(A-2)}$$

where

$$G(x,\Delta t|\xi,\tau) = -\frac{1}{2\sqrt{\pi(\Delta t - \tau)}}\, EXP[-\frac{(\xi - x)^2}{4(\Delta t - \tau)}] \quad \text{(A-3)}$$

is the Green's function for equation (A-1). The first term in equation(A-2) describes the influence of the inhomogeneous reaction term, while the second term describes the redistribution of energy from the previous time step by the homogeneous diffusion operator $\partial(\bullet)/\partial t - \partial^2(\bullet)/\partial x^2 = 0$. Note that the second term does not contain Q.

The difficulty with obtaining numerical solutions of equations such as equation (A-1) arises from the largeness of D. This usually necessitates taking very small time steps, of order Δt_c. Rational means for avoiding this requirement (and therefore speeding up the computation substantially) are sought by analyzing equation (A-2) as $D \to \infty$.

In order that all three terms in equation (A-2) balance as $D \to \infty$, the time interval Δt in the first integral must become very small; in fact, Δt must be of order $D^{-1} \approx \Delta t_c$. Thus, by defining $s = D\tau$ as a new O(1) variable of integration, one finds, as $D \to \infty$,

$$T(x,\Delta t) \doteq - D\Delta t \int_{-\infty}^{\infty} G(x,\Delta t|\xi,0)Q(\xi,0)d\xi - \int_{-\infty}^{\infty} T_o(\xi)G(x,\Delta t|\xi,0)d\xi, \quad \text{(A-4)}$$

where Δt is now $0(\Delta t_c)$. For very small Δt the Green's functions in (A-4) reduce to the Dirac delta function $-\delta(\xi-x)$, whereby

$$T(x,\Delta t \leq \Delta t_c) \doteq \Delta t\, DQ(x,0) + T_o(x), \quad \text{(A-5)}$$

which is valid for $\Delta t \leq \Delta t_c \approx D^{-1}$.

For the remainder of the time step a finite solution for T is possible only if $Q(x,t \geq \Delta t_c) = 0$. This means that equation (A-1) describes a transport-limited process (convection, or diffusion, or both), in which an increment of combustible gas is transported to the reaction zone, where it reacts "instantaneously", thereby producing heat and depleting the increment of combustible gas. The heat generated by reaction is transported away from the reaction zone, and further reaction cannot occur [i.e., Q is now zero] until another increment of combutible gas has been transported into the reaction zone. Thus, the overall time interval for this process is approximately one characteristic transport time Δt_d [i.e., $\Delta t \approx \Delta t_d$ in equation(A-2).] Since chemical reaction and heat release occur at the beginning of this time interval, equation (A-5) may be used as an initial condition for the calculation of the change in T over the remainder of the time step. Thus, equation (A-2) gives

$$T(x,\Delta t) \simeq - \int_{-\infty}^{\infty} T(x,\Delta t_c)G(x,\Delta t|\xi,0)d\xi, \quad \text{(A-6)}$$

where $T(x,\Delta t_c)$ is given by equation (A-5), and G may be evaluated at $\Delta t = 0$ instead of at $\Delta t = \Delta t_c$.

In sum, the solution of equation (A-1) over the time interval Δt can be obtained by first solving the spatially-homogeneous equation $\partial T/\partial t = DQ$, giving $T(x,\Delta t_c) = T_o(x) + \Delta t_c\ DQ(x,0)$[which is equation (A-5)], and then using this as a modified initial condition for the solution over the remainder of the time step. Then one solves $\partial T/\partial t = \partial^2 T/\partial x^2$, obtaining equation (A-6).

The preceding physical and mathematical discussion implies that this integration procedure can be implemented wherever the local reaction rate quickly consumes the local <u>excess</u> combustible. If this were not the case, then the proposed integration scheme could be applied only to diffusion flames with infinitely fast chemistry in infinitesimally thin reaction zones. In general, computational methods are unnecessary for such problems. Consequently, this integration procedure is expected to apply for diffusion flames with "slow" chemistry <u>and</u> premixed flames; for diffusion flames the excess component is fuel or oxidizer, while for premixed flames it is the combustible mixture itself. Such a general level of applicability is important because most currently challenging problems in combustion theory involve flames of mixed character. Therefore, the first test of this solution procedure is a premixed-flame-speed calculation.

A.3. <u>The Premixed Laminar Flame</u>

The premixed flame equations solved here are

$$\left.\begin{aligned} &\text{i)}\ \frac{\partial T}{\partial t} = \frac{\partial^2 T}{\partial x^2} + DR \quad ; \quad R = Y\ \mathrm{EXP}\left[-\frac{\beta(1-T)}{1-\alpha(1-T)}\right] \\ &\text{ii)}\ \frac{\partial Y}{\partial t} = \frac{1}{\mathrm{Le}}\frac{\partial^2 Y}{\partial x^2} - DR, \end{aligned}\right\} \qquad \text{(A-7)}$$

where β is the Zeldovich number, and D is the "Damkohler number". Over the reaction time interval one solves $\partial T/\partial t = DR$, $\partial Y/\partial t = -DR$. The Schvab-Zeldovich procedure gives $Y = C(x) - T$, thereby requiring the solution of only one nonlinear equation, viz.,

$$\frac{\partial T}{\partial t} = D(C(x) - T)\mathrm{EXP}\left[-\frac{\beta(1-T)}{1 - \alpha(1 - T)}\right] \qquad \text{(A-8)}$$

This equation was integrated with a fourth-order Runge-Kutta scheme over the <u>entire</u> time step, Δt, giving $T_i^{n+1} = T_{ih}^{n}$, $Y_i^{n+1} = Y_{ih}^{n}$, which were then used as augmented (local) initial conditions for the final calculation of T_i^{n+1}, Y_i^{n+1} from the homogeneous diffusion equations [put $R = 0$ in Eqs. (A-7)]. This calculation employed a simple (implicit) centered-difference scheme, viz.,

$$\left.\begin{aligned} &\text{i)}\ T_i^{n+1} - \alpha\left[T_{i+1}^{n+1} - 2T_i^{n+1} + T_{i-1}^{n+1}\right] = T_{ih}^{n} \\ &\text{ii)}\ Y_i^{n+1} - \frac{\alpha}{\mathrm{Le}}\left[Y_{i+1}^{n+1} - 2T_i^{n+1} + Y_{i-1}^{n+1}\right] = Y_{ih}^{n} \end{aligned}\right\} \qquad \text{(A-9)}$$

where $\alpha = \Delta t/\Delta x^2$.

The parameter values used were Le = (0.5, 1.0), β = (10,20), Δx = (0.25, 0.1, 0.0625), and Δt = (0.0005, 0.001, 0.002, 0.005, 0.01, 0.02, 0.05). Note that asymptotic analysis gives $D = \beta^2/2\mathrm{Le}$; note also

that $\beta^2/2Le \gg 0(1)$, as required for the anaylsis of Sec. II.

A.4. Benefit of the Analytical-Numerical Method

The numerical integration scheme of Sec. III was compared to the flame-speed calculations presented in the GAMM workshop [Peters (1982)], and to calculations of the same problem using an explicit numerical scheme[1] and an implicit numerical scheme (iterate with the reaction term). An example of these latter comparisons is shown in Table 1 for the case Le = 0.5, β = 10. The numerical scheme of Sec. III converges to a solution in all cases, whereas the other schemes develop convergence and overflow problems. The required CPU time is less than for the implicit scheme, though the explicit method is fastest when it works. In multiple space dimensions it is believed that this method will be much quicker and easier to implement than other, more sophisticated algorithms. In addition, flames of mixed (diffusion/premixed) character are not expected to produce excessive computational difficulties.

Remarks: [1]. The scheme of Sec. III is essentially "adiabatic", while the explicit scheme is "constant temperature". Therefore, they represent, in a sense, thermodynamic extremes. Explicit schemes have also been used by Reitz(1981).

Table A-1: Flame= Velocity for Le=0.5, β=10, V=flame velocity, N=number of time step calculated, (CPU time, by Digital micro VAX II, unit sec).

	t = 0.001	0.002	0.005	0.01	0.02	0.05	0.1
Δx=0.25	method 1, case 1						
	V=0.962	V=0.960	V=0.945	V=0.944	V=0.927	V=0.850	V=0.624
	N=900	N=450	N=150	N=100	N=120	N=40	N=40
	CPU 173.04	88.54	32.17	22.98	46.28	37.79	70.54
	method 2, case 1	V=0.965	V=0.965	V=0.959	not		
		N=900	N=450	N=150	convergent		
	CPU	204.66	172.91	162.76			
	method 3, case 1	V=0.964	V=0.963	V=0.954	V=0.938	V=0.952	over
		N=900	N=450	N=150	N=240	N=50	
	CPU	39.67	21.69	10.32	13.63	6.22	
Δx=0.10	method 1, case 2						
	V=0.962	V=0.960	V=0.951	V=0.936	V=0.907	V=0.852	V=0.777
	N=900	N=450	N=150	N=60	N=30	N=40	N=40
	CPU 425.34	214.73	74.74	32.25	30.56	87.87	169.94
	method 2, case 2	V=0.965	V=0.966	V=0.968	not		
		N=900	N=450	N=150	convergent		
	CPU	584.5	429.57	284.78			
	method 3, case 2	V=0.964	V=0.964	V=0.961	V=0.955	V=0.945	over
		N=900	N=450	N=150	N=60	N=30	flow
	CPU	92.4	48.32	18.7	9.95	6.69	
Δx=0.063	method 1, case 3						
	V=0.962	V=0.959	V=0.952	V=0.936	V=0.906	V=0.853	V=0.777
	N=900	N=450	N=150	N=60	N=30	N=40	N=40
	CPU 678.98	341.2	117.27	49.53	46.19	138.48	269.18
	method 2, case 3	V=0.965	V=0.965	V=0.965	not		
		N=900	N=450	N=150	convergent		
	CPU	792.4	498.34	286.5			
	method 3, case 3	V=0.963	V=0.963	V=0.960	V=0.954	V=0.944	over
		N=900	N=450	N=150	N=60	N=30	flow
	CPU	146.12	74.9	27.71	13.71	9.17	

Remarks:
1. V=0.944 (analytical solution)
2. Method 1, analytical numerical method.
3. Method 2, Implicit method.
4. Method 3, Explicit the chemical reaction term and implicit for the convection diffusion term.

APPENDIX B

PROGRAM LISTING FOR THE PILOT IGNITION MODEL

```
C     ************************************************************************
C     COMPUTER MODEL FOR THE PILOT IGNITION OF WOOD
C                          by: Lin-Shyang Tzeng
C                              FIRDI in Taiwan
C                          P. O. Box 246 Hsinchu 300,Taiwan R. O. C.
C                           SEPTEMBER 1990
C     ************************************************************************
C     The following five lines is the example of input data (see next page
C     under C "input data")
C 0.0276 0.0000276 0.000276 0.00666 0.0037 0.00666 0.02 0 0 0 .218 1.0 1.657
C 0.866 9.59 18.2 3.33E7 0.25 3.8 2.00 298. 0.6 0.197 6.0E7 .75 0.232
C 48000 560 110 21 221 241 3 40 10 0 241 20 1 0
C 0.135 1.657 0.69 0.07 0.01 31.0
C PNM1F38.DAT
C The case shown above is in the file named PNM1F38.DAT
C     combined analytical & numerical method
C     solve chem reac. analytically when T(I). gt. 0.95
C     including the surface temp.
C     solve the solid equation numerically
C     not dumping the data after turn on the ignition source
```

```
C     Le number not = 1.
      PROGRAM ONEDPISN
      COMMON T(401),YF(401),YO(401),XX(401),A(6),B(6),D(6),N,NDUM
     1,NIGS,DTOD,IM,IN,IO,NODUF,TIME,DT,IFLAG,IDUMP,HL,NMAX,SMA
     1,I,DT1,DT2,DT3,CF,CO,AF,BT,Q,DA,FS,REAC,CLA,CSM,STP
     1,AFU(6),DF(6),BF(6),YFS
      COMMON/WDATA/WTD(451),WTDO(451),WAMD(451),WAMDO(451),WDN(451)
     1   ,WDNA(451),WDNC(451),WHCP(451),WCND(451),WA(451),WD(451),SIGM
     1   ,WD1(451),WDNO(451),WB(451),WR(451),DNWF,DNF,HCPA,HCPC,CNDC
     1   ,WDX,WTIME,EACT
      DIMENSION TOD(401),YFOD(401),YOD(401),TTD(401),YFTD(401)
     1,YOTD(401)
      DOUBLE PRECISION WDN,WDNO,WDX
      CHARACTER*16 SFTPDAT
      OPEN(UNIT=10,FILE='IGDUFLN.DAT',TYPE='NEW')
      OPEN(UNIT=11,FILE='DAISN.DAT',TYPE='OLD')
      OPEN(UNIT=12,FILE='OUPTN.DAT',TYPE='NEW')
      OPEN(UNIT=13,FILE='HTFXN.DAT',TYPE='NEW')
C     IGDUFLN.DAT data for check if there is ignition
C     DAISN.DAT input data file
C     OUPTN.DAT file for temperature and species profile
C     HTFXN.DAT file for wave of heat flux
C     input data
      READ(11,*)DT,DT2,DT3,DX1,DX2,DX3,SM1,SM2,ST1,ST2,YFS,RLE
      READ(11,*)AF,BT,Q,DA,FS,HSF,CVF,TAMB,DNS,RKK,APS,EPSL,YOS
      READ(11,*)NMAX,NIG,IG,IM,IN,IO,IGN,NDUP,NHS,NW,IDUMP,NCH,M
      READ(11,*)DNF,HCPA,HCPC,CNDC,WDX,EACT
```

```
      READ(11,2400)SFTPDAT
 2400 FORMAT(A16)
      OPEN(UNIT=14,FILE=SFTPDAT,TYPE='NEW')
      WRITE(14,*)DT,DT2,DT3,DX1,DX2,DX3,SM1,SM2,ST1,ST2,YFS,RLE
      WRITE(14,*)AF,BT,Q,DA,FS,HSF,CVF,TAMB,DNS,RKK,APS,EPSL,YOS
      WRITE(14,*)NMAX,NIG,IG,IM,IN,IO,IGN,NDUP,NHS,NW,IDUMP,NCH,M
      WRITE(14,*)DNF,HCPA,HCPC,CNDC,WDX,EACT
      WRITE(14,2500)SFTPDAT
 2500 FORMAT(1X,A16)
C     DT = time step of no chem. react.
C     DT2 = time step of premixed flame
C     DT3 = time step of diffusion flame
C     DX1 = grid space near the surface
C     DX2 = grid space in the middle area
C     DX3 = grid space near the upper surface
C     SM1 = const fuel flow rate
C     SM2 = coeff. of linear fuel flow rate
C     ST1 = constant surface temp.
C     ST2 = coeff. of linear surface temp.
C     SM1,SM2,ST1,ST2 in this program are only dummy variable
C     YFS = fuel concentration in the solid phase
C     RLE = Lewis number
C     AF = non-dimensional flame temperature
C     BT = non-dimensional activation energy of fuel
C     Q = non-dimensional heat of reaction of fuel
C     DA = Damkohler number
C     FS = stoichiometry ratio
```

```
C     HSF =  radiation heat flux imposed on the wood
C     CVF = convection heat transfer coeff. (W/m2 k)
C     TAMB = ambient temperature k
C     DNS = density of wood g/cm3
C     RKK = thermal conductivity of wood W/m k
C     APS = pre-exponential factor of pyrolysis of wood
C     EPSL = surface emissivity
C     YOS = oxygen concentration of ambient air
C     NMAX = maximum number of step
C     NIG = number of time step to turn on the ignition source
C     IG = grid location of the ignition source
C     IM = number of the grid near the surace
C     IN = number of the grid in the middle area
C     IO = total number of the grid
C     IGN = number of grids for ignition source
C     NDUP = number of step between calling subroutine DUMP
C     NHS = number of step between turn on the ignition source
C     NW = flag to control if write down data of temp. fuel and time
C     IDUMP = number of data grids to be dumped
C     NCH = interval of step to write down the surface temp. with respect
C     to time.
C     M = number of step to calculate the chemical reaction term
C     DNF = final char density
C     HCPA = specific heat of active wood
C     HCPC = specific heat of char
C     CNDC = thermal conductivity of char
C     WDX = grid space of wood
```

```
C     EACT =  activation energy of wood (kcal/g mole)
C     DX1*(IM-1)+DX2*(IN-IM)+DX3*(IO-IN) = 1.00 for boundary layer thickness
C     = 1.5 cm
      TRES=0.0011
      TMAX=(DT+DT3)*0.5*NMAX+1.5
C     initial condition
      DO 100 I=1,IO
       T(I)=0.
       YF(I)=0.
       YO(I)=YOS
  100 CONTINUE
C     coefficient of matrix and boundary cond.
      B(1)=0.
      A(1)=(-1.)/DX1
      AFU(1)=-1./(DX1*RLE)
      NIGA=0
      NIGB=0
      NIGS=0
      NDUM=0
      NODUF=0
      NTD=0
      NTD1=0
      MA=0
      NIGT=NIG
      DTTD=DT
      NDUPTD=NDUP
      NHSTD=NHS
```

```
      IIGN=IG+(IGN/2)
      TIGPS=0
      DTOD=DT
      TIME=DT
      ERRO1=0.0
      ERRO=1.E-8
      N=1
      IFLAG=0
      INOWR=0
C     specify the x-coordinate XX(I) (Variable grid)
      XX(1)=0.
      DO 102 I=2,IM
       XX(I)=XX(I-1)+DX1
  102 CONTINUE
      DO 104 I=IM+1,IN
       XX(I)=XX(I-1)+DX2
  104 CONTINUE
      DO 106 I=IN+1,IO
       XX(I)=XX(I-1)+DX3
  106 CONTINUE
C     send data to temporary file
  110 CONTINUE
      DO 108 I=1,IO
       TOD(I)=T(I)
       YFOD(I)=YF(I)
       YOD(I)=YO(I)
  108 CONTINUE
```

```
C     start the new time step
  111 CONTINUE
      IF(TIME.GT.TMAX) GO TO 400
      IF((MA-M).GT.2) GO TO 150
      NCH1=(N/NCH)*NCH*NW
      NCH2=(N/NCH)*NCH
      IF(N.EQ.NCH1) WRITE(13,1100)TIME,T(2),T(IG)
     1,T(IN),YF(2),YF(IG),YF(IN),YO(2),YO(IG),YO(IN)
      CALL SFTN(SMA,STP,DT,TIME,HSF,CVF,TAMB,DNS,RKK,APS,EPSL,N)
      IF(N.EQ.NCH2) THEN
C     locate the max temp
      IDUF=2
      TDUF=0.
      DO 40 I=2,IO-1
       IF(T(I).GT.TDUF) GO TO 30
       GO TO 40
   30  CONTINUE
       IDUF=I
       TDUF=T(I)
   40 CONTINUE
      TISEC=TIME/0.55187
      WRITE(14,2200)TISEC,SMA,T(4),T(1),TDUF,IDUF,N
      END IF
 2200 FORMAT(1X,'tsec,SMA,ST21,TPM,I,N=',F9.4,4F9.5,1X,I4,1X,I5)
      IF(SMA.GT.2.) GO TO 400
      T(1)=STP
      YF(1)=SMA*YFS
```

```
 YO(1)=0.
 D(1)=SMA+(1./DX1)
 A(2)=DT*((SMA/DX1)-(1./(DX1**2)))
 D(2)=1.-(SMA*DT/DX1)+(2.*DT/(DX1**2))
 B(2)=(-1.)*DT/(DX1**2)
 A(3)=SMA*DT/DX2-2.*DT/((DX1+DX2)*DX2)
 D(3)=1.+2.*DT/((DX1+DX2)*DX2)+2.*DT/((DX1+DX2)*DX1)
1-SMA*DT/DX2
 B(3)=(-2.)*DT/((DX1+DX2)*DX1)
 A(4)=(SMA*DT/DX2)-DT/(DX2**2)
 D(4)=1.-(SMA*DT/DX2)+(2.*DT/(DX2**2))
 B(4)=(-1.)*DT/(DX2**2)
 A(5)=SMA*DT/DX3-2.*DT/((DX2+DX3)*DX3)
 D(5)=1.+2.*DT/((DX2+DX3)*DX3)+2.*DT/((DX2+DX3)*DX2)
1-SMA*DT/DX3
 B(5)=(-2.)*DT/((DX2+DX3)*DX2)
 A(6)=(SMA*DT/DX3)-DT/(DX3**2)
 D(6)=1.-(SMA*DT/DX3)+(2.*DT/(DX3**2))
 B(6)=(-1.)*DT/(DX3**2)
 DF(1)=SMA+(1./(DX1*RLE))
 AFU(2)=DT*((SMA/DX1)-(1./((DX1**2)*RLE)))
 DF(2)=1.-(SMA*DT/DX1)+(2.*DT/((DX1**2)*RLE))
 BF(2)=-1.*DT/((DX1**2)*RLE)
 AFU(3)=SMA*DT/DX2-2.*DT/(((DX1+DX2)*DX2)*RLE)
 DF(3)=1.+2.*DT/(((DX1+DX2)*DX2)*RLE)+2.*DT/(((DX1+DX2)*DX1)*
1 RLE)-SMA*DT/DX2
 BF(3)=-2.*DT/(((DX1+DX2)*DX1)*RLE)
```

```
      AFU(4)=(SMA*DT/DX2)-DT/((DX2**2)*RLE)
      DF(4)=1.-(SMA*DT/DX2)+(2.*DT/((DX2**2)*RLE))
      BF(4)=-1.*DT/((DX2**2)*RLE)
      AFU(5)=SMA*DT/DX3-2.*DT/(((DX2+DX3)*DX3)*RLE)
      DF(5)=1.+2.*DT/(((DX2+DX3)*DX3)*RLE)+2.*DT/(((DX2+DX3)
     1 *DX2)*RLE)-SMA*DT/DX3
      BF(5)=-2.*DT/(((DX2+DX3)*DX2)*RLE)
      AFU(6)=SMA*DT/DX3-DT/((DX3**2)*RLE)
      DF(6)=1.-(SMA*DT/DX3)+(2.*DT/((DX3**2)*RLE))
      BF(6)=-1.*DT/((DX3**2)*RLE)
C     calculate the homogeneous chemical reaction
      DT1=DT/M
      MA=M
      DO 140 I=2,IO-1
C     assume that if T(I). less 1.E-12 ,then no chem reac.
      IF(T(I).LT.1.E-12) GO TO 140
      IF(T(I).GT.0.95) GO TO 112
       GO TO 113
  112  CONTINUE
       CF1=Q*YF(I)
       CO1=FS*Q*YO(I)
       CFO=CF1+CO1
       CLA=0.5*(CFO+ABS(CF1-CO1))
       CSM=CFO-CLA
       CF=CF1+T(I)
       CO=CO1+T(I)
       CALL AS
```

```
      GO TO 121
  113 CONTINUE
      CF=T(I)+(Q*YF(I))
      CO=T(I)+(FS*Q*YO(I))
      TB=T(I)
      IF(T(I).LT.0.2) GO TO 115
      CALL CHEM
      T(I)=TB+REAC
      IF((CF-T(I)).LT.ERRO.OR.(CO-T(I)).LT.ERRO) THEN
       T(I)=TB
       GO TO 112
      END IF
      GO TO 121
  115 CONTINUE
      DO 120 J=1,MA
       TA=T(I)
       CALL CHEM
       AR=REAC
       T(I)=TA+(0.5*AR)
       CALL CHEM
       BR=REAC
       T(I)=TA+(0.5*BR)
       CALL CHEM
       CR=REAC
       T(I)=TA+CR
       CALL CHEM
       T(I)=TA+((AR+2.*BR+2.*CR+REAC)/6.)
```

```
      IF((CF-T(I)).LT.ERRO1.OR.(CO-T(I)).LT.ERRO1) THEN
      T(I)=TB
      GO TO 112
      END IF
  120 CONTINUE
  121 CONTINUE
      YF(I)=(CF-T(I))/Q
      YO(I)=(CO-T(I))/(FS*Q)
  140 CONTINUE
C     solve the temperature and species equation
      CALL SY
      IF(IFLAG.EQ.2) GO TO 150
      GO TO 160
  150 CONTINUE
      IF(INOWR.EQ.1) GO TO 152
      WRITE(10,*)'IFLAG,N,DT=',IFLAG,N,DT
  152 CONTINUE
      IFLAG=0
      DT=DT/2.
      NDUP=NDUP*2
      NHS=NHS*2
      NTD1=N+20
      MA=0
      DO 155 I=1,IO
       T(I)=TOD(I)
       YF(I)=YFOD(I)
       YO(I)=YOD(I)
```

```
  155 CONTINUE
      GO TO 110
  160 CONTINUE
C     check if there is ignition
      IF(N.LT.NIG) GO TO 200
      GO TO 210
  200 N=N+1
      TIME=TIME+DT
      GO TO 110
  210 CONTINUE
      IF(NIGS.EQ.1) GO TO 217
      IF(N.LE.NIGT) GO TO 213
      IF(T(IIGN).LT.0.15) GO TO 211
      IF((TIME-TIMETD).GT.TRES.AND.T(IIGN).LT.0.2) GO TO 211
      IF((N-NIGT).GT.4500.AND.T(IIGN).GT.0.4) GO TO 400
      GO TO 213
C     not dump data, that pick the data at N=N+1
  211 CONTINUE
      NHS=NHSTD
      NIGT=N+NHS
      N=N+1
      DT=DTTD
      NDUP=NDUPTD
      TIME=TIME+DT
      INOWR=0
      NCH=NCH/40
      GO TO 110
```

```
213 CONTINUE
    IF((N-220).GT.NTD)DT=DT3
    DO 214 I=2,IG
     IF(T(I).GT.1.0) THEN
     NIGS=1
     II=I
     WRITE(10,*)'pilot ign at n,t,i,T=',N,TIME,I,T(I)
     TIMETDS=TIMETD-DT1
     WRITE(10,*)'NTD,TIMETD=',NTD,TIMETDS
     WRITE(10,*)'T,YF,YO,at t,I=',TTD(II),YFTD(II),YOTD(II)
   1 ,TIMETDS,II
     WRITE(10,*)'T,YF,YO,at t,IG=',TTD(IG),YFTD(IG),YOTD(IG)
   1 ,TIMETDS,IG
     WRITE(13,*)'pilot ign at n,t,i,T=',N,TIME,I,T(I)
     WRITE(13,*)'NTD,TIMETD=',NTD,TIMETDS
     WRITE(13,*)'T,YF,YO,at t,I=',TTD(II),YFTD(II),YOTD(II)
   1 ,TIMETDS,II
     WRITE(13,*)'T,YF,YO,at t,IG=',TTD(IG),YFTD(IG),YOTD(IG)
   1 ,TIMETDS,IG
     END IF
214 CONTINUE
    DO 216 I=IG+IGN+1,IN
     IF(T(I).GT.0.99) THEN
     NIGS=1
     II=I
     WRITE(10,*)'pilot ign at n,t,i,T=',N,TIME,I,T(I)
     TIMETDS=TIMETD-DT1
```

```
      WRITE(10,*)'NTD,TIMETD=',NTD,TIMETDS
      WRITE(10,*)'T,YF,YO,at t,I=',TTD(II),YFTD(II),YOTD(II)
     1 ,TIMETDS,II
      WRITE(10,*)'T,YF,YO,at t,IG=',TTD(IG),YFTD(IG),YOTD(IG)
     1 ,TIMETDS,IG
      WRITE(13,*)'pilot ign at n,t,i,T=',N,TIME,I,T(I)
      WRITE(13,*)'NTD,TIMETD=',NTD,TIMETDS
      WRITE(13,*)'T,YF,YO,at t,I=',TTD(II),YFTD(II),YOTD(II)
     1 ,TIMETDS,II
      WRITE(13,*)'T,YF,YO,at t,IG=',TTD(IG),YFTD(IG),YOTD(IG)
     1 ,TIMETDS,IG
      END IF
  216 CONTINUE
  217 CONTINUE
      IF((N-400).GT.NTD) DT=DT3
      NB=(N/NDUP)*NDUP
      IF(NB.EQ.N) CALL DUMP
      IF(NB.EQ.N) WRITE(10,*)'N,DT=',N,DT
      IF(NIGS.EQ.1) GO TO 232
C     turn on the ignition source
      IF(N.EQ.NIGT)GO TO 220
      GO TO 232
  220 CONTINUE
      DO 225 I=1,IO
       TTD(I)=T(I)
       YFTD(I)=YF(I)
       YOTD(I)=YO(I)
```

```
  225 CONTINUE
      NTD=N+1
      NCH=NCH*40
      TIMETD=DT+TIME
C     if TDUF gt 0.28 not turn on ign source
      DT=DT2
      DO 230 I=1,IGN
       T(IG+I)=1.
  230 CONTINUE
  232 CONTINUE
      N=N+1
      TIME=TIME+DT
      IF(N.GT.NMAX) GO TO 400
      IF(N.EQ.NTD1) THEN
      DT=DT2
      NDUP=NDUPTD
      NHS=NHSTD
      INOWR=1
      END IF
      GO TO 110
  400 CONTINUE
      REWIND(UNIT=12)
      WRITE(10,*)'N,t,DT=',N,TIME,DT
      WRITE(12,*)'data for t,N=',TIMETD,NTD
      DO 410 I=2,IO
       WRITE(12,1200)I,XX(I),TTD(I),YFTD(I),YOTD(I)
  410 CONTINUE
```

```
 1100 FORMAT(' t,TFO2,IG,IN',F8.3,1X,9F5.2)
 1200 FORMAT(' I,X,T,YF,YO=',I5,1X,F11.4,3F7.4)
      NN=NMAX+450
      WRITE(12,*)'   NMAX+450=',NN
      WRITE(13;*)'   NMAX+450=',NN
      IF(IFLAG.EQ.1) WRITE(10,*)'IFLAG,N=',IFLAG,N
      CLOSE(UNIT=10)
      CLOSE(UNIT=11)
      CLOSE(UNIT=12)
      CLOSE(UNIT=13)
      STOP
      END
C     ***************************************
C     This subroutine is to calculate the solution of tri-diagonal matrix
      SUBROUTINE SY
C     ***************************************
      COMMON T(401),YF(401),YO(401),XX(401),A(6),B(6),D(6),N,NDUM
     1 ,NIGS,DTOD,IM,IN,IO,NODUF,TIME,DT,IFLAG,IDUMP,HL,NMAX,SMA
     1 ,I,DT1,DT2,DT3,CF,CO,AF,BT,Q,DA,FS,REAC,CLA,CSM,STP
     1 ,AFU(6),DF(6),BF(6),YFS
      DIMENSION DD(401),DD1(401),AA(401),BB(401)
      DO 10 I=2,IM-1
       DD(I)=D(2)
       AA(I)=A(2)
       BB(I)=B(2)
   10 CONTINUE
      DD(IM)=D(3)
```

```
      AA(IM)=A(3)
      BB(IM)=B(3)
      DO 20 I=IM+1,IN-1
       DD(I)=D(4)
       AA(I)=A(4)
       BB(I)=B(4)
   20 CONTINUE
      DD(IN)=D(5)
      AA(IN)=A(5)
      BB(IN)=B(5)
      DO 30 I=IN+1,IO-1
       DD(I)=D(6)
       AA(I)=A(6)
       BB(I)=B(6)
   30 CONTINUE
C     solve the temp equ.
      DD(1)=1.
      AA(1)=0.
      DD(IO)=1.
      BB(IO)=0.
C     solve by Gauss elimination
      DD1(1)=DD(1)
      DO 40 I=2,IO-1
       CC=BB(I)/DD1(I-1)
       DD1(I)=DD(I)-(CC*AA(I-1))
       T(I)=T(I)-(CC*T(I-1))
   40 CONTINUE
```

```
      DO 50 I=2,IO-1
       II=IO-I+1
       T(II)=(T(II)-AA(II)*T(II+1))/DD1(II)
       IF(T(II).LT.1.E-22)T(II)=0.
   50 CONTINUE
C     solve the fuel & Oxygen equ.
      DD(1)=DF(1)
      AA(1)=AFU(1)
      DD1(1)=DD(1)
      DO 52 I=2,IM-1
       DD(I)=DF(2)
       AA(I)=AFU(2)
       BB(I)=BF(2)
   52 CONTINUE
      DD(IM)=DF(3)
      AA(IM)=AFU(3)
      BB(IM)=BF(3)
      DO 54 I=IM+1,IN-1
       DD(I)=DF(4)
       AA(I)=AFU(4)
       BB(I)=BF(4)
   54 CONTINUE
      DD(IN)=DF(5)
      AA(IN)=AFU(5)
      BB(IN)=BF(5)
      DO 56 I=IN+1,IO-1
       DD(I)=DF(6)
```

```
      AA(I)=AFU(6)
      BB(I)=BF(6)
   56 CONTINUE
      DO 60 I=2,IO-1
      CC=BB(I)/DD1(I-1)
      DD1(I)=DD(I)-(CC*AA(I-1))
      YF(I)=YF(I)-(CC*YF(I-1))
      YO(I)=YO(I)-(CC*YO(I-1))
   60 CONTINUE
      DO 70 I=2,IO
      II=IO-I+1
      YF(II)=(YF(II)-AA(II)*YF(II+1))/DD1(II)
      YO(II)=(YO(II)-AA(II)*YO(II+1))/DD1(II)
      IF(YF(II).LT.1.E-22)YF(II)=0.
      IF(YO(II).LT.1.E-22)YO(II)=0.
   70 CONTINUE
      RETURN
      END
C     ****************************************
C     This subroutine is to dump the data
      SUBROUTINE DUMP
C     ****************************************
      COMMON T(401),YF(401),YO(401),XX(401),A(6),B(6),D(6),N,NDUM
     1 ,NIGS,DTOD,IM,IN,IO,NODUF,TIME,DT,IFLAG,IDUMP,HL,NMAX,SMA
     1 ,I,DT1,DT2,DT3,CF,CO,AF,BT,Q,DA,FS,REAC,CLA,CSM,STP
     1 ,AFU(6),DF(6),BF(6),YFS
      IA=IO/IDUMP
```

```
      HX=0.8299
      NDUM=NDUM+1
      IF(NDUM.GT.1.5) GO TO 20
      IF(NIGS.EQ.1) GO TO 5
      NDUM=0
      REWIND(UNIT=12)
    5 CONTINUE
      IF(NIGS.EQ.1) WRITE(10,*)'Pilot ignition at N,T=',N,TIME
      IF(NIGS.EQ.1) WRITE(13,*)'Pilot ignition at N,T=',N,TIME
      WRITE(12,*) '  N,TIME,DT=',N,TIME,DT
      DO 10 I=2,IO,IA
       HFX=HX*(T(I)-T(I-1))/(XX(I)-XX(I-1))
       WRITE(12,2000)I,XX(I),T(I),YF(I),YO(I),HFX
   10 CONTINUE
      GO TO 70
   20 CONTINUE
      IF(N.EQ.NMAX) GO TO 5
C     check if there is diffusion flame
      IDUF=2
      TDUF=0.
      DO 40 I=2,IO-1
       IF(T(I).GT.TDUF) GO TO 30
       GO TO 40
   30  CONTINUE
       IDUF=I
       TDUF=T(I)
   40 CONTINUE
```

```
      IF(TDUF.LT.0.28) THEN
      WRITE(10,*)'flame quenched at N,T=',N,TIME
      WRITE(13,*)'flame quenched at N,T=',N,TIME
      NDUM=0
      NIGS=0
      NODUF=0
      NMAX=N+25000
      REWIND(UNIT=12)
      GO TO 5
      END IF
      IF(((NDUM/20)*20).EQ.NDUM) GO TO 60
      IF(NODUF.EQ.1) GO TO 70
      NODUF=0
      CC=0.
      IF(TDUF.GT.0.6.AND.YO(1).LT.0.001) THEN
       DT=DT3
       NMAX=N+4500
       NODUF=1
      END IF
   60 CONTINUE
      IF(NODUF.EQ.0) GO TO 70
      WRITE(10,*)'There is a diffusion flame at'
      WRITE(10,*)'I,N,TIME=',IDUF,N,TIME
      WRITE(10,*)'SMA,STP=',SMA,STP
      WRITE(13,*)'There is a diffusion flame at'
      WRITE(13,*) 'I,N,TIME,DT=',IDUF,N,TIME,DT,'HX, J/CM2 S'
       I=IDUF
```

```
      HFX=HX*(T(I)-T(I-1))/(XX(I)-XX(I-1))
      WRITE(13,2000)I,XX(I),T(I),YF(I),YO(I),HFX
     WRITE(12,*) '  N,TIME,DT=',N,TIME,DT
     DO 65 I=2,IO,IA
      HFX=HX*(T(I)-T(I-1))/(XX(I)-XX(I-1))
      WRITE(12,2000)I,XX(I),T(I),YF(I),YO(I),HFX
  65 CONTINUE
  70 CONTINUE
2000 FORMAT(' I,X,T,YF,YO=',I5,1X,F11.4,3F7.4,F9.4)
     RETURN
     END
C    ****************************************
C    This subroutine is to calculate the chemical reaction rate
     SUBROUTINE CHEM
C    ****************************************
     COMMON T(401),YF(401),YO(401),XX(401),A(6),B(6),D(6),N,NDUM
    1 ,NIGS,DTOD,IM,IN,IO,NODUF,TIME,DT,IFLAG,IDUMP,HL,NMAX,SMA
    1 ,I,DT1,DT2,DT3,CF,CO,AF,BT,Q,DA,FS,REAC,CLA,CSM,STP
    1 ,AFU(6),DF(6),BF(6),YFS
      C1=1.-T(I)
     IF(T(I).LT.1.E-20) THEN
     GO TO 112
     END IF
      C2=BT*C1/(1.-AF*C1)
      IF(ABS(C2).GT.30.) GO TO 112
      C3=1./EXP(ABS(C2))
      IF(C2.LT.0.) C3=1./C3
```

```
      GO TO 114
  112 C3=0.
      IF(C2.LT.0.) IFLAG=1
  114 CONTINUE
      C4=C3*DT1/(FS*Q)
      REAC=DA*(CF-T(I))*(CO-T(I))*C4
      RETURN
      END
C     ********************************
C     This subroutine is to calculate the chemical reaction rate near
C     flame temperature
      SUBROUTINE AS
C     ********************************
      COMMON T(401),YF(401),YO(401),XX(401),A(6),B(6),D(6),N,NDUM
     1 ,NIGS,DTOD,IM,IN,IO,NODUF,TIME,DT,IFLAG,IDUMP,HL,NMAX,SMA
     1 ,I,DT1,DT2,DT3,CF,CO,AF,BT,Q,DA,FS,REAC,CLA,CSM,STP
     1 ,AFU(6),DF(6),BF(6),YFS
       C1=1.-T(I)
      IF(T(I).LT.1.E-20) THEN
      GO TO 112
      END IF
       C2=BT*C1/(1.-AF*C1)
       IF(ABS(C2).GT.30.) GO TO 112
       C3=1./EXP(ABS(C2))
       IF(C2.LT.0.) C3=1./C3
       GO TO 114
  112  C3=0.
```

```
      IF(C2.LT.0.) IFLAG=1
  114 CONTINUE
      C4=DA*CLA*DT/(FS*Q)
      IF(C4.LT.1.) GO TO 116
      IF(C3.GT.(50./C4)) THEN
       T(I)=T(I)+CSM
       GO TO 120
      END IF
  116 CONTINUE
      C5=C4*C3
      C6=1./EXP(C5)
      T(I)=T(I)+CSM*(1.-C6)
  120 CONTINUE
      RETURN
      END
C     this subroutine solves the solid equations numerically
      SUBROUTINE SFTN(SMA,STP,DT,TIME,HSF,CVF,TAMB,DNW,CNDA,APS,EPSL,N)
C     ****************************************************************
      COMMON/WDATA/WTD(451),WTDO(451),WAMD(451),WAMDO(451),WDN(451)
     1  ,WDNA(451),WDNC(451),WHCP(451),WCND(451),WA(451),WD(451),SIGM
     1  ,WD1(451),WDNO(451),WB(451),WR(451),DNWF,DNF,HCPA,HCPC,CNDC
     1  ,WDX,WTIME,EACT
      DOUBLE PRECISION CC1,CC2,CC3,WDT,WDX,WDN,WDNO
C     DNW= Virgin wood density
C     DNF= Final char density
C     HCPA= Specific heat active wood
C     HCPC= Specific heat of char
```

```
C     CNDA= Thermal condcutivity of active wood
C     CNDC= Thermal conductivity of char
C     EPSL= Emissivity
C     HSF= Imposed heat flux
C     CVF= h/EPSL ,h is convective heat transfer coefficient
C     TAMB= Ambient temperature
C     SIGM= 5.6696E-12
C     APS= Ad, pre-exponential factor of wood
C     NMAX= Maximum number of step
C     WDX= Grid space of wood
C     DT= Time step
C     IO= number of grid space
C     initial condition
      IO=350
      IF(N.GT.1) GO TO 200
C     change the unit of input data
      CNDA=0.01*CNDA
      CNDC=0.01*CNDC
      CVF=0.0001*CVF/EPSL
      EACT=EACT*1000./1.987
      DO 100 I=1,IO
       WTD(I)=TAMB
       WTDO(I)=TAMB
       WDN(I)=DNW
       WDNO(I)=DNW
       WAMD(I)=0.
       WAMDO(I)=0.
```

```
100 CONTINUE
    SIGM=5.6696E-12
    WDX2=WDX**2
    DNWF=DNW-DNF
160 CONTINUE
    WTIME=TIME
    DO 170 I=1,IO
     WDN(I)=WDNO(I)
     WTD(I)=WTDO(I)
170 CONTINUE
200 CONTINUE
    WDT=DT/0.55187
    IF((WTIME-TIME).GT.1.E-12) GO TO 160
     WDNA(1)=DNW*(WDN(1)-DNF)/DNWF
     WDNC(1)=DNF*(DNW-WDN(1))/DNWF
     WHCP(1)=(WDNA(1)*HCPA+WDNC(1)*HCPC)/WDN(1)
     WCND(1)=(WDNA(1)*CNDA/DNW)+(WDNC(1)*CNDC/DNF)
     WA(1)=-WCND(1)/WDX2
     WB(1)=WA(1)
     WD(1)=(-WA(1)-WB(1))+(WDN(1)*WHCP(1)/WDT)
     WR(1)=WDN(1)*WHCP(1)*WTD(1)/WDT
    DO 210 I=2,IO
     WDNA(I)=DNW*(WDN(I)-DNF)/DNWF
     WDNC(I)=DNF*(DNW-WDN(I))/DNWF
     WHCP(I)=(WDNA(I)*HCPA+WDNC(I)*HCPC)/WDN(I)
     WCND(I)=(WDNA(I)*CNDA/DNW)+(WDNC(I)*CNDC/DNF)
     WA(I)=-WCND(I)/WDX2
```

```
      WB(I)=WA(I-1)
      WD(I)=(-WA(I)-WB(I))+(WDN(I)*WHCP(I)/WDT)
      WR(I)=WDN(I)*WHCP(I)*WTD(I)/WDT
  210 CONTINUE
      WA(1)=1.
      WD(1)=-1.
      WB(1)=0.
      WA(IO)=0.
      WD(IO)=1.
      WB(IO)=-1.
      WR(1)=(-WDX*EPSL/WCND(1))*(HSF-CVF*(WTD(1)-TAMB)-SIGM*((WTD(1)**4)
     1 -(TAMB**4)))
C     where CVF=h/EPSL
      WR(IO)=0.
C     solve the temperature equation
      DO 220 I=1,IO
       WD1(I)=WD(I)
  220 CONTINUE
      DO 230 I=2,IO
       CC=WB(I)/WD1(I-1)
       WD1(I)=WD1(I)-(CC*WA(I-1))
       WR(I)=WR(I)-(CC*WR(I-1))
  230 CONTINUE
      WR(IO)=WR(IO)/WD1(IO)
      WTDO(IO)=WTD(IO)
      WTD(IO)=WR(IO)
      DO 240 I=2,IO
```

```
      II=IO-I+1
      WR(II)=(WR(II)-WA(II)*WR(II+1))/WD1(II)
      WTDO(II)=WTD(II)
      WTD(II)=WR(II)
  240 CONTINUE
      WTD(IO+1)=WTD(IO)
      DO 250 I=1,IO
      CC=EACT/WTD(I)
      CC1=APS/EXP(CC)
C     APS=Ad
      CC2=CC1+(1./WDT)
      CC3=(WDN(I)/WDT)+CC1*DNF
      WDNO(I)=WDN(I)
      WDN(I)=CC3/CC2
  250 CONTINUE
      DO 260 I=2,IO
      II=IO-I+1
      WAMD(II)=WAMD(II+1)-WDX*(WDN(II)-WDNO(II))/WDT
  260 CONTINUE
      STP=(WTD(1)-TAMB)/(2230.-TAMB)
      SMA=WAMD(1)*3230.
      WTIME=TIME
      RETURN
      END
C
C     ***********************************************************************
```

APPENDIX C

PROGRAM LISTING FOR THE STEADY STATE DIFFUSION FLAME

(FINITE DIFFERENCE METHOD AND ACTIVATION ENERGY ASYMPTOTICS)

C.1 Finite difference numerical code

```
C     PROGRAM FOR THE STEADY STATE DIFFUSION FLAME
C                    by: Lin-Shyang Tzeng
C     solve T,YF,YO separately
C     for steady state diffusing flame
C     example for the input data of this program
C     0.0037 0.0037 0.0037 0.2 0.1656 0.7 0 0.002 0 0 1.0 1.0
C     0.866 9.6 18.2 3.33E7 0.25 0.232
C     2000 2 101 181 191 273 0 1.0 10 1 10 10
C     The result is writing on the file 'IGDUFLS.DAT'
C     In the IGDUFLS.DAT, the last line SMA,SMAO are the fuel flow rate ,
C     SMA is the fuel flow rate where there is not a diffusion flame
C     SMAO is the fuel flow rate where there is a diffusion flame
      PROGRAM ONEDSL
      COMMON T(401),YF(401),YO(401),XX(401),A(6),B(6),D(6),N,SMA
     1 ,RR(401),BT,AF,DA,FS,IM,IN,IO,NODUF,DX1,DX2,DX3,IFLAG,IDUMP
     2,PM1,NDST,YFS,RLE,AFU(6),BF(6),DF(6),ERR
      COMMON DDF(401),AAF(401),BBF(401),DD(401),DD1(401),AA(401)
     1 ,BB(401),DDO(401),AAO(401),BBO(401)
```

```
      DIMENSION TOD(401),YFOD(401),YOD(401)
      OPEN(UNIT=10,FILE='IGDUFLS.DAT',TYPE='NEW')
      OPEN(UNIT=11,FILE='DAINS.DAT',TYPE='OLD')
      OPEN(UNIT=12,FILE='OUPTS.DAT',TYPE='NEW')
C     input data
      READ(11,*)DX1,DX2,DX3,SMA,STP,PARM,PM1,PSM,IPM,MX,YFS,RLE
      READ(11,*)AF,BT,Q,DA,FS,YOS
      READ(11,*)NMAX,NDST,IG,IM,IN,IO,IRA,RAD,NHS,NW,IDUMP,NCH
C     IRA=1 including the radiation
C     NDST=1 the density and the conductivity is not constant
C     RLE ; Levise number
C     PARM ; the ratio of the old and new data for the iteration
C     PM1 ; maximum error for convergerne
C     PSM ; error for the fuel flow rate of two
C     NMAX ; maximum number for iteration
C     IG ; initial flame location
C     IDUMP ; number of dumped data (IA=IO/IDUMP)
C     RAD Planck mean absorption coeff Kp (/m)
C     NCH,NHS undefined
      HL=(IM-1)*DX1+(IN-IM)*DX2+(IO-IN)*DX3
      HL2=HL**2
      XF=1.-(LOG(0.058/YFS+1.))/SMA
      IG=IO*XF
C     initial condition
      SMAO=SMA
      SMB=0.
      ERO=1.E-3
```

```
C     coefficient of matrix and boundary cond.
      B(1)=0.
      A(1)=(-1.)/DX1
      AFU(1)=A(1)/RLE
      N=1
      NL=0
      IFLAG=0
      XX(1)=0.
      DO 102 I=2,IM
       XX(I)=XX(I-1)+DX1
  102 CONTINUE
      DO 104 I=IM+1,IN
       XX(I)=XX(I-1)+DX2
  104 CONTINUE
      DO 106 I=IN+1,IO
       XX(I)=XX(I-1)+DX3
  106 CONTINUE
C     initial condition
      DO 107 I=1,IG-3
       T(I)=XX(I)/XX(IG)
       YF(I)=SMA*(1.-T(I))
       YO(I)=0.
       T(I)=T(I)+STP
  107 CONTINUE
      DO 108 I=IG+3,IO
       T(I)=(XX(IO)-XX(I))/(XX(IO)-XX(IG))
       YF(I)=0.
```

```
      YO(I)=YOS*(1.-T(I))
  108 CONTINUE
      DO 109 I=1,7
       II=I-3
      T(IG+II)=1.
      YF(IG+II)=YF(IG-4)
      YO(IG+II)=YO(IG+4)
  109 CONTINUE
C     start the new iteration
  110 CONTINUE
      IF(SMA.LT.1.E-9) GO TO 400
      DO 111 I=1,IO
       TOD(I)=T(I)
       YFOD(I)=YF(I)
       YOD(I)=YO(I)
  111 CONTINUE
      IF(IPM.EQ.1) GO TO 400
      ERR=0.
C     calculate the old chemical reaction
      CALL CHEM
      DO 120 I=2,IO-1
       RTP=0.
       IF(IRA.EQ.1)THEN
       TP=T(I)*1932.+298
       DNST=0.3528/TP
       RTP=RAD*(TP**4)*1.576E-16/DNST
       END IF
```

```
      RR(I)=Q*YF(I)*YO(I)*RR(I)-RTP
      IF(RR(I).LT.0.) RR(I)=0.
  120 CONTINUE
      CALL COEF
      IF(IFLAG.EQ.1) GO TO 400
C     solve the diffusion
      CALL SY
      DO 130 I=2,IO-1
       ER=ABS(T(I)-RR(I))
       IF(ER.GT.ERR) ERR=ER
       T(I)=(1.-PARM)*T(I)+PARM*RR(I)
  130 CONTINUE
      CALL CHEM
      CALL COEF
      IF(((N/2)*2).EQ.N) GO TO 142
      CALL SYF
      DO 135 I=1,IO-1
       ER=ABS(YF(I)-RR(I))
       IF(ER.GT.ERR) ERR=ER
       YF(I)=YF(I)*(1.-PARM)+PARM*RR(I)
  135 CONTINUE
      CALL CHEM
      CALL COEF
      CALL SYO
      DO 140 I=1,IO-1
       ER=ABS(YO(I)-RR(I))
       IF(ER.GT.ERR) ERR=ER
```

```
      YO(I)=YO(I)*(1.-PARM)+PARM*RR(I)
  140 CONTINUE
      GO TO 148
  142 CONTINUE
      CALL SYO
      DO 145 I=1,IO-1
       ER=ABS(YO(I)-RR(I))
       IF(ER.GT.ERR) ERR=ER
       YO(I)=YO(I)*(1.-PARM)+PARM*RR(I)
  145 CONTINUE
      CALL CHEM
      CALL COEF
      CALL SYF
      DO 147 I=1,IO-1
       ER=ABS(YF(I)-RR(I))
       IF(ER.GT.ERR) ERR=ER
       YF(I)=YF(I)*(1.-PARM)+PARM*RR(I)
  147 CONTINUE
  148 CONTINUE
      IF(IFLAG.EQ.2) ERR=1.
      N=N+1
      IF(N.GT.NMAX) THEN
       WRITE(10,*)'not converge for N=',N
       GO TO 400
      END IF
      IF(ERR.GT.ERO) GO TO 111
      ERO=1.E-4
```

```
      N=1
      TMX=0.
      II=0
      DO 210 I=2,IO-1
       IF(T(I).GT.TMX) THEN
        TMX=T(I)
        II=I
       END IF
  210 CONTINUE
      WRITE(10,*)'SMA,TMX,II,X=',SMA,TMX,II,XX(II)
      IF(NW.EQ.0) GO TO 410
      IF(MX-1)220,230,240
  220 CONTINUE
      IF(TMX.GT.0.27) THEN
       SMAO=SMA
       SMA=0.5*(SMA+SMB)
      SMR=ABS(1.-(SMA/SMAO))
      IF(SMR.LT.PSM) THEN
       SMA=SMA*0.5
       SMB=SMA
       END IF
       N=1
       GO TO 110
      END IF
      DO 225 I=1,IO
       T(I)=TOD(I)
       YF(I)=YFOD(I)
```

```
      YO(I)=YOD(I)
  225 CONTINUE
      SMB=SMA
      SMA=0.5*(SMAO+SMA)
      SMR=ABS(1.-(SMA/SMAO))
      IF(SMR.LT.PSM) GO TO 400
      N=1
      GO TO 111
  230 CONTINUE
      IF(TMX.GT.0.1) THEN
      DX1=DX1-0.0035
      DX2=DX2-0.00035
      DX3=DX3-0.0035
      A(1)=(-1.)/DX1
      DO 232 I=2,IM
       XX(I)=XX(I-1)+DX1
  232 CONTINUE
      DO 234 I=IM+1,IN
       XX(I)=XX(I-1)+DX2
  234 CONTINUE
      DO 236 I=IN+1,IO
       XX(I)=XX(I-1)+DX3
  236 CONTINUE
      N=1
      GO TO 110
      END IF
      GO TO 400
```

```
240 CONTINUE
    WRITE(10,*)'T(1),YF(1)=',T(1),YF(1)
    IF(TMX.GT.0.27) THEN
    YFS=YFS-0.01
    N=1
    GO TO 110
    END IF
400 CONTINUE
    SMA=SMA*1000.0/3230.0
    SMAO=SMAO*1000.0/3230.0
    IF(MX.EQ.0)  WRITE(10,*)'minimum fuel flow rate (mg/cm2 sec),SMA
   1 ,SMAO=',SMA,SMAO
    IF(MX.EQ.1)  WRITE(10,*)'minimum quench dist.XX(IO),DX1,DX2
   1 =',XX(IO),DX1,DX2
    IF(MX.EQ.2) WRITE(10,*)'min fuel con YFS=',YFS
    IF(IFLAG.EQ.2) GO TO 410
    IF(ERR.GT.0.01) THEN
     WRITE(10,*)'ERR=',ERR
     GO TO 410
    END IF
    DO 410 I=2,IO-1
     T(I)=TOD(I)
     YF(I)=YFOD(I)
     YO(I)=YOD(I)
410 CONTINUE
    CALL DUMP
    IF(IFLAG.EQ.2) WRITE(10,*)'IFLAG,N=',IFLAG,N
```

```
      IF(IFLAG.EQ.1) WRITE(10,*)'IFLAG,N=',IFLAG,N
      CLOSE(UNIT=10)
      CLOSE(UNIT=11)
      CLOSE(UNIT=12)
      STOP
      END
C     ***************************************
C     This subroutine solve the tri-diagonal matrix
      SUBROUTINE SY
C     ***************************************
      COMMON T(401),YF(401),YO(401),XX(401),A(6),B(6),D(6),N,SMA
     1 ,RR(401),BT,AF,DA,FS,IM,IN,IO,NODUF,DX1,DX2,DX3,IFLAG,IDUMP
     2 ,PM1,NDST,YFS,RLE,AFU(6),BF(6),DF(6),ERR
      COMMON DDF(401),AAF(401),BBF(401),DD(401),DD1(401),AA(401)
     1 ,BB(401),DDO(401),AAO(401),BBO(401)
      RR(1)=T(1)
      RR(IO)=T(IO)
      IF(NDST.EQ.1) THEN
       DO 100 I=2,IM-1
       CDT=900./(T(I)*1932.+298.)
       CDA=900./(T(I+1)*1932.+298.)
       CXT=1./(DX1*DX1*CDT)
       CXA=1./(DX1*DX1*CDA)
       SMX=SMA/DX1
       DD(I)=CXA+CXT-SMX
       AA(I)=SMX-CXA
       BB(I)=-CXT
```

```
100  CONTINUE
     CDT=900./(T(IM)*1932.+298.)
     CDA=900./(T(IM+1)*1932.+298.)
     CXT=1./(DX2*DX1*CDT)
     CXA=1./(DX2*DX2*CDA)
     SMX=SMA/DX2
     DD(IM)=CXA+CXT-SMX
     AA(IM)=SMX-CXA
     BB(IM)=-CXT
     DO 200 I=IM+1,IN-1
     CDT=900./(T(I)*1932.+298.)
     CDA=900./(T(I+1)*1932.+298.)
     CXT=1./(DX2*DX2*CDT)
     CXA=1./(DX2*DX2*CDA)
     SMX=SMA/DX2
     DD(I)=CXA+CXT-SMX
     AA(I)=SMX-CXA
     BB(I)=-CXT
200  CONTINUE
     CDT=900./(T(IN)*1932.+298.)
     CDA=900./(T(IN+1)*1932.+298.)
     CXT=1./(DX2*DX3*CDT)
     CXA=1./(DX3*DX3*CDA)
     SMX=SMA/DX3
     DD(IN)=CXA+CXT-SMX
     AA(IN)=SMX-CXA
     BB(IN)=-CXT
```

```
      DO 300 I=IN+1,IO-1
      CDT=900./(T(I)*1932.+298.)
      CDA=900./(T(I+1)*1932.+298.)
      CXT=1./(DX3*DX3*CDT)
      CXA=1./(DX3*DX3*CDA)
      SMX=SMA/DX3
      DD(I)=CXA+CXT-SMX
      AA(I)=SMX-CXA
      BB(I)=-CXT
  300 CONTINUE
     GO TO 35
     END IF
     DO 10 I=2,IM-1
      DD(I)=D(2)
      AA(I)=A(2)
      BB(I)=B(2)
   10 CONTINUE
     DD(IM)=D(3)
     AA(IM)=A(3)
     BB(IM)=B(3)
     DO 20 I=IM+1,IN-1
      DD(I)=D(4)
      AA(I)=A(4)
      BB(I)=B(4)
   20 CONTINUE
     DD(IN)=D(5)
     AA(IN)=A(5)
```

```
      BB(IN)=B(5)
      DO 30 I=IN+1,IO-1
       DD(I)=D(6)
       AA(I)=A(6)
       BB(I)=B(6)
   30 CONTINUE
   35 CONTINUE
C     solve the temp equ.
      DD(1)=1.
      AA(1)=0.
      DD(IO)=1.
      BB(IO)=0.
C     solve by Gauss elimination
      DD1(1)=DD(1)
      DO 40 I=2,IO-1
       CC=BB(I)/DD1(I-1)
       DD1(I)=DD(I)-(CC*AA(I-1))
       RR(I)=RR(I)-(CC*RR(I-1))
   40 CONTINUE
      DO 50 I=2,IO-1
       II=IO-I+1
       RR(II)=(RR(II)-AA(II)*RR(II+1))/DD1(II)
       IF(RR(II).LT.(-1.E-12)) THEN
        RR(II)=PM1*RR(II)
        IFLAG=2
       END IF
   50 CONTINUE
```

```
      GO TO 80
   80 CONTINUE
      RETURN
      END
C     ******************************************
C     This subroutine dump the data to a temporary file
      SUBROUTINE DUMP
C     ******************************************
      COMMON T(401),YF(401),YO(401),XX(401),A(6),B(6),D(6),N,SMA
     1 ,RR(401),BT,AF,DA,FS,IM,IN,IO,NODUF,DX1,DX2,DX3,IFLAG,IDUMP
     2 ,PM1,NDST,YFS,RLE,AFU(6),BF(6),DF(6),ERR
      COMMON DDF(401),AAF(401),BBF(401),DD(401),DD1(401),AA(401)
     1 ,BB(401),DDO(401),AAO(401),BBO(401)
      IA=IO/IDUMP
      DO 10 I=1,IO,IA
       WRITE(12,2000)I,XX(I),T(I),YF(I),YO(I)
   10 CONTINUE
C     check if there is diffusion flame
      NODUF=0
      IDUF=2
      TDUF=0.
      DO 40 I=2,IO-1
       IF(T(I).GT.TDUF) GO TO 30
       GO TO 40
   30  CONTINUE
       IDUF=I
       TDUF=T(I)
```

```
   40 CONTINUE
      WRITE(10,*)'max temp N,T,I=',N,TDUF,IDUF
 2000 FORMAT(' I,X,T,YF,YO=',I5,1X,F11.4,3F7.4)
      RETURN
      END
C     ************************************
C     This subroutine calculate the chemical reaction rate
      SUBROUTINE CHEM
C     ************************************
      COMMON T(401),YF(401),YO(401),XX(401),A(6),B(6),D(6),N,SMA
     1 ,RR(401),BT,AF,DA,FS,IM,IN,IO,NODUF,DX1,DX2,DX3,IFLAG,IDUMP
     2 ,PM1,NDST,YFS,RLE,AFU(6),BF(6),DF(6),ERR
      COMMON DDF(401),AAF(401),BBF(401),DD(401),DD1(401),AA(401)
     1 ,BB(401),DDO(401),AAO(401),BBO(401)
      DO 120 I=2,IO-1
       C1=1.-T(I)
       C2=BT*C1/(1.-AF*C1)
       IF(ABS(C2).GT.50.) GO TO 112
       C3=1./EXP(ABS(C2))
       IF(C2.LT.0.) C3=1./C3
       GO TO 114
  112  C3=0.
       IF(C2.LT.0.) IFLAG=1
      IF(IFLAG.EQ.1) PRINT *,'I,N,T=',I,N,T(I)
  114  CONTINUE
       IF(NDST.EQ.1) THEN
C      Density is not constant
```

```
      DA1=DA*943.4/(T(I)*1932.+298.)
      GO TO 115
      END IF
      DA1=DA
  115 CONTINUE
      RR(I)=C3*DA1
  120 CONTINUE
      RETURN
      END
C     ****************************************
C     This subroutine calculate the coefficient of the tri-diagonal matrix
      SUBROUTINE COEF
C     ****************************************
      COMMON T(401),YF(401),YO(401),XX(401),A(6),B(6),D(6),N,SMA
     1 ,RR(401),BT,AF,DA,FS,IM,IN,IO,NODUF,DX1,DX2,DX3,IFLAG,IDUMP
     2 ,PM1,NDST,YFS,RLE,AFU(6),BF(6),DF(6),ERR
      COMMON DDF(401),AAF(401),BBF(401),DD(401),DD1(401),AA(401)
     1 ,BB(401),DDO(401),AAO(401),BBO(401)
      D(1)=SMA+(1./DX1)
      A(2)=1.0*((SMA/DX1)-(1./(DX1**2)))
      D(2)=0.-(SMA*1.0/DX1)+(2.*1.0/(DX1**2))
      B(2)=(-1.)*1.0/(DX1**2)
      A(3)=SMA*1.0/DX2-2.*1.0/((DX1+DX2)*DX2)
      D(3)=0.+2.*1.0/((DX1+DX2)*DX2)+2.*1.0/((DX1+DX2)*DX1)
     1 -SMA*1.0/DX2
      B(3)=(-2.)*1.0/((DX1+DX2)*DX1)
      A(4)=(SMA*1.0/DX2)-1.0/(DX2**2)
```

```
      D(4)=0.-(SMA*1.0/DX2)+(2.*1.0/(DX2**2))
      B(4)=(-1.)*1.0/(DX2**2)
      A(5)=SMA*1.0/DX3-2.*1.0/((DX2+DX3)*DX3)
      D(5)=0.+2.*1.0/((DX2+DX3)*DX3)+2.*1.0/((DX2+DX3)*DX2)
     1 -SMA*1.0/DX3
      B(5)=(-2.)*1.0/((DX2+DX3)*DX2)
      A(6)=(SMA*1.0/DX3)-1.0/(DX3**2)
      D(6)=0.-(SMA*1.0/DX3)+(2.*1.0/(DX3**2))
      B(6)=(-1.)*1.0/(DX3**2)
      DF(1)=SMA+(1./(DX1*RLE))
      AFU(2)=(SMA/DX1)-(1./((DX1**2)*RLE))
      DF(2)=(2./((DX1**2)*RLE))-(SMA/DX1)
      BF(2)=(-1.)/((DX1**2)*RLE)
      AFU(3)=SMA/DX2-2./((DX1+DX2)*DX2*RLE)
      DF(3)=2./((DX1+DX2)*DX2*RLE)+2./((DX1+DX2)*DX1
     1 *RLE)-SMA/DX2
      BF(3)=(-2.)/((DX1+DX2)*DX1*RLE)
      AFU(4)=(SMA/DX2)-1./((DX2**2)*RLE)
      DF(4)=2./((DX2**2)*RLE)-(SMA/DX2)
      BF(4)=(-1.)/((DX2**2)*RLE)
      AFU(5)=SMA/DX3-2./((DX2+DX3)*DX3*RLE)
      DF(5)=2./((DX2+DX3)*DX3*RLE)+2./((DX2+DX3)*DX2
     1 *RLE)-SMA/DX3
      BF(5)=(-2.)/((DX2+DX3)*DX2*RLE)
      AFU(6)=SMA/DX3-1./((DX3**2)*RLE)
      DF(6)=2./((DX3**2)*RLE)-SMA/DX3
      BF(6)=(-1.)/((DX3**2)*RLE)
```

```
      RETURN
      END
C     **********************************
C     This subroutine solves the tri-diagonal matrix for fuel
      SUBROUTINE SYF
C     **********************************
      COMMON T(401),YF(401),YO(401),XX(401),A(6),B(6),D(6),N,SMA
     1 ,RR(401),BT,AF,DA,FS,IM,IN,IO,NODUF,DX1,DX2,DX3,IFLAG,IDUMP
     2 ,PM1,NDST,YFS,RLE,AFU(6),BF(6),DF(6),ERR
      COMMON DDF(401),AAF(401),BBF(401),DD(401),DD1(401),AA(401)
     1 ,BB(401),DDO(401),AAO(401),BBO(401)
      RR(1)=SMA*YFS
      RR(IO)=YF(IO)
      IF(NDST.EQ.1) THEN
       DO 100 I=2,IM-1
       CDT=900./(T(I)*1932.+298.)
       CDA=900./(T(I+1)*1932.+298.)
       CXT=1./(DX1*DX1*CDT*RLE)
       CXA=1./(DX1*DX1*CDA*RLE)
       SMX=SMA/DX1
       DDF(I)=CXA+CXT-SMX
       AAF(I)=SMX-CXA
       BBF(I)=-CXT
  100  CONTINUE
       CDT=900./(T(IM)*1932.+298.)
       CDA=900./(T(IM+1)*1932.+298.)
       CXT=1./(DX2*DX1*CDT*RLE)
```

```
      CXA=1./(DX2*DX2*CDA*RLE)
      SMX=SMA/DX2
      DDF(IM)=CXA+CXT-SMX
      AAF(IM)=SMX-CXA
      BBF(IM)=-CXT
      DO 200 I=IM+1,IN-1
      CDT=900./(T(I)*1932.+298.)
      CDA=900./(T(I+1)*1932.+298.)
      CXT=1./(DX2*DX2*CDT*RLE)
      CXA=1./(DX2*DX2*CDA*RLE)
      SMX=SMA/DX2
      DDF(I)=CXA+CXT-SMX
      AAF(I)=SMX-CXA
      BBF(I)=-CXT
  200 CONTINUE
      CDT=900./(T(IN)*1932.+298.)
      CDA=900./(T(IN+1)*1932.+298.)
      CXT=1./(DX2*DX3*CDT*RLE)
      CXA=1./(DX3*DX3*CDA*RLE)
      SMX=SMA/DX3
      DDF(IN)=CXA+CXT-SMX
      AAF(IN)=SMX-CXA
      BBF(IN)=-CXT
      DO 300 I=IN+1,IO-1
      CDT=900./(T(I)*1932.+298.)
      CDA=900./(T(I+1)*1932.+298.)
      CXT=1./(DX3*DX3*CDT*RLE)
```

```
      CXA=1./(DX3*DX3*CDA*RLE)
      SMX=SMA/DX3
      DDF(I)=CXA+CXT-SMX
      AAF(I)=SMX-CXA
      BBF(I)=-CXT
300   CONTINUE
     DO 310 I=2,IO-1
     DDF(I)=RR(I)*YO(I)+DDF(I)
310  CONTINUE
     CDA=900./(T(2)*1932.+298.)
     DDF(1)=(1./(RLE*CDA*DX1))+SMA
     AAF(1)=-1./(RLE*CDA*DX1)
     GO TO 32
     END IF
     DO 10 I=2,IM-1
      DDF(I)=RR(I)*YO(I)+DF(2)
      AAF(I)=AFU(2)
      BBF(I)=BF(2)
 10  CONTINUE
     DDF(IM)=RR(I)*YO(I)+DF(3)
     AAF(IM)=AFU(3)
     BBF(IM)=BF(3)
     DO 20 I=IM+1,IN-1
      DDF(I)=RR(I)*YO(I)+DF(4)
      AAF(I)=AFU(4)
      BBF(I)=BF(4)
 20  CONTINUE
```

```
      DDF(IN)=RR(I)*YO(I)+DF(5)
      AAF(IN)=AFU(5)
      BBF(IN)=BF(5)
      DO 30 I=IN+1,IO-1
       DDF(I)=RR(I)*YO(I)+DF(6)
       AAF(I)=AFU(6)
       BBF(I)=BF(6)
   30 CONTINUE
C     solve the fuel equ.
      DDF(1)=DF(1)
      AAF(1)=AFU(1)
   32 CONTINUE
      DO 35 I=2,IO-1
       RR(I)=0.
   35 CONTINUE
      DDF(IO)=1.
      BBF(IO)=0.
C     solve by Gauss elimination
      DD1(1)=DDF(1)
      DO 40 I=2,IO-1
       CC=BBF(I)/DD1(I-1)
       DD1(I)=DDF(I)-(CC*AAF(I-1))
       RR(I)=RR(I)-(CC*RR(I-1))
   40 CONTINUE
      DO 50 I=2,IO
       II=IO-I+1
       RR(II)=(RR(II)-AAF(II)*RR(II+1))/DD1(II)
```

```
      IF(RR(II).LT.(-1.E-12)) THEN
       RR(II)=PM1*RR(II)
       IFLAG=2
      END IF
   50 CONTINUE
      RETURN
      END
C     **********************************
C     This subroutine solves the tri-diagonal matrix for oxygen
      SUBROUTINE SYO
C     **********************************
      COMMON T(401),YF(401),YO(401),XX(401),A(6),B(6),D(6),N,SMA
     1 ,RR(401),BT,AF,DA,FS,IM,IN,IO,NODUF,DX1,DX2,DX3,IFLAG,IDUMP
     2 ,PM1,NDST,YFS,RLE,AFU(6),BF(6),DF(6),ERR
      COMMON DDF(401),AAF(401),BBF(401),DD(401),DD1(401),AA(401)
     1 ,BB(401),DDO(401),AAO(401),BBO(401)
      RR(1)=0.
      RR(IO)=YO(IO)
      IF(NDST.EQ.1) THEN
       DO 100 I=2,IM-1
       CDT=900./(T(I)*1932.+298.)
       CDA=900./(T(I+1)*1932.+298.)
       CXT=1./(DX1*DX1*CDT*RLE)
       CXA=1./(DX1*DX1*CDA*RLE)
       SMX=SMA/DX1
       DDO(I)=CXA+CXT-SMX
       AAO(I)=SMX-CXA
```

```
      BBO(I)=-CXT
  100 CONTINUE
      CDT=900./(T(IM)*1932.+298.)
      CDA=900./(T(IM+1)*1932.+298.)
      CXT=1./(DX2*DX1*CDT*RLE)
      CXA=1./(DX2*DX2*CDA*RLE)
      SMX=SMA/DX2
      DDO(IM)=CXA+CXT-SMX
      AAO(IM)=SMX-CXA
      BBO(IM)=-CXT
      DO 200 I=IM+1,IN-1
      CDT=900./(T(I)*1932.+298.)
      CDA=900./(T(I+1)*1932.+298.)
      CXT=1./(DX2*DX2*CDT*RLE)
      CXA=1./(DX2*DX2*CDA*RLE)
      SMX=SMA/DX2
      DDO(I)=CXA+CXT-SMX
      AAO(I)=SMX-CXA
      BBO(I)=-CXT
  200 CONTINUE
      CDT=900./(T(IN)*1932.+298.)
      CDA=900./(T(IN+1)*1932.+298.)
      CXT=1./(DX2*DX3*CDT*RLE)
      CXA=1./(DX3*DX3*CDA*RLE)
      SMX=SMA/DX3
      DDO(IN)=CXA+CXT-SMX
      AAO(IN)=SMX-CXA
```

```
      BBO(IN)=-CXT
      DO 300 I=IN+1,IO-1
      CDT=900./(T(I)*1932.+298.)
      CDA=900./(T(I+1)*1932.+298.)
      CXT=1./(DX3*DX3*CDT*RLE)
      CXA=1./(DX3*DX3*CDA*RLE)
      SMX=SMA/DX3
      DDO(I)=CXA+CXT-SMX
      AAO(I)=SMX-CXA
      BBO(I)=-CXT
  300 CONTINUE
      DO 310 I=2,IO-1
      DDO(I)=DDO(I)+(RR(I)*YF(I)/FS)
  310 CONTINUE
      CDA=900./(T(2)*1932.+298.)
      DDO(1)=(1./(RLE*CDA*DX1))+SMA
      AAO(1)=-1./(RLE*CDA*DX1)
      GO TO 32
      END IF
      DO 10 I=2,IM-1
      DDO(I)=(RR(I)*YF(I)/FS)+DF(2)
      AAO(I)=AFU(2)
      BBO(I)=BF(2)
   10 CONTINUE
      DDO(IM)=(RR(I)*YF(I)/FS)+DF(3)
      AAO(IM)=AFU(3)
      BBO(IM)=BF(3)
```

```
      DO 20 I=IM+1,IN-1
       DDO(I)=(RR(I)*YF(I)/FS)+DF(4)
       AAO(I)=AFU(4)
       BBO(I)=BF(4)
   20 CONTINUE
      DDO(IN)=(RR(I)*YF(I)/FS)+DF(5)
      AAO(IN)=AFU(5)
      BBO(IN)=BF(5)
      DO 30 I=IN+1,IO-1
       DDO(I)=(RR(I)*YF(I)/FS)+DF(6)
       AAO(I)=AFU(6)
       BBO(I)=BF(6)
   30 CONTINUE
C     solve the Oxygen equ.
      DDO(1)=DF(1)
      AAO(1)=AFU(1)
   32 CONTINUE
      DO 35 I=2,IO-1
       RR(I)=0.
   35 CONTINUE
      DDO(IO)=1.
      BBO(IO)=0.
C     solve by Gauss elimination
      DD1(1)=DDO(1)
      DO 40 I=2,IO-1
       CC=BBO(I)/DD1(I-1)
       DD1(I)=DDO(I)-(CC*AAO(I-1))
```

```
      RR(I)=RR(I)-(CC*RR(I-1))
   40 CONTINUE
      DO 50 I=2,IO
       II=IO-I+1
       RR(II)=(RR(II)-AAO(II)*RR(II+1))/DD1(II)
       IF(RR(II).LT.(-1.E-12)) THEN
        RR(II)=PM1*RR(II)
        IFLAG=2
       END IF
   50 CONTINUE
      RETURN
      END
C
C     ***********************************************************************
```

C.2 Program for the calculation of extintion Damkohler number

(Activation energy asymptotics method)

```
C     This program is to calculate the minimum fuel flow rate by using the
C     extinction Damkohler number derived by Linan
C     example for the input data, assume the fuel is metnane
C     SMA=0.0002,    YOX=0.232,    HCM=1.5,    TL=640.0,    YFS=0.25,
C     ACTV=48.0,     AEXF=2.424E15,
      PROGRAM EXTIN
      FS=0.25
```

```
C     FS is the stoichiometry ratio of the fuel
      N=0
      PRINT *,'input SMA(g/cm2 sec),HCM(cm),YOX,TL(k),YFS'
      READ(5,*)SMA,HCM,YOX,TL,YFS
C     SMA is the fuel flow rate at the surface
C     HCM is the boundary layer thickness
C     YOX is the Oxygen mass fraction
C     TL is the surface temperature, (absolute temperature k)
C     YFS is the fuel mass fraction beneath the solid surface
      SMD=0.000001
      PRINT *,'input activation energy, pre-exponedtial factor'
      PRINT *,'kcal/mole,cm3/g sec'
      READ(5,*)ACTV,AEXF
C     ACTV is the activation energy of the gas fuel
C     AEXF is the frequency factor of the gas fuel
  100 CONTINUE
      N=N+1
      IF(N.GT.1000) THEN
       PRINT *,' NOT CONVERGE AT N=',N
       PRINT *,'REDAE,REDA',REDAE,REDA
       GO TO 220
      END IF
      IF(SMA.LT.1.E-12) GO TO 200
      SMAD=SMA*3230.
      YFSO=YFS-(YFS+FS*YOX)/EXP(SMAD)
      TPND=35155.*YFSO
      STPL=TL/TPND
```

```
      STPU=298./TPND
      DL=3230.*SMA
      ARFA=FS*YOX/YFSO
      BETA=STPL-STPU
      TACE=ACTV/(0.001983*TPND)
      TDEF=STPL+(ARFA-BETA)/(1.+ARFA)
      EBS=(TDEF**2)/TACE
      GAMA=1.-2.*(ARFA-BETA)/(1.+ARFA)
      ZETO=1.-(1./EXP(DL))
      DAMKO=4.*0.000374*AEXF*YFSO*5.61E-8/(0.323*(SMA**2))
      CN1=4.*DAMKO*(ZETO**2)*(EBS**3)
      CN2=((1.-(ZETO*ARFA/(1.+ARFA)))**2)*((1.+ARFA)**2)
      CN3=1./EXP(TACE/TDEF)
      REDA=CN1*CN3/CN2
      CN4=1.-GAMA
      REDAE=2.7183*(CN4-(CN4**2)+0.26*(CN4**3)+0.055*(CN4**4))
      IF(REDA.GT.REDAE) THEN
      SMA=SMA-SMD
      N=N+1
      GO TO 100
      END IF
  200 CONTINUE
      IF(((REDAE-REDA)/(REDAE+REDA)).GT.0.01) THEN
       SMA=SMA+SMD
       SMD=SMD*0.1
       GO TO 100
      END IF
```

```
  220 CONTINUE
      PRINT *,'SMA,HCM,YOX,REDA,REDAE=',SMA,HCM,YOX,REDA,REDAE
      TDEFD=TDEF*TPND
      IF(N.EQ.1) PRINT *,'SMA too small,re-test again'
      PRINT *,'diffusion flame temp.=',TDEFD
      STOP
      END
C
C     ***********************************************************************
```

Appendix D

ESTIMATION OF SOLID PHASE PARAMETERS FROM PILOTED IGNITION EXPERIMENTAL DATA

D.1. Experimental Data

A series of piloted ignition experiments have been conducted by Abu-Zaid (1988). A combustion wind tunnel was used to perform these experiments in a well-controlled atmosphere under external radiation. This tunnel consists of three main sections, the inlet section, the test section, and the exhaust section; it is schematically shown in Figure D-1. The crossectional area for air flow is 15cm x 8.5 cm, and the wood sample (14.5 cm long, 7.5 cm width and 3.75 cm high) is placed 30cm downstream of the leading edge. These wood samples were carefully instrumented by surface, bottom and in-depth thermocouples.

During the experiments, the heaters were turned on at the desired radiant heat flux, and were allowed to warm up for about 15-20 minutes. The wood sample was then placed on the weighing table with its top surface flat along the tunnel base. A small natural gas pilot flame was used downstream of the tunnel to initiate piloted ignition. The output of gas analyzers, thermocouples and the load cell was stored and processed by a microcomputer in real time.

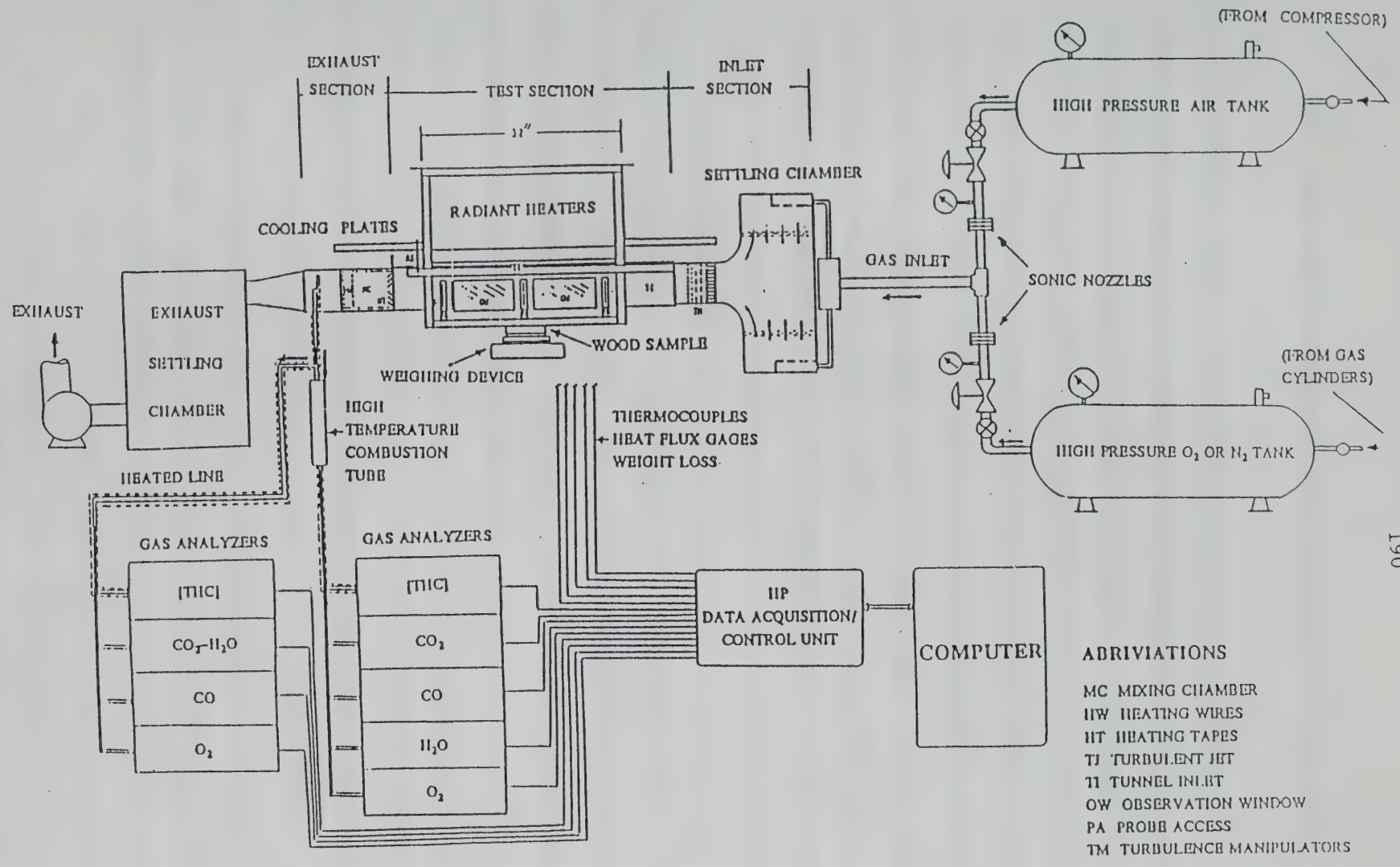

FIGURE D-1 Schematic diagram of the experimental facility.

D.2. Estimation of Convective Heat Transfer Coeffeicient.

The evaluation of the convective heat transfer coefficient during piloted ignition is complicated, because (i) the surface temperature of the sample is continuously changing, and (ii) the heat losses from the surface do not occur primarily by convection. In fact, a major portion of the incident heat flux is lost by re-radiation. Thus, the use of correlations for the convective heat transfer coefficient obtained from either constant surface temperature or constant heat flux is questionable. Furthermore, there is a reduction in convective heat transfer due to blowing effects from the evolution of pyrolysis gases, although these are expected to be negligible for piloted ignition.

In view of the above complications only an approximate value of convective heat transfer can be obtained from the Nusselt number correlations available in the literature. Also it seems more appropriate to use the constant surface temperature condition because the surface temperature at piloted ignition is nearly constant (since and the rate of change of surface temperature is small when it is in the neighborhood of the piloted ignition temperature). The estimation of the convective heat transfer coefficient is now described below. The mass flow rate in the wind tunnel during the piloted ignition experiments was about 0.4625g/sec. Assuming the density of air in the wind tunnel to be 0.8585 Kg/m^3, gives a free steam flow velocity of 4.22 cm/sec. Other properties of air (at 650 ^oK) are taken as: $\nu = 58.5 \times 10^{-6}$ m^2/sec; λ_a (thermal conductivity of air) = 0.0495 W/m^2 K and Pr = 0.7. Also, the Nusselt number expression for laminar flow is used, viz.,

$$Nu_x = 0.332\ P_r^{1/3}\ Re_x^{1/2}.$$

Since the leading edge of the thermal boundary layer is about 30 cm downstream of the (actual) physical leading edge, Re_x at the begining of the wood sample is $Re(x=30cm) = U_\infty x/\nu = 337.7$ Hence, the convective heat transfer coefficient is $\overline{h}(x=30\ cm) = 0.8927$ W/m^2K. The leading edge of the thermal boundary layer at the end of wood is about 44.5 cm. Thus, $Re(x=44.5\ cm) = 503.8$, and $\overline{h}(x=44.5\ cm) = 0.733\ W/m^2K$. Hence, the average convective heat transfer coefficient is taken as $= 0.812\ W/m^2K$. This value is used to calculate the surface temperature from the analytical (integral) solution.

Although this estimate of the convective heat transfer coefficient is approximate, the convective heat transfer itself is not very important because the major heat loss from the surface occurs by radiation. The effect of $\overline{h}$ on the prediction of thermal conductivity by inverse calculations will be discussed later.

D.3. Comparison of the Analytical Solution and Experimental Data

In order to predict the experimental heat and mass transfer, a least square curve fitting program has been written to determine the optimal thermal conductivity.

D.3.1 Determination of Thermal Properties of Wood

In view of equation (5-17), if the convective heat transfer coefficient and the external heat flux have been determined, then the quantity inside the brackets is fixed. (say, equal to BX), and the constant K can be calculated by a least-square fit of the experimental values of t and BX.

By using the equation (5-25) of Beck and Arnold (1977), the optimal value of K is given by

$$K = \Sigma t_i BX_i / \Sigma (BX_i)^2 .$$

A computer program, SQFT, see Appendix E was written to calculate the optimal thermal properties from the measured surface temperature. Figure D-2 shows a comparison of the experimental and the least-square-error fitted surface temperature. The continuous line is the experimental data, and the dashed line is the least square fit. The thermal conductivity of the wood calculated by this procedure is listed in Table D-1. The average value of the thermal conductivity is 0.25 W/mK, which is within the range of literature-listed values. (the thermal conductivities for various woods, determined by Atreya (1983), range between 0.135 and 0.263 W/mK. (Assume λ_w is a constant).

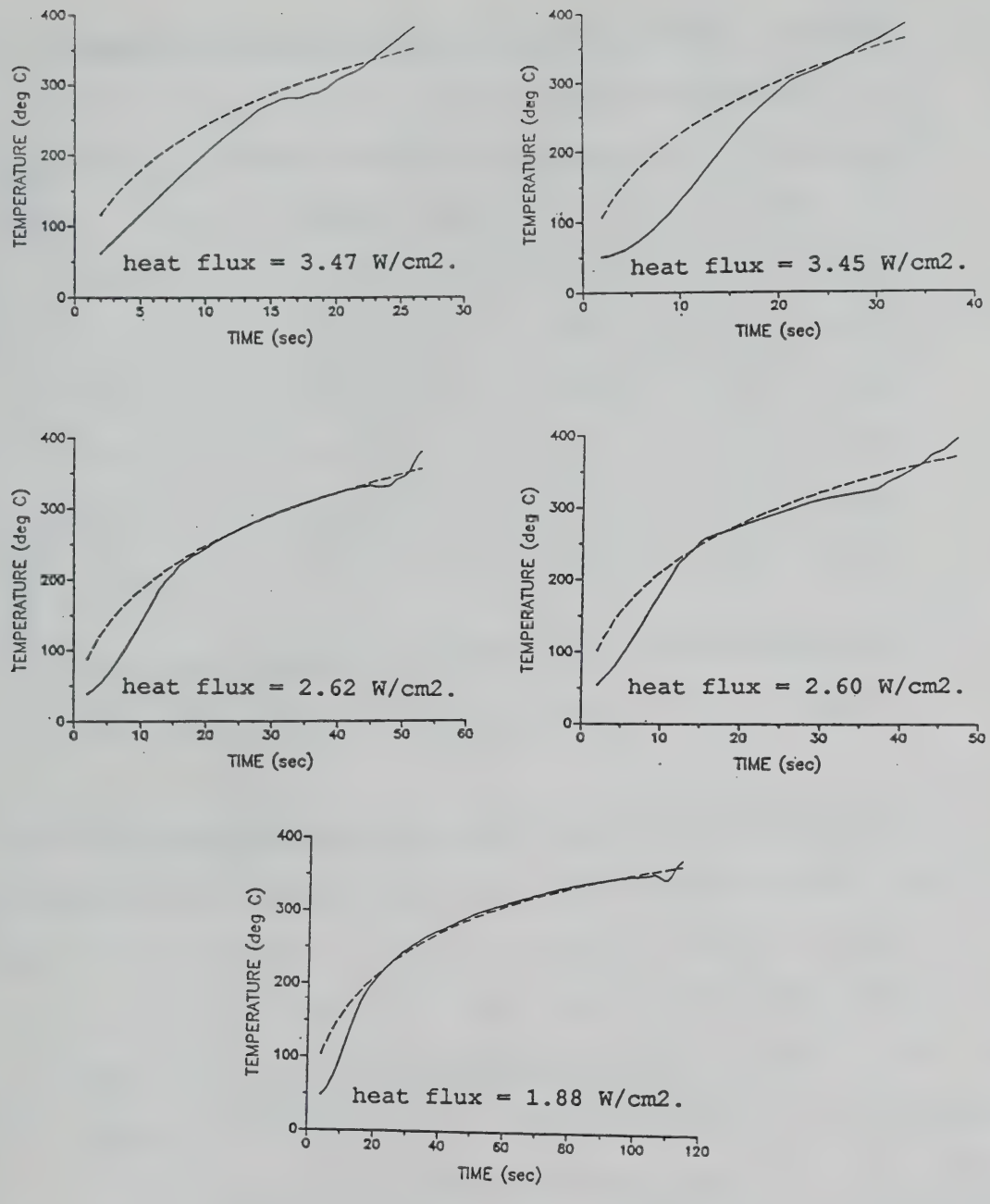

FIGURE D-2 Comparison of measured and predicted surface temperature.

Table D-1. Thermal conductivity calculated from measured surface temperature.

heat flux W/cm^2	thermal conductivity W/mK
1.88	0.226
2.6	0.223
2.62	0.188
3.45	0.315
3.47	0.299

D.3.2 The Effect of $\bar{h}$ on the Prediction of Thermal Conductivity of Wood.

Since the major heat loss from the surface at piloted ignition is due to radiation, small changes in the convective heat transfer coefficient may not have a significant effect on the determination of the thermal conductivity of wood. Table D-2 shows the comparison of the thermal conductivity of wood calculated by least-square surface temperature curve fitting for different convective heat transfer coefficients. It is seen that even a 100% increase or decrease in the heat transfer coefficient results in only a small error in the determination of the thermal conductivity (~2%).

Table D-2. Comparison of thermal conductivity for different $\bar{h}$.

Heat flux W/cm^2	$\bar{h}$=0.812 $W/m^{2o}K$	$\bar{h}$=0.406$W/m^{2o}K$	$\bar{h}$=1.624$W/m^{2o}K$
1.88	0.226	0.229	0.216
2.6	0.223	0.227	0.217
2.62	0.188	0.191	0.181
3.45	0.315	0.318	0.309
3.47	0.299	0.301	0.293
Average	0.250	0.253	0.243

D.3.3 The Pre-Expermental Factor Calculation

The pre-exponential factor for wood pyrolysis is also not well known. In view of the fuel production rate equation, let $M_s^* = \eta_i$, A^*=b, and

$$x_i \equiv \frac{(1-\delta^*)}{\Phi_s E^*} T_s^{*2} EXP(-E^*/T_s^*)\left[1- \frac{EXP(-E^*(1-1/T_s^*)}{T_s^{*2}}\right] .$$

By using equation (5-25) Beck and Arnold (1977), the approperiate pre-exponential factor can be estimated from the equation

$$A^* = \Sigma\eta_i X_i/\Sigma X_i^2 ,$$

where the thermal conductivity was assumed equal to 0.245 W/mK,

the activation energy equal to 30 kcal/gm-mole, and the char yield δ equal to 0.25. A computer program, SQFM, was written to calculate the optimal pre-exponential factor and the theoretical fuel evolution rate by using equation (5-18). The numerical code is listed in Appendix E.

Figure D-3 compares the experimental and theoretical fuel flow rates. The continuous lines are the experimentally measured data, while the dashed lines are the fuel evolution rate calculated from the analytical solution. (The analytical solution for the pyrolysis of wood shows the same trend as the numerical calculation of pyrolysis at the very beginning). The shapes of the fuel evolution rate curves for the experimental data are different than the analytical solution curves. The experimental fuel evolution rate rises very quickly, then falls a bit; the drop to zero of the experimental data might occur because of the measurement error. Most of the gas flow out of the wood in the early stages of pyrolysis is water vapor. Wood contains much water (even "dry" wood). The experimental dry wood is only arbitrarily defined (heated at $105^{\circ}C$ for 8 hours and allowed to cool over anhydrous $CaSO_4$). The sharp rise for the fuel evolution rate at the beginning may occur because of the evaporation of the moisture contained in the wood.

The pre-exponential factors calculated by the computer program are listed in Table D-3.

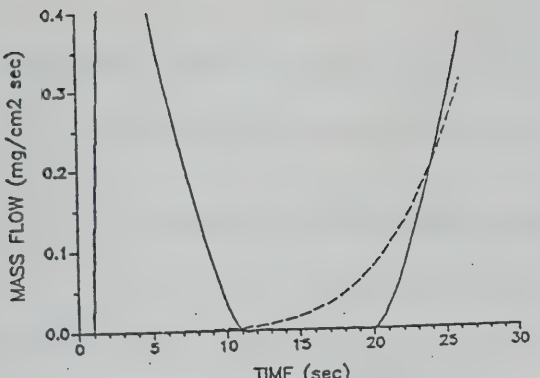

heat flux = 3.47 W/cm2.

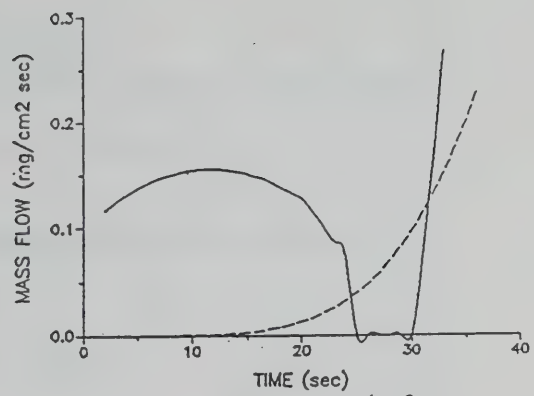

heat flux = 3.45 W/cm2.

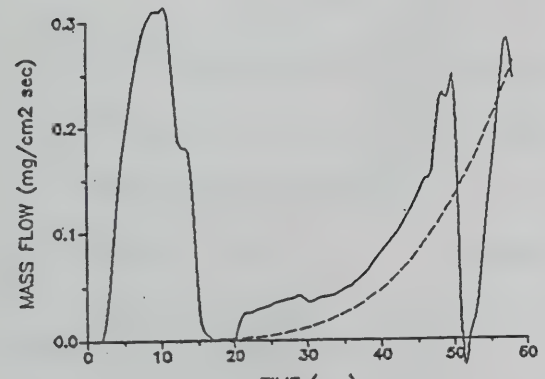

heat flux = 2.62 W/cm2.

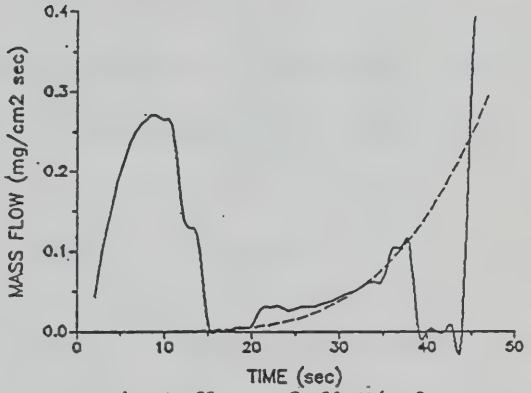

heat flux = 2.60 W/cm2.

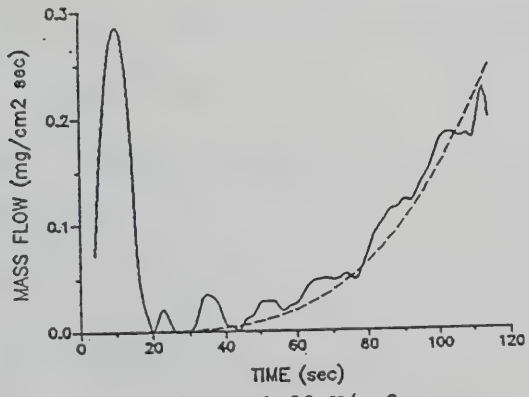

heat flux = 1.88 W/cm2.

FIGURE D-3 Comparison of measured and predicted mass flux at the surface.

Table D-3. Pre-exponential factor for the pyrolysis, obtained by the best fitting of the experimental data.

heat flux W/cm^2	pre-exponential factor (sec-1)
1.88	1.55E8
2.6	1.59E8
2.62	8.5E7
3.45	3.5E7
3.47	2.14E7

average A = 1.296E8 (sec-1)

The average pre-exponential factor is within the range of literature values $6.0*10^{7}$ ~$7.5*10^{8}$ (data from Tinney (1965)).

APPENDIX E

PROGRAM LIST FOR THE PARAMETER ESTIMATION OF WOOD

E.1 Program for the surface temperature

(least square fitting for optimum heat flux and thermal cond.)

```
C     This program least square fits the surface temperature of wood
C     to estimate the convective heat transfer coefficient and thermal
C     conductivity of wood
      PROGRAM SQFT
      DIMENSION TI(800),TA(800),CSS(800),SSQTP(80)
      OPEN(UNIT=11,FILE='SQIN.DAT',TYPE='OLD')
      OPEN(UNIT=12,FILE='SQOU.DAT',TYPE='NEW')
      PRINT *,'input conv,T,DNST,EPSL,in W/cm2,W/m2k,k,g/cm3'
      READ(5,*)CVF,TAMB,DNS,EPSL
      PRINT *,'Input higher and lower conv Rads heat flux'
      READ(5,*)HSFH,HSFL
      SIGM=5.6696E-12
C     RLNTH=0.126*TAMB/(HSF*85.)
      CVF=CVF/EPSL
C     HH=HH/EPSL
C     HL=HL/EPSL
C     HSF=HSF-(0.05/EPSL)
      HSF=HSFH
```

```
      HSFD=(HSFH-HSFL)/80.
      PRINT *,'Input # of data'
      READ(5,*)NDATA
      DO 20 I=1,NDATA
       READ(11,*)TI(I),TA(I)
   20 CONTINUE
C     Least square fit of RKK then calculate sum of square of temp.
C     CVF=HH
C     CVFD=(HH-HL)/80.
      HSFM=0.
      RKKM=0.
      SSQTM=1.E30
C     HSFM is the minimum heat flux
C     SSQTM is the minimum sum of square err SSQT
C     RKKM is the minimum of RKK
C     HSFM is dimensional, while RKKM is defined by Atreya's thesis
      DO 400 K1=1,80
C      CVF=CVF-CVFD
       HSF=HSF-HSFD
       AHTC=-(CVF*0.0001+(4.*SIGM*(TAMB**3)))
       SBC=-25.*SIGM*(TAMB**2)/3.
      BTAB=(AHTC**2)-(4.*SBC*HSF)
      SSQ=0.
      SYX=0.
      DO 40 I=1,NDATA
C     TEMP1=T-Tamb , Tamb=25.
       TEMP1=TA(I)-25.
```

```
      AB1=HSF+AHTC*TEMP1+SBC*(TEMP1**2)
      CC=(TEMP1*(AHTC+2.*SBC*TEMP1)/(BTAB*AB1))
      CCA=2.*SBC*TEMP1
      CCB=AHTC-(BTAB**0.5)
      CCC=AHTC+(BTAB**0.5)
      CCD=(CCA+CCB)*CCC/((CCA+CCC)*CCB)
      CC2=-(AHTC/(BTAB**1.5))*LOG(ABS(CCD))
      TIME1=(0.5*(TEMP1**2)/(AB1**2)-CC2-CC)
      SSQ=SSQ+TIME1**2
      SYX=SYX+TI(I)*TIME1
   40 CONTINUE
      RKK=SYX/SSQ
      TEMP=0.
      DTI=1.
      SSQT=0.
      DO 280 I=1,NDATA
       TIME=TI(I)
      TEMP1=TEMP+DTI
      DTI1=DTI
C     IF(TIME.LE.1.E-7) GO TO 240
  100 CONTINUE
      AB1=HSF+AHTC*TEMP1+SBC*(TEMP1**2)
      CC=(TEMP1*(AHTC+2.*SBC*TEMP1)/(BTAB*AB1))
      CCA=2.*SBC*TEMP1
      CCB=AHTC-(BTAB**0.5)
      CCC=AHTC+(BTAB**0.5)
      CCD=(CCA+CCB)*CCC/((CCA+CCC)*CCB)
```

```
C     PRINT *,'CCD=',CCD
      CC2=-(AHTC/(BTAB**1.5))*LOG(ABS(CCD))
      TIME1=RKK*(0.5*(TEMP1**2)/(AB1**2)-CC2-CC)
      ERR=(TIME1-TIME)/TIME
      IF(ABS(ERR).LE.1.E-3) GO TO 200
      IF(ERR.LT.0.) THEN
       TEMP=TEMP1
       TEMP1=TEMP+DTI1
       GO TO 100
      END IF
      DTI1=DTI1*0.5
      TEMP1=TEMP+DTI1
      GO TO 100
  200 CONTINUE
      SSQT=SSQT+(TEMP1-TA(I)+25.)**2
  280 CONTINUE
      HHF=CVF*EPSL
      IF(SSQT.LT.SSQTM) THEN
       SSQTM=SSQT
       HSFM=HSF
       RKKM=RKK
      END IF
      PRINT *,'HSF,SSQT,RKK=',HSF,SSQT,RKK
      WRITE(12,1100)HSF,SSQT,RKK
 1100 FORMAT(1X,'HSF,SSQT,RKK=',3F16.9)
  400 CONTINUE
      PRINT *,'Input HSF,RKK',HSFM,RKKM
```

```
      READ(5,*)HSF,RKK
C     CVF=CVF/EPSL
       AHTC=-(CVF*0.0001+(4.*SIGM*(TAMB**3)))
       SBC=-25.*SIGM*(TAMB**2)/3.
      BTAB=(AHTC**2)-(4.*SBC*HSF)
      TEMP=0.
      DTI=1.
      IF(CVF.LE.1.E-7) GO TO 480
      SSQT=0.
      REWIND(UNIT=12)
      DO 480 I=1,NDATA
       TIME=TI(I)
      TEMP1=TEMP+DTI
      DTI1=DTI
  420 CONTINUE
      AB1=HSF+AHTC*TEMP1+SBC*(TEMP1**2)
      CC=(TEMP1*(AHTC+2.*SBC*TEMP1)/(BTAB*AB1))
      CCA=2.*SBC*TEMP1
      CCB=AHTC-(BTAB**0.5)
      CCC=AHTC+(BTAB**0.5)
      CCD=(CCA+CCB)*CCC/((CCA+CCC)*CCB)
      CC2=-(AHTC/(BTAB**1.5))*LOG(ABS(CCD))
      TIME1=RKK*(0.5*(TEMP1**2)/(AB1**2)-CC2-CC)
      ERR=(TIME1-TIME)/TIME
      IF(ABS(ERR).LE.1.E-3) GO TO 440
      IF(ERR.LT.0.) THEN
       TEMP=TEMP1
```

```
       TEMP1=TEMP+DTI1
       GO TO 420
      END IF
      DTI1=DTI1*0.5
      TEMP1=TEMP+DTI1
      GO TO 420
  440 CONTINUE
      TEMP1=TEMP1+25.
      PRINT *,'TA(I),TEMP1=',TA(I),TEMP1
      WRITE(12,1200)TI(I),TEMP1
 1200 FORMAT(2X,F10.5,1X,E12.5)
  480 CONTINUE
      STOP
      END
C
C     ***********************************************************************
```

E.2 Program listing of the least square fitting of pyrolysis of wood

```
C     least square fitting for optimum pre-exponential factor
      PROGRAM SQFM
      DIMENSION TI(800),FUMA(800),CSS(800),SSQTP(80)
      OPEN(UNIT=11,FILE='SQIN.DAT',TYPE='OLD')
      OPEN(UNIT=12,FILE='SQOU.DAT',TYPE='NEW')
      PRINT *,'input rads,T,DNST,EPSL,RTK,in W/cm2,k,g/cm3,W/mk'
```

```
C     RTK is the thermal conductivity in W/mk
      READ(5,*)HSF,TAMB,DNS,EPSL,RTK
      CVF=0.812
      RKK=0.66667*DNS*1.38*RTK*0.01/(EPSL**2)
C     assume Cp = 0.33 cal/gk
C     assume conv heat trans. coeff. = 0.812 W/cm2k
      SIGM=5.6696E-12
      RLNTH=RTK*TAMB/(HSF*85.)
      TD=(RLNTH**2)*DNS*1.38/(RTK*0.01)
      CVF=CVF/EPSL
C     HH=HH/EPSL
C     HL=HL/EPSL
      PRINT *,'Input # of data'
      READ(5,*)NDATA
 1100 FORMAT(2X,F10.5,14X,E12.5)
      DO 20 I=1,NDATA
       READ(11,1100)TI(I),FUMA(I)
   20 CONTINUE
C     least square fit for optimum pre-exponential factor
C     CVF=HH
C     HSFM is the minimum heat flux
C     SSQTM is the minimum sum of square err SSQT
C     RKKM is the minimum of RKK
C     HSFM is dimensional, while RKKM is defined by Atreya's thesis
       AHTC=-(CVF*0.0001+(4.*SIGM*(TAMB**3)))
       SBC=-25.*SIGM*(TAMB**2)/3.
      BTAB=(AHTC**2)-(4.*SBC*HSF)
```

```
      SSQ=0.
      SYX=0.
      TEMP=0.
      DTI=1.
      IF(CVF.LE.1.E-7) GO TO 480
      SSQT=0.
      REWIND(UNIT=12)
      DO 480 I=1,NDATA
       TIME=TI(I)
      TEMP1=TEMP+DTI
      DTI1=DTI
  420 CONTINUE
      AB1=HSF+AHTC*TEMP1+SBC*(TEMP1**2)
      CC=(TEMP1*(AHTC+2.*SBC*TEMP1)/(BTAB*AB1))
      CCA=2.*SBC*TEMP1
      CCB=AHTC-(BTAB**0.5)
      CCC=AHTC+(BTAB**0.5)
      CCD=(CCA+CCB)*CCC/((CCA+CCC)*CCB)
      CC2=-(AHTC/(BTAB**1.5))*LOG(ABS(CCD))
      TIME1=RKK*(0.5*(TEMP1**2)/(AB1**2)-CC2-CC)
      ERR=(TIME1-TIME)/TIME
      IF(ABS(ERR).LE.1.E-3) GO TO 440
      IF(ERR.LT.0.) THEN
       TEMP=TEMP1
       TEMP1=TEMP+DTI1
       GO TO 420
      END IF
```

```
      DTI1=DTI1*0.5
      TEMP1=TEMP+DTI1
      GO TO 420
  440 CONTINUE
      TEMP=TEMP1/TAMB
      TEMPS=TEMP+1.
      AB2=AB1/HSF
      RMS=(0.75*(TEMPS**2)/(50.*AB2*EXP(50./TEMPS))*(1.-(1./
     1 ((TEMPS**2)*EXP(50.*(1.-(1./TEMPS)))))))
      SMAND=FUMA(I)*0.001*TD/(DNS*RLNTH)
C     SMAND is the non-dimensional mass flow rate
      SSQ=SSQ+(RMS**2)
      SYX=SYX+RMS*SMAND
  480 CONTINUE
      APND=SYX/SSQ
      APS=APND/TD
C     APND is the non-dimensional pre-exponential factor
C     APS is dimensional in sec-1
      TEMP=0.
      DTI=1.
      DO 280 I=1,NDATA
       TIME=TI(I)
      TEMP1=TEMP+DTI
      DTI1=DTI
  100 CONTINUE
      AB1=HSF+AHTC*TEMP1+SBC*(TEMP1**2)
      CC=(TEMP1*(AHTC+2.*SBC*TEMP1)/(BTAB*AB1))
```

```
      CCA=2.*SBC*TEMP1
      CCB=AHTC-(BTAB**0.5)
      CCC=AHTC+(BTAB**0.5)
      CCD=(CCA+CCB)*CCC/((CCA+CCC)*CCB)
      CC2=-(AHTC/(BTAB**1.5))*LOG(ABS(CCD))
      TIME1=RKK*(0.5*(TEMP1**2)/(AB1**2)-CC2-CC)
      ERR=(TIME1-TIME)/TIME
      IF(ABS(ERR).LE.1.E-3) GO TO 200
      IF(ERR.LT.0.) THEN
       TEMP=TEMP1
       TEMP1=TEMP+DTI1
       GO TO 100
      END IF
      DTI1=DTI1*0.5
      TEMP1=TEMP+DTI1
      GO TO 100
  200 CONTINUE
      TEMP=TEMP1/TAMB
      TEMPS=TEMP+1.
      AB2=AB1/HSF
      RMS=(APND*0.75*(TEMPS**2)/(50.*AB2*EXP(50./TEMPS))*(1.-(1./
     1 ((TEMPS**2)*EXP(50.*(1.-(1./TEMPS)))))))
      RMSFX=RMS*DNS*RLNTH*1000./TD
      PRINT *,'RMS,FUMA(I)mg/cm2 sec',RMSFX,FUMA(I)
      WRITE(12,*)TI(I),RMSFX
  280 CONTINUE
      PRINT *,'APS (sec-1),APND,TD',APS,APND,TD
```

```
      CLOSE(UNIT=11)
      CLOSE(UNIT=12)
      STOP
      END
C
C     ***************************************************************************
```

LIST OF REFERENCES

Abu-Zaid, M. [1988], "Effect of Water on Piloted Ignition of Cellulosic Materials", Ph. D. Thesis, Michigan State University, E. Lansing, MI.

Aly, S. L. and Hermance, C. E. [1981], "A Two-dimensioal Theory of Laminar Flame Quenching", Combustion and Flame 40, 173-185.

Amos, B., and Fernandez-Pello, A. C. [1988], "Model of the Ignition and Flame Development on a Vaporizing Combustible Surface in a Stagnation Point Flow: Ignition by Vapor Fuel Radiation Absorption", Combust. Sci. and Tech., 62,331-343.

Anderson, D. A., Tannehill, J. C., and Pletcher, R. H. [1984], "Combustional Fluid Mechanics and Heat Transfer", New York: Hemisphere Publishing Co.

Atreya, A. [1983], Pyrolysis, Ignition and Fire Spread on Horizontal Surfaces of Wood", Ph. D. Thesis, Harvard University, Cambridge, MA.

Atreya, A., Carpentier, C., and Harkleroad, M.[1986],"Effects of Sample Orientation on Piloted Ignition and Flame Spread,"First International Symposium on Fire Safety Science, V. 1, pp. 97-109.

Atreya, A. and Wichman, I.S.[1987],"Heat and Mass Transfer during Piloted Ignition of Cellulosic Solids,"2nd ASME-JSME Thermal Engineering Joint Conference, V. 1, pp. 433-440.

Atreya, A., and Wichman, I. S. [1989], "Heat and Mass Transfer During Piloted Ignition of Cellulosic Solids", Journal of Heat Transfer, 111, pp.7.

Bamford, C., Crank, J., and Malan, D., [1946], "The Combustion of Wood", Proc. Cambridge Phil. Soc., Vol. 42, p.166.

Baum, H. R., and Corley, D. M. [1981], "Finite Reaction Rate and Lewis Number Effects on Diffusion Flames in Channels", Presented at the Eastern State Section of the Combustion Institute, Pittsburgh, PA.

Beck, J. V., and Arnold, K. J. [1977], "Parameter Estimation in Engineering and Science", New York, John Wilery & Sons.

Blackshear, P. L., and Kanury, A. M. [1970], "On the Combustion of Wood I: A Scale Effect in the Pyrolysis of Solids", Combust. Sci. and Tech., 2, pp.1-4.

Buckmaster, J. D. [1975], "A New Large Damkohler Number Theory of Fuel Droplet Burning", Combustion and Flame, 24, pp.79-88.

Coffee, T.P., Kotlar, A. J., and Miller, M. S. [1983]," The Overall

Reaction Concept in Premixed, Laminar, Steady-State Flames", Combustion and Flame, 54, 155.

Gandhi, P. D. and Kanury, A. M. [1986], "Criteria for Spontaneous Ignition of Radiantly Heated Organic Solids", Comb. Sci. Tech., 50, 233.

Glassman, I. [1977], "Combustion", New York, Academic press.

Goos, A. (1952), "The Thermal Decomposition of Wood", Wood Chemistry, 2, ACS Nomograph Series No. 97, 2nd Ed., Reinhold Pub. Co., New York.

Hshieh, F. Y., and Richards, G. N. [1989], "Factors Influencing Chemisorption and Ignition of Wood Chars", Combustion and Flame, 76, pp. 37-47.

Ishizuka, S., and Tsuji, H. [1981], "An Experimental Study of the Effect of Inert Gases on Extinction of Laminar Diffusion Flames, "Eighteenth Symposium (International) on Combustion, The Combustion Institute, Pittsburgh, PA, pp.695-703.

Kanury, A. M., and Blackshear, P. L. [1970A], "Some Considerations Pertaining to the Problem of Wood-Burning", Combust. Sci. and Tech., 1, pp.339-355.

Kanury, A. M., and Blackshear, P. L. [1970B], "On the Combustion of Wood II: The Influence of Internal Convection on the Transient Pyrolysis of Cellulose", Combust. Sci. and Tech., 2, pp.5-9.

Kanury, A. M. [1972A],"Ignition of Cellulosic Solids - A Review,"Fire Research Abstracts and Reviews, V. 14, pp. 24-52.

Kanury, A. M. [1972B], "Thermal Decomposition Kinetics of Wood Pyrolysis", Combustion and Flame, 18, pp.75-83.

Kanury, A. M. [1974], "Ignition of Cellulosic Solids, Minimum Surface Temperature Criterion", Combust. Sci. and Tech., 9, pp.171-172.

Kanury, A. M. [1975], "Introduction to Combustion Phenomena", New York, Gordon and Beach.

Kansa, E. J. Perlee, H. E., and Chaiken, R. F. [1977], "Mathematical Model of Wood Pyrolysis Including Internal Forced Convection", Combustion and Flame, 29, pp.311-324.

Kashiwagi, T. [1974], "A Radiation Ignition Model of a Solid Fuel", Comb. Sci. Tech., 8, pp.225.

Kashiwagi, T. [1981],"Radiative Ignition Mechanism of Solid Fuels, "Fire Safety Journal, V. 3, pp. 185-200.

Kashiwagi, T. [1982], "Effect of Sample Orientation on Radiative Ignition", Combustion and Flame, 44,223-245.

Kashiwagi, T., Ohlemiller, T. J., and Werner, K. [1987], "Effect of External Radiation Flux and Ambient Oxygen Concentration on Nonflaming Gasification Rate and Evolved Products of White Pine", Combustion and Flame, 69, pp.331-345.

Kent, J. H., and Williams, F. A. [1974], "Extinction of Laminar Diffusion Flames for Liquid Fuels". Fifteenth Symposium (International) on Combustion, The Combustion Institute, Pittsburgh, Pennsylvania, pp.315-325.

Kindelan, M. and William, F. A. [1975], "Radiant Ignition of a Comstible Solid with Gas-Phase Exothermicity", Acta Astronautica, 2,pp.955.

Kung, H. C. [1972], "A Mathematical Model of Wood Pyrolysis", Combustion and Flame, 18, pp.185-195.

Kung, H. C. [1974], "The burning of Vertical Wooden Slabs", Fifteenth Symposium (International) on Combustion, The Combustion Institute, Pittsburg. pp.243-253.

Law, C. K. [1975], "Asymptotic theory for Ignition and Extinction in Droplet Burning". Combustion and Flame, 24, pp.89-98.

Linan, A. [1974], "The Asymptotic Structure of Counterflow Diffusion Flames for Large Activation Energies", Acta Astronautica, 1, pp. 1007-1039.

Martin, S. [1965], " Diffusion-Controlled Ignition of Cellulosic Materials by Intensive Radiant Energy", Tenth Symposium (International) on Combustion, pp.877.

Nurbakhsh, S. [1989], "Thermal Decomposition of Charring Materials", Ph.D. Thesis, Michigan State University, E. Lansing, MI.

Parker, W. J. [1988], "Prediction of Heat Release Rate of Wood" Ph.D. Thesis, The George Washington University.

Puri, I. K., and Seshadri, K. [1986], "Extinction of Diffusion Flames Burning Diluted Methane and Diluted Propane in Diluted Air", Combustion and Flame, 65, pp.137-150.

Roberts, A. F. [1970], "A Review of Kinetic Data for the Pyrolysis of Wood and Related Substances", Combustion and Flame, 14, pp.261-272.

Sauer, F. [1956], "The Charring of Wood During Exposure to Thermal Radiation: Correlation Analysis for Semi-infinite solids", Intrim, T. AFSWP-868 U.S.D.A. Forest Service.

Schwenker, R., and Beck, L (1963), "Study of the Pyrolytic Decomposition of Cellulose by Gas Chromatography", J. Polymer Sci. Part C, 1, No.2, pp.331.

Sibulkin, M., Kulkarni, A. K., and Annamali, K. [1982], "Burning on

a Vertical Fuel Surface with Finite Chemical Reaction Rate", Combustion and Flame, 44, pp.187.

Simms, D. L., [1960], "Ignition of Cellulosic Materials by Radiation", Combustion and Flame, 4, pp.293-300.

Simms, D. L., [1961], "Experiments on the Ignition of Cellulosic Materials by Thermal Radiation", Combustion and Flame, 5, pp.369-375.

Simms, D. L., [1962], "Damage to Cellulosic Solids by Thermal Radiation", Combustion and flame, 6, pp.303-318.

Simms, D. L., [1963], "On the Pilot Ignition of Wood by Radiation" Combustion and Flame, 7, pp.253.

Simms, D. L., and Law, M. [1967], "The Ignition of Wet and Dry Wood by Radiation", Combustion and Flame, 11, pp.377-388.

Spalding, D. B. [1953], Aircraft Engineering 25, 264; Proc. Roy. Soc. London 245A, 352 (1958).

Spalding, D. B. [1956], Phil. Trans. Roy. Soc. London, A249, 1.

Tzeng, L. S., Wichman, I.S. and Baum, H.R. [1987],"A Combined Analytical-Numerical Solution Procedure for Chemically-Reacting Flows", Central States Meeting of the Combustion Institute, pp.426-431.

Tzeng, L. S., Atreya, A., and Wichman, I. S. [1990],"A One-Dimensional Model of Piloted Ignition", Combustion and Flame, 80, pp.94-107. 1990.

Wang, C. Y. [1972], "Lecture Notes, Perturbation Methods", Department of Mathematics, National Taiwan University.

Wesson, H. R., Welker, J. R., and Sliepcevich, C. M. [1971], "The Piloted Ignition of Wood by Thermal Radiation", Combustion and Flame, 16, pp.303-310.

Westbrook, C. K., and Dryer, F. L. [1981], "Simplified Reaction Mechanisms for the Oxidation of Hydrocarbon Fuel in Flames", Combustion Science and Technology, Vol.27, pp.31-43.

Westbrook, C. K., and Dryer, F. L. [1984], "Chemical Kinetic Modeling of Hydrocarbon Combustion", Prog. Energy Combust. Sci., Vol.10. pp.1-57.

Williams, F. A. [1982], "Urban and Wildland Fire Phenomenology", Prog. Energy Combust. Sci., 8, pp.317-354.

Williams, F. A. [1985],"Combustion Theory,"The Benjamin/Cummings Publishing Co., Second Edition.

Wichman, I. S., and Atreya, A. [1987], "A Simplified Model for the

Pyrolysis of Charring Materials", Combustion and Flame, 68, pp.231-247.

Wichman, I. S., "On the Use of Operator-Splitting Methods for the Equations of Combustion", Combustion and Flame, to appear (1990).

NIST-114A
(REV. 3-90)

U.S. DEPARTMENT OF COMMERCE
NATIONAL INSTITUTE OF STANDARDS AND TECHNOLOGY

BIBLIOGRAPHIC DATA SHEET

1. PUBLICATION OR REPORT NUMBER
NIST-GCR-91-595

2. PERFORMING ORGANIZATION REPORT NUMBER

3. PUBLICATION DATE
August 1991

4. TITLE AND SUBTITLE

Theoretical Investigation of Piloted Ignition of Wood

5. AUTHOR(S)

Lin-Shyang Tzeng and Arvind Atreya

6. PERFORMING ORGANIZATION (IF JOINT OR OTHER THAN NIST, SEE INSTRUCTIONS)

Michigan State University
Department of Mechanical Engineering
East Lansing, MI 48824

7. CONTRACT/GRANT NUMBER
NIST Grant No. 60NANB8D0861

8. TYPE OF REPORT AND PERIOD COVERED

9. SPONSORING ORGANIZATION NAME AND COMPLETE ADDRESS (STREET, CITY, STATE, ZIP)
U.S. Department of Commerce
National Institute of Standards and Technology
Gaithersburg, MD 20899

10. SUPPLEMENTARY NOTES

11. ABSTRACT (A 200-WORD OR LESS FACTUAL SUMMARY OF MOST SIGNIFICANT INFORMATION. IF DOCUMENT INCLUDES A SIGNIFICANT BIBLIOGRAPHY OR LITERATURE SURVEY, MENTION IT HERE.)

A theoretical model for piloted ignition of a flame in the gas phase above a vaporizing or pyrolyzing solid has been developed. Using this model it has been found that (i) The postulated simplified governing equations adequately explain the pre-ignition flashes that are often observed experimentally; (ii) A rational criterion for positioning the pilot flame exists; (iii) The heat losses to the surface play an important role, indicating that the fuel evolution rate by itself is insufficient for predicting the onset of piloted ignition. In this investigation, a numerical integration scheme is developed that accounts for the often vastly different rates between chemical reaction and convection or diffusion processes in the equations of combustion theory. This new numerical scheme is found to be very efficient for the piloted ignition problem, which involves both pre-mixed and diffusion flames. Finally, a numerical model for piloted ignition of wood which includes transient solid-phase decomposition has been developed. It has been found that the activation energy for the combustion of the evolved fuel is 49 Kcal/mole.

12. KEY WORDS (6 TO 12 ENTRIES; ALPHABETICAL ORDER; CAPITALIZE ONLY PROPER NAMES; AND SEPARATE KEY WORDS BY SEMICOLONS)

diffusion flames; equations; pilot ignition; premixed flames; wood

13. AVAILABILITY

[X] UNLIMITED

[ ] FOR OFFICIAL DISTRIBUTION. DO NOT RELEASE TO NATIONAL TECHNICAL INFORMATION SERVICE (NTIS).

[ ] ORDER FROM SUPERINTENDENT OF DOCUMENTS, U.S. GOVERNMENT PRINTING OFFICE, WASHINGTON, DC 20402.

[X] ORDER FROM NATIONAL TECHNICAL INFORMATION SERVICE (NTIS), SPRINGFIELD, VA 22161.

14. NUMBER OF PRINTED PAGES
230

15. PRICE
A11

ELECTRONIC FORM